4-18-2017

Anticipating the Effects of Economic Displacement in Marine Space with Agent Based Models

Kevin P. Nebiolo
University of Connecticut - Storrs, kevin.nebiolo@uconn.edu

Anticipating the Effects of Economic Displacement in Marine Space with Agent Based Models

Kevin Patrick Nebiolo, PhD

University of Connecticut, 2017

As marine space is managed into appropriate resource use areas, it is inevitable that some is allocated towards a mutually exclusive spatial activity. This exclusion results in displacement that has real economic consequences. When a wind energy area is placed in coastal waters, navigable space is reduced and vessels are displaced from their former routes. The USCG is concerned that re-routing will result in vessels navigating within closer proximity than they would otherwise in an open ocean scenario, and fear that this will increase the risk of vessel collision (USCG 2016). They recommend research into tools that are capable of predicting changes in vessel traffic patterns (USCG 2016). Agent based models are a method capable of predicting these traffic patterns, and are composed individual, autonomous goal directed software objects that form emergent behavior of interest. Agents are controlled by a simple behavioral rule, they must arrive at their destination without colliding with an obstacle or other vessel. They enforce this rule with the gravitational potential that exists between two objects. Attractive forces pull each agent towards their destination, while repulsive forces push them away from danger. We validated simulated vessel tracks against real turning circle test data, tested for the presence of chaotic systems, developed metrics to assess transportation costs, and applied the method to assess a WEA located outside of the entrance to the Port of New York and New Jersey.

Anticipating the Effects of Economic Displacement in Marine Space with Agent Based Models

Kevin Patrick Nebiolo

B.A., University of Connecticut, 2004

M.A., University of Connecticut, 2012

A Dissertation

Submitted in Partial Fulfillment of the

Requirements for the Degree of

Doctor of Philosophy

at the

University of Connecticut

2017

APPROVAL PAGE

Doctor of Philosophy Dissertation

Anticipating the Effects of Economic Displacement
in Marine Space with Agent Based Models

Presented by

Kevin Patrick Nebiolo, B.A., M.A.

Major Advisor _____
Robert Cromley

Associate Advisor _____
Thomas Meyer

Associate Advisor _____
Carol Atkinson-Palombo

Associate Advisor _____
Nathaniel Trumbull

University of Connecticut
2017

Acknowledgements

I'd like to thank my advising committee for their support, guidance and patience throughout the years.

To my family, close friends and colleagues for believing in me and giving me carte-blanche to gripe over the years.

Most importantly, I'd like to thank my wife. Tina, you gave me the strength to keep pushing on, I wouldn't be here today without you.

Thank you.

Table of Contents

Chapter 1
Introduction

1.1 Introduction

With the Bureau of Ocean Energy Management (BOEM) siting Wind Energy Areas (WEAs) within navigable water and fisheries management agencies enforcing Marine Protected Areas (MPAs) that shelter resources from harvesters, spatial regulations manage resource use within appropriate areas in marine space. In contrast to a traditional sectoral resource management paradigm, Marine Spatial Planning (MSP) conceptualizes marine space as a coupled socio-ecological system. Resource managers allocate space towards a restricted set of resources uses that exclude certain activities, leading to economic, social and environmental change within a system. Socio-economic systems that are not resilient, (i.e. cannot endure too much stress), may decline or fail. Therefore, a successful MSP will

implement spatial management decisions that do not erode the ability of individual system components to adapt to change, thus ensuring their sustainability.

Sustainable, ecosystem based MSP is an integrated planning framework that allocates marine space among competing resource uses (Foley, et al. 2010). MSP is necessary because of the uncoordinated expansion of existing and emerging uses of marine space such as renewable energy and large-scale aquaculture. Along with a rapidly growing coastal population, these conditions are likely to exacerbate the decline of marine ecosystem health (Foley, et al. 2010). Ecosystem-based MSP provides economic, ecological and administrative benefits for practitioners and resource users alike. Most importantly, ecosystem based marine spatial planning seeks to resolve conflict among competing users of ocean space and to reduce the cumulative impacts of these activities on the marine environment (Douvere and Ehler 2009). Ecosystem based MSP accomplishes this by taking into account the entire marine ecosystem, rather than individual sites, and it ensures that economic and social objectives respect environmental limits (Ehler 2008). As a result, implementing sustainable, ecosystem based MSP requires that planners utilize methods that take into consideration the interconnected nature of complex systems in order to anticipate the consequences of spatial management decisions.

1.2 Statement of the Problem

When siting competing mutually exclusive ocean uses, many MSP applications lack the ability to anticipate the consequences of economic displacement resulting from foregone space. Foregone space represents the area lost to a particular use when exclusive rights for that space are granted to a competing use. MPAs represent foregone space for fishers, while WEAs are foregone space for marine trade. Their siting results in displacement, which simply means that effort is moved from one place to another (Agardy, Notarbartolo di Sciara and Christie 2011). For example, ocean renewable energy infrastructure (OREI) displaces commercial traffic because vessels cannot safely navigate within a project boundary (MCA 2008). Recently, the United States Coast Guard (USCG) ruled that creating routing measures

where structures currently do not exist (i.e. displacing navigational channels), would more than likely result in an increase in risk due to vessel navigation in closer proximity to each other in than they would otherwise in an open ocean scenario (USCG, 2016). They recommend creating modeling and analysis tools that are capable of predicting changes in vessel traffic patterns, and much more stringent spatial planning protocols (USCG, 2016). OREI can also impact commercial fishing, as fishers are hesitant to deploy mobile gear (long lines, gillnets and trawls) near these facilities as they risk entanglement with anchoring structures (Fayram and de Risi 2007). For some spatial plans, displacement is intended as a measure to protect resources and habitats (MPAs), while for others, displacement is a consequence of siting a mutually exclusive use (WEAs). For either case, the socio-economic consequences of displacement can have broader implications for the region.

Displacement has real economic costs for marine industry, it leads to increased time at sea, greater fuel costs and lower profit margins. For fishers, their efficiency is further reduced in terms of catch per unit effort because of the costs associated with learning where the productive areas are in new fishing grounds (Agardy, Notarbartolo di Sciara and Christie 2011). Displacement costs reduce the profitability of marine industrial sectors, making them less resilient to change. Because of the interconnected nature of human socio-economic systems, these consequences can also follow through onto land as well. In the outlying coastal counties of the Northeastern United States, the location quotient for the marine economy was high, meaning these areas are more dependent upon the marine sector than on average. Spatial management decisions that affect the profitability of marine trade and fishing can have severe repercussions for regions that are dependent upon the marine economy. As these industries falter or even fail, coastal economies dependent upon them will retract as well. Therefore, limiting access to resources (including space itself) has the potential to disrupt the socio-economic stability of coastal communities, and result in conflict among user groups with competing interests over the same limited resources (Agardy, Notarbartolo di Sciara and Christie 2011). Understanding and anticipating the negative consequences from displacement is necessary for a successful MSP.

Displacement related impacts are often indirect consequences of a MSP, few researchers have addressed them, and those that have primarily address fishery sectors. Agardy, Notarbartolo di Sciara and Christie (2011) found that few analytical studies actually quantify displacement impacts, let alone address the long-term resiliency of socio economic sectors. Those that have were inconclusive or lacked the rigor of quantitative analysis. Marine Protected Areas (MPAs) conserve important habitat areas for fisheries resources by prohibiting fishing, thereby directly displacing effort. They were found to affect the social well-being and political power of fishers, but there was no clear effect on the economic well-being of coastal communities (Mascia, Claus and Naidoo 2010). Greenstreet, Fraser and Piet (2009) developed a fisheries effort displacement model that reallocated effort to areas outside of an MPA. Their method assumes that a fisher will focus their effort on a new, empty area, regardless of that area's prior productivity. In other words, they assumed fishers will simply spread out without attempting to maximize catch. However, their assumptions were incorrect. Actual fishing data suggests that fishers congregate along the boundary of an MPA in an effort to catch biological spillover, a phenomenon known as "fishing the line" (Kellner, et al. 2007). Campbell, et al. (2014) employed vessel management system (VMS) data to map and characterize fishery activity within the English Channel. They designed their output to be incorporated into a multi-criteria decision analysis that minimized impacts to fisheries. While their approach demonstrates the utility of high-resolution use data (VMS) for making informed management decisions, it cannot anticipate the consequences of an MPA. Their method has no way of calculating displacement related effects, planners can only locate an MPA in areas less frequented by fishers. In an analysis of the noncompliant behavior that results from poor MPA design, Peterson and Stead (2011) found that displacement generally leads to four options for fishers: fish illegally, change fishing grounds, change fishing gears, or move effort to alternative methods. However, their method stops short of quantifying any real economic cost resulting from a spatial management decision. Besides fishing, marine trade is impacted by MSPs as well. However, studies have not addressed displacement of commercial shipping, feedback effects associated with rerouting commercial vessels, nor the long-term

economic sustainability of the commercial shipping industry due to these impacts. Therefore, current MSP practices still have a long way to go before a plan anticipates the sustainability for socio-economic sectors dependent upon the space they are restricting.

1.3 Purpose

The purpose of this study is to implement methods that can anticipate the displacement of mutually exclusive activities resulting from foregone space. Particularly, it will study the effects of a WEA on the marine trade and transport industry. The resulting displacement has real economic costs, which can potentially lower the industry's profit margin. The rerouting of vessels will not only result in longer voyages in both time and distance, but routing all vessels into narrower navigational channels may lead to traffic congestion and increased risk of vessel collision. These secondary effects could lead to even longer voyage times and worse, loss of life and property. Currently, MSPs do not account for these effects, and often times they are addressed after the fact through adaptive management protocols. Planners can test the sustainability of spatial regulations by developing simulation methods that anticipate these effects.

1.4 Theoretical Framework

Agent based models (ABM) are comprised of autonomous interacting agents that produce emergent behavior on a simulated landscape (Macal and North 2005). They offer a way to experiment prior to a plan's implementation. ABMs examine the sustainability of potential configurations without having to enact a plan in real life and study its affects after the fact. ABMs are also an approach to modeling complex adaptive systems through individual interaction. In the case of competition over marine space, individual agents are the mariners piloting the ships in the marine trade industry. Agent behavior can range from primitive stimulus-reaction decision rules to complex adaptive intelligence (Macal and North 2005). These adaptive traits are behavioral rules or simple heuristics that allow an

individual agent to make decisions (Jorgensen and Fath 2011). Through complex interactions between individuals, emergent patterns of agent behavior manifest on the landscape. Then, as the system is constrained in some way, agents will adapt to the new conditions, producing new emergent states (Abbott 2007). Emergence is a property of the system; it is not reducible to, nor readily predictable from the properties of the individual agents (Halley and Winkler 2008). This is because emergence results from individual interaction between rational, goal-directed agents that combine to produce novel behavioral patterns. While useful for exploring the consequences of plan options, their implementation is quite difficult.

In work that paved the way for complex systems thought, Lorenz (1963) developed a simple abstraction capturing the essence of a three-dimensional convection model with intention of modeling weather, and he found that the prediction of the sufficiently distant future was impossible by any method unless the present conditions are known exactly. Therefore, in the view of imperfect models and information, long-term prediction is impossible (Lorenz, 1963). Given that these models lose predictability over time, their duration must be short. Therefore, the model durations herein are on the magnitude of a single voyage. Aside from short, but meaningful durations, model validation is important.

Reproducing past observations, or verifying the structural similarity between the model and present knowledge of the system validates ABMs (Gross and Strand, 2000). However, given the complexity of real systems, there can probably be no true one-to-one validation of system components in terms of structural similarity (Gross and Strand, 2000). Therefore, the marine planner must validate their model by comparing the emergent states of many iterations with empirical data from past events.

1.5 Research Questions

A major concern for the marine spatial planner should be that of the effect of foregone space (in total area and configuration) and resultant economic displacement of mutually exclusive spatial activities.

WEAs reduce the navigable area for commercial vessels. It is thought that this can lead to an increase in voyage duration, greater transportation costs, and an increased risk of collision with infrastructure and other vessels in congested channels, thereby reducing the resiliency and safety of the marine trade sector. An ABM, designed to simulate the marine trade and transport industry, will anticipate the negative consequences of a WEA with a population of autonomous ship-agents.

1.6 Importance of the Study

This study is timely considering energy derived from marine renewables (wind, wave and tides) are poised to reduce reliance on fossil fuel for energy production in the northeast United States and to reduce the current rates of $C0_2$ emissions affecting global climate. However, siting WEAs may have unforeseen consequences for the marine trade sector, a globally and regionally important socio-economic sector that is closely tied to the economic well-being of the coastal counties within the northeast United States. In 2016, economic downturn in advanced economies reduced exports coming from China, and the industry is projected to experience zero growth (Northam, 2016). Following the announcement of troubles for the global shipping industry, Hanjin Shipping company, one of the world's largest shipping companies filed for bankruptcy protection while leaving some 500,000 containers stranded at sea (Northam, 2016a). The industry is showings signs of stress, and improper planning could apply more pressure. The current plans for WEAs along the Northeast's coastline place some developments close to major shipping channels. However, these plans do not take into consideration that marine traffic, especially tug and barge traffic, do not always navigate within the confines of marked channels. The much slower and much less maneuverable barge traffic could impede the movements of faster vessels leading to congestion and an increased risk of collision.

1.7 Scope of the Study

An ABM, simulating the marine trade and transport sector will anticipate the socio-economic impacts following the implementation of a marine spatial plan off the coast of the northeastern United States. This project will address three important research priorities. The first will develop a series of computational experiments and analytical methods designed to quantify economic displacement as a function of the plan's size and configuration and the number of individuals in the population. The first will assess the ability of an agent-based model to simulate a socio-economic sector and reproduce emergent pattern as depicted with actual ship trajectory scenarios from a theoretical and analytical perspective.

1.8 Summary

Ecosystem based MSP gives planners and regulators the tools they need to create sustainable plans that balance mutually exclusive uses of marine space. However, current methodologies lack the ability to anticipate the negative consequences of a plan, potentially leading to the degradation of globally and regionally important marine socio-economic sectors. These sectors are complex adaptive systems comprised of autonomous agents maximizing their own wellbeing and competing for space. Following plan implementation, they will interact in novel ways producing new emergent states that may lead to economic hardship or a reduction in the safety of the industry. ABMs are a tool that can anticipate these negative consequences and give planners and regulators the insight they need to make better, more informed decisions.

Chapter 2
Literature Review

2.1 Traditional and Expanding Uses of Marine Space

Traditional socio-economic uses of marine space include the fishing and marine trade and transport industry. In capture fisheries, fish are hunted in wild ecosystems using techniques ranging from spears, traps and hooks, to massive nets guided by sophisticated equipment (Campling, Havice, & Howard, 2012). Because fish are mobile and inhabit expansive swaths of coastal ocean, capture fisheries spread out to find the most productive areas for exploitation. Prior to the development of MPAs, the only spatial regulations on capture fisheries that were enforced were to abide by the exclusive economic zone of sovereign states (Campling, Havice, & Howard, 2012). Over time, as fishers identified the most productive areas and developed effective gear, fishery stocks began to feel pressures from

overexploitation. Now, approximately 75% of the world's fisheries are at or beyond exploitation rates, and their populations are expected to decline (Campling, Havice, & Howard, 2012), forcing many natural resource agencies to enact spatial regulation.

MPAs are spatially defined marine units in which one or more human activities are restricted (McKay and Jones 2011). A majority of the MPAs prohibit fishing, while some restrict recreational uses as well. MPAs displace fishers that at one time directed their effort into these locations, forcing them to find new areas to exploit. Displaced fishers can mitigate economic losses if they can relocate to another productive area (Carter 2003) or if biological spillover occurs resulting in higher catches along the margins of MPAs (Kellner, et al. 2007). Displacement has other unintended consequences. Fishing fleets are rational economic entities, meaning they make decisions that maximize their well-being within the constraints placed on them through spatial management (Hilborn 2007). If an MPA displaces a fisher from their traditional fishing grounds, they will find new species and habitats to target. Therefore, efforts to protect an imperiled species through spatial measures inadvertently increase harvesting pressure on others (Abbott and Hayne 2012). Aside from displaced effort, a reallocation of resource use and access rights also occurs. This affects the economic well-being, health, education, social capital, and the culture of traditional resource users, local communities and other social groups (Mascia and Claus 2008). The unintended consequences and socio-economic ripple effects of spatial management plans have the greatest effect on the sustainability of coastal communities. Spatial management can erode the resiliency of traditional fishing communities, and regulators need to anticipate these impacts. The fishing industry is not the only traditional marine industry at odds with new uses of marine space.

The marine trade and transport industry is a traditional socio-economic use of marine space, and consists of several different industries, including freight transportation, passenger transportation, transportation logistics, warehousing, electronics, and the ancillary land based sectors dependent upon the marine economy (Kildow, Colgan, and Scorse, 2009). Consequently, this expansive industry is a major

sector in coastal economies. In a study of the marine economy in Ireland, Morrissey, O'Donoghue, and Hynes (2011) found that the shipping and marine transport made up a significant portion of the economy. In Europe, the promise of short-sea-shipping, or short-run coastal freight shipping, is expected to alleviate pressures on already overcrowded transportation infrastructure (Baird, 2007). As the 21st century witnesses an increase in the use of maritime trade corridors, we are also expanding our footprint into the coastal ocean by constructing OREI infrastructure.

OREI has the potential to make significant contributions to future energy supplies (Kerr, 2007) as well as reduce emissions of greenhouse gases. Technologies are available that can harness mechanical power from waves and tides, while offshore platforms are constructed to support traditional wind turbines. Tidal power (referring to instream hydrokinetics and not tidal barrages) is highly predictable and reliable compared with other renewables (Pelc and Fujita, 2002), but it requires site-specific conditions that accelerate tidal flows into currents greater than 2 m/s (Kerr, 2007). Therefore, finding appropriate sites for tidal development is difficult. Regardless, marine hydrokinetic technology could harness considerable power from sites with favorable conditions. A numerical study of the central Maine coast found peak power densities as high as 6.5 kW/m^2 (Brooks, 2011). Harnessing this resource will produce 2700 MWh, or enough power for 150 homes (Brooks, 2011). As the depth of the structure increases, navigational concerns diminish, but environmental concerns may remain. Collision impacts with marine organisms are a concern; however, their proper location can mitigate impacts (Cada and Bevelhimer 2011). OREI technologies that reduce the hydrokinetic energy of some systems by extracting tidal or wave energy may produce environmental conditions that are at odds with the ecological communities that have adapted to these high-energy environments (Shields, et al. 2011). Again, proper location can mitigate these impacts. At this time, tidal power and wave energy is not expected to reach the scale of development as proposed with offshore wind; therefore, the expected impact to navigability from these technologies is low. Meanwhile, offshore wind, another OREI technology, requires large tracts of contiguous and empty ocean space.

The amount of space required for an offshore wind project with sufficient economies of scale is great. For example, to maximize the efficiency of offshore windfarm turbines, the required inter-array spacing is as high as 7 – 10.5 rotor diameters (Barthelmie, et al., 2010). A 6 MW turbine with a 126-meter rotor diameter will require a buffer area between 882 and 1,323 m^2. Therefore, a 90 MW wind farm (30 turbines) requires at least 26.46 to 36.69 km^2 of the coastal ocean. Since some large commercial vessels cannot safely navigate within a wind farm, renewable energy infrastructure that is near shipping corridors may increase vessel density, affecting the navigability of the region causing mariners to reduce their speed, change course, or implement collision avoidance procedures. The Maritime and Coastguard Agency, the United Kingdom's equivalent of the United States Coast Guard, recommends shipping routes be at least 0.45 nautical miles (800 m) from a turbine (MCA, 2008). Exclusion could lead to navigational, safety or routing problems as vessels must follow a less than optimum route (MCA, 2008). Not only will voyage distances increase as vessels must now navigate around obstructions, but an increase in vessel density could lead to congestion effects that reduce the serviceability of ports because vessels are competing over limited space in navigational approach corridors. Removing navigable space that was once available to the marine trade and transport industry can have significant consequences. Longer navigation routes and increased vessel density will lead to higher transportation costs (Clark, Dollar, and Micco, 2004). Removal of navigable space may reduce the marine trade and transport industry's capacity to absorb economic impacts from other external forces. These forces could be new forms of industry regulation, competition from terrestrial or aerial forms of commercial transportation, or natural events that cause an increase in industry costs.

2.2 Displacement Impacts on Navigation

Displacement affects the marine trade and transport industry. From farther distances travelled and more time at sea, to increased traffic congestion and density related impacts around installations, the

industry will incur greater costs as the result of OREI development. Measuring an increase in the distance travelled and the cost incurred for a vessel to navigate around an OREI development is somewhat trivial. Rather, it is the impacts of congestion and or vessel safety that may affect industry the most, and consequently, are the most difficult to anticipate. For maritime transport, voyage costs are influenced by distance travelled and time spent at sea (Cullinane and Khanna 2000). A small reduction in voyage efficiency (lower vessel speeds due to higher congestion) can have severe economic costs (Fagerholt 2004). Vessel interaction, particularly meeting and passing maneuvers, are the most critical navigation problem (Hewlett 1994), and when congestion is increased, the frequency of these critical moments increase. Aside from the at-sea impacts, the land-based marine economic sectors will also face displacement related impacts.

Any time a vessel is operating at speeds below cruising, they will incur economic penalties associated with a longer time at sea, and the shipping line may choose another port with easier access. In an analysis of large container ships, Cullinane and Khanna (2000), found that when ports are congested or inefficient, diseconomies of scale have greater significance. In other words, the greater the size and cargo capacity of a vessel, the more congestion hurts their profitability. Congestion is a significant problem around access channels to ports and can represent bottlenecks in global maritime transportations systems (Notteboom 2006). OREI developments that lead to greater congestion and delays can have significant impacts in worldwide transportation networks, where unexpected vessel waiting times in strategic locations can cascade throughout the whole loop (Notteboom 2006). As congestion increases and liner profitability decreases, shipping firms may choose other ports with better serviceability.

Maintaining port serviceability is critical for the economic viability of the port and tertiary sectors dependent upon steady maritime traffic. Following containerization and deregulation, maritime carriers set contracts with rail services to establish rates independent of location, resulting in intensified competition between ports (Malchow and Kanafani 2004). Regional ports compete with one another to

become destinations for large shipping alliances (Chang, Lee and Tongzon 2008). Chang, Lee and Tongzon (2008) found that cargo volume, terminal handling changeover, berth availability, location, and feeder connection are important predictor variables in port choice. They also found that feeder ports must compete with other feeder ports to provide more comprehensive and value-added services. Nir, Lin, and Liang (2003) found that travel time and cost explained port choice. Tongzon and Sawant (2007) conducted a stated preference survey, and found port efficiency to be of prime importance followed by charges, economic connectivity, location, infrastructure, ancillary port services, and maximum cargo size. With efficiency the primary factor in port choice, any reduction may prompt shippers to find another port. Displacement related congestion could tip the balance in favor of another port. Therefore, the economic viability of a port and local economy hinges on how efficient they can load and offload goods. Ports that are a long distance from demand centers are at a greater risk of impact from congestion related impacts because they are less resilient than ports closer to demand centers. Other sectors within the marine trade industry are also affected by congestion.

Ferries transport human cargo across open expanses of water in an effort to bypass congested road networks or to connect island populations to the mainland. Their long-term sustainability depends upon safe and timely service. In 2003, a study was commissioned to assess the safety of increased ferry services within San Francisco Bay (Merrick, et al. 2003). The authors conducted a traffic simulation study and found areas of greater congestion and increased risk of accidents. They concluded that the current safety levels enjoyed by San Francisco's ferry operators cannot be maintained under the planned expansion scenarios (Merrick, et al. 2003). Clearly, congestion related impacts to the marine trade and transport industry far outweigh those of greater distance travelled. Marine spatial plans that lead to increased congestion can affect safety of ferry traffic, the sustainability of trade industries, the ports they choose, and the coastal economies that service them as well. In an analysis of coastal counties, the location quotient for outlying counties reliant upon the marine sector was high (Figure 2.1). Within large metropolitan areas, the coastal economy is primarily

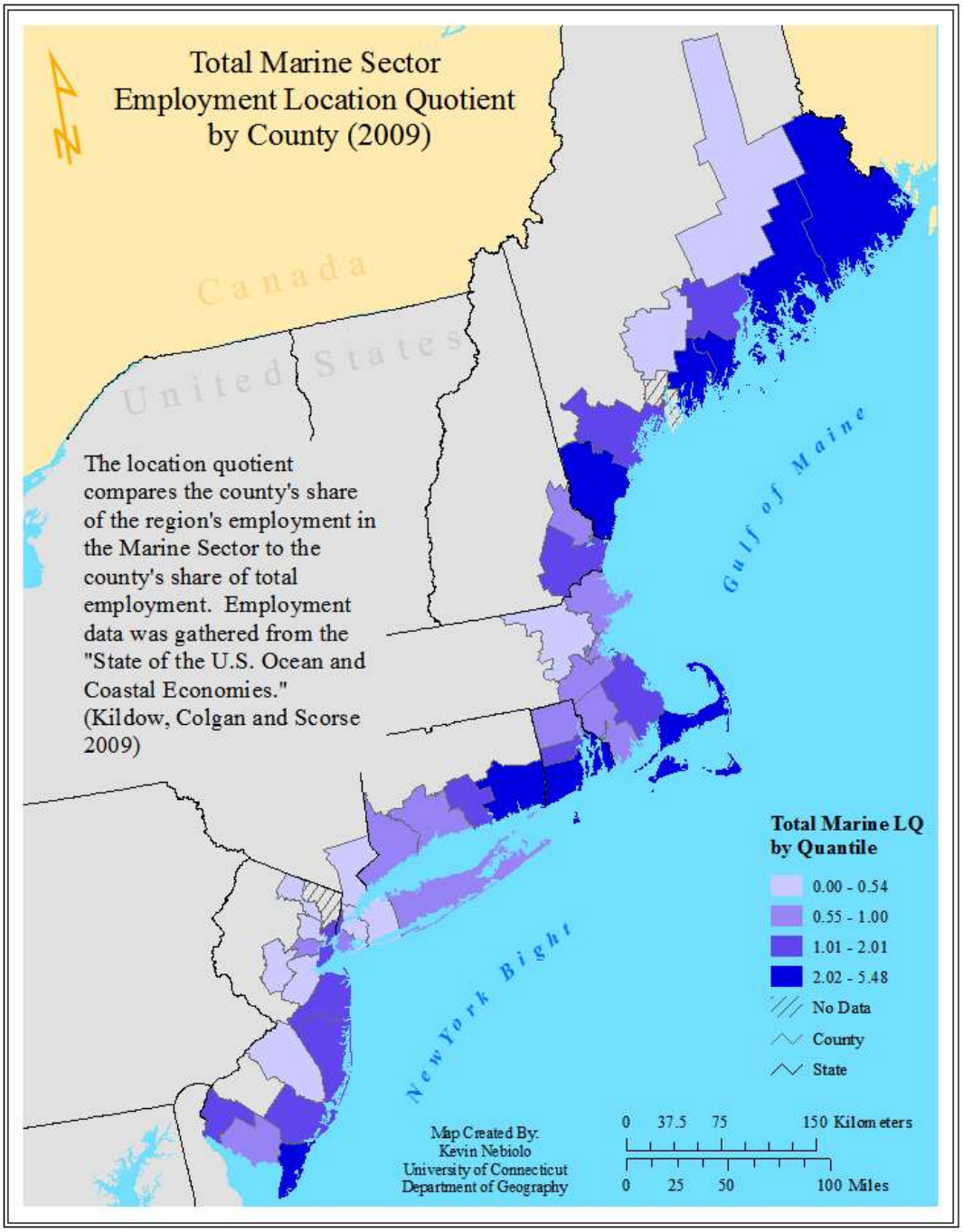

Figure 2.1 a depiction of the location quotient for the total marine industry within the coastal counties of the Northeastern United States.

professional service based (Kildow, Colgan, & Scorse, 2009). However, outside of the economically diverse metropolitan areas, the periphery relies upon a few key marine-based sectors. In the northeast United States, these are the living resource industries (fisheries), tourism and recreation industry, marine trade, and marine manufacturing and construction. However, with few shipyards and no mineral or oil and gas exploration, this last sector makes up only a tiny fraction of the region's marine based economy.

Economies change and adapt over time to patterns of supply and demand in much the same manner an ecosystem would adapt to new environmental stimuli. For an ecosystem to evolve, selection operates on the system's individual components (Levin & Lubichenco, 2008). The ability of a system to alter its composition in a changing environment is maintained through diversity and heterogeneity (Holling, 1973 and Levin & Lubichenco, 2008). The more homogenous the system, the more likely it is to have low resilience or robustness (Holling, 1973). Therefore, any development that may reduce the sustainability of marine industries will also have repercussions for land based economy that provides critical support services for marine trades.

The remainder of the 21st century will see a continued development in coastal areas placing considerably more stress onto coastal ecosystems and socio-economic sectors than current exploitation does now. With new uses for marine space directly competing with traditional uses and ecosystem services in steep decline, natural resource managers must embrace systems thinking else we risk eroding our current systems further and to the point they are no longer sustainable.

2.3 Ecosystem Based Marine Spatial Planning

The term Ecosystem Based Management can be misleading. It is not solely focused on the stewardship of biodiversity, but also considers the complex mix of property rights, local customs and regulations, and the diverse range of human use activities in the marine region (Peel and Lloyd, 2004). The ultimate goal is to allow existing and emerging uses while supporting healthy ecosystems and

sustaining their production of goods and services for future generations (Foley, et al., 2010 and Levin and Lubichenco, 2008). Managers and planners must consider who will be affected by management decisions, along with how and where the changes will take place (Harrill, 1999). EBM seeks to resolve the inadequacies of sectoral management by developing a method that views the ecosystem as a whole, where all drivers and their impacts are considered for their effect on ecosystem functioning (Curtin and Prezello, 2010). EBM has solid foundations in classical and contemporary ecological thought (Crowder and Norse, 2008 and Curtin and Prezello, 2010). It takes into account the behavior of complex adaptive systems (Gunderson and Holling, 2002 and Crowder and Norse, 2008), the maintenance of ecosystem resilience through heterogeneity (Holling, 1973 and Reynolds, 2002 and Levin and Lubichenco, 2008 and Mori, 2011), the study of thresholds (Jogiste, Moser, and Mandre, 2005 and Samhouri, Levin, and Ainsworth, 2010), and connectivity and flow of materials and information between system elements (Crowder and Norse, 2008 and Foley, et al., 2010).

EBM understands that each socioeconomic sector is made up of individual components that interact and produce their own emergent patterns of use. These sectors include recreational users, the marine trade and transport industry, and even offshore energy installations. Meanwhile there is connectivity and flow within and between sectors, occurring across multiple spatial scales. Fisheries will compete with the burgeoning offshore renewables sector, as both require vast expanses of ocean space. Offshore renewable energy installations require multiple devices spread across a seascape to achieve utility size economies of scale (Johnson, Kerr, and Side, 2013). Competition arises between sectors because development of offshore renewable energy installations limit access and navigation, and can have potential negative impacts upon commercially fished species (Alexander, Wilding, and Heymans, 2012) as well as closing large areas of ocean once open to fishing. To date this conflict has not been addressed. Models incorporating multiple uses and examining tradeoffs are being developed that incorporate multi criteria decision analysis (Villa, Tunesi, and Agardy, 2002), numerical optimization (Klein, Steinback, Watts, Scholz, and Possingham, 2010), fuzzy logic (Teh, Teh, and Meitner, 2012) and spatial decision

support systems (Alexander, Janssen, Arciniegas, O'Higgins, Eikelboom, and Wilding, 2012). However, these methods have yet to produce robust management recommendations. They are still focused on single sectors and fail to incorporate interactions among system components. Methods emulating complex adaptive systems can produce a robust management solution that has adapted to the most probable system states. Therefore, resiliency is built into the management recommendations. The solution is robust; because it has been shown to withstand future changes in system states. EBM requires the spatial planner to identify, describe and understand interaction among its component parts, as well as how these interactions form patterns of behavior across the marine landscape.

2.4 Embracing Complexity

Complexity science is the study of complex and complex adaptive systems (CAS). These systems are collections of individual autonomous objects competing for some type of limited resource (Johnson N. F., 2009), in the case of MSP, that limited resource is space. Causal connections among these autonomous components impairs top-down modeling (Gross and Strand, 2000), making complexity anti-reductionist. Martin and Sunley (2007) write, "a system is complex when it comprises non-linear interactions between its parts, such that an understanding of the system is not possible through a simple reduction to its component elements." Further, interaction provides a means for a complex system to restructure itself over time (Martin and Sunley, 2007), a property called emergence. A traditional reductionist approach to studying systems is to correlate these emergent system states with management directives. However, complexity allows us to produce emergent system states through individual interaction. It is a bottom up approach to understanding emergent pattern in systems. Complexity therefore studies the spatial ordering that arises from injections of energy (Thrift, 1999) that lead to novel interaction among its components. Natural forcing or human induced changes in system state provide Thrift's energy. An emergent property is the spatial ordering that results in response to energy input. Complexity provides a descriptive link between emergent geographical pattern, individual system

components whose interaction produced that pattern, and the change in system state that instigated novel interaction among its individuals. Understanding complex systems requires an understanding of determinism, particularly path dependence, from inputs of energy to emergent pattern.

Under determinism, Ruelle (1991) stated that if someone were to toss a coin, the laws to classical mechanics determine with certainty how it will fall. If the present state of a system is known exactly, and its physics have been properly defined, it is possible to predict with precision the future state of a system. This of course assumes perfect information. Further, complex systems are sensitive to initial conditions. In complex systems, small changes in the initial state of a system at time zero produce a later change that grows exponentially with time (Ruelle 1991). Therefore, uncertainty in the present state can lead to dramatic changes in the future state of a system. Ruelle describes this phenomenon with a thought experiment using billiard balls (Ruelle 1991). If two billiard balls were to start from the same position, but their trajectories altered ever so slightly by an angle of a, the billiard balls will only diverge by a degrees per second until they strike a convex obstacle and form a divergence angle a' which is twice the original angle a (Ruelle 1991). After the second collision, a' is now 4 times a and after 10 collisions a' is now 1024 times larger than a (Ruelle 1991). It does not take many interactions for the final state of the billiard balls to become completely different from a model with nearly identical starting conditions. Incrementally small changes will produce an output that is completely unpredictable from the simulation that came before it. A simulation of the marine trade and transport industry will behave in much the same way as Ruelle's billiard balls with added potential for complexity because each billiard ball is goal directed.

Because of sensitivity to initial conditions, complex systems are not forwardly predictable in the long term (Abbott, 2007), repeated simulations demonstrating a propensity towards an attractor, or singular emergent state, could allow it to anticipate the implications of spatial plans. The validation of a predictive model based on complex interactions pose significant verification challenges that are hard to

meet (Gross and Strand, 2000). Our aim for assessing the sustainability of a spatial management program requires prediction. Gross and Strand (2000) state that validating a predictive model requires comparing its predictions with past observations. However, a certain degree of accuracy and precision must accompany these predictions so that spatial planners can anticipate the most probable emergent states. Only under carefully controlled scenarios, designed to anticipate impact across a range of probable system states, can we have faith in the predictive capacities of models that invoke complexity. Assuming a validated model of a complex socio-economic system exists, applying CAS theory to quantify a metric of sustainability is straightforward.

2.5 Resiliency as a Measure of Sustainability

A system's resilience determines the persistence of relationships within a system and is a measure of its ability to absorb change and persist in its present state (Holling, 1973). Resilience bounds the amount of disturbance, or impact, that a system can withstand before it changes state. Researchers have found that the heterogeneity and diversity of habitats and species assemblages increases the resilience of an ecosystem (Levin and Lubichenco, 2008; Foley, et al., 2010). Likewise, the heterogeneity and diversity in socio-economic systems increase their resiliency. Without variability, there can be no adaptation, and without adaptive capacity, populations cannot respond to change (Levin and Lubichenco, 2008). Preserving the diversity of habitat (the physical space in which species interact) is as important as maintaining species diversity and is often a goal of EBM (Crowder and Norse, 2008; Levin and Lubichenco, 2008). Robustness is not only the system's resistance to change, but also the ability to return to a steady state (Levin and Lubichenco, 2008; Crowder and Norse, 2008; Gunderson and Holling, 2002). Achieving robustness typically requires the maintenance of sufficient variability so that adaptation can operate, and that the system can survive a catastrophic loss in redundancy after a species or habitat is removed (Levin and Lubichenco, 2008). A system is able to maintain resiliency until anthropogenic or natural forcing arrives at a threshold, leading to a change in system state, and ushering in adaptive

responses. An ecological threshold is the point at which an incrementally small change in an environmental variable can produce large and abrupt responses in the state of an ecosystem (Samhouri, Levin, and Ainsworth, 2010) including irreversible events (i.e. extinction). Understanding resiliency is a matter of understanding thresholds. How much change can a system withstand before it ushers in a new state? Methods that find these thresholds can inform spatial managers on the best course of action to take.

2.6 Leveraging Complex Adaptive Systems for Ecosystem Based Management

Few methods exist that model and provide understanding of complex adaptive systems, and to leverage their explanatory power to aid in natural resource decision-making is even more daunting. One promising area of research -- agent based modeling -- has made significant progress into this area, with many applications in geography and natural resources.

2.6.1 Agent Based Modeling

Agent based models have direct historical roots in complex systems (Macal and North, 2005). With agent-based models, the relations and descriptions of the global variables of traditional (top-down) models are replaced by an explicit representation of the microscopic features of the system (Gross and Strand, 2000). Specifically, the study of complex systems concerns itself with the question of how emergent behaviors arise in nature among autonomous agents (Macal and North, 2005). Agents are autonomous objects within an object oriented simulation framework. They are situated/living in a simulated environment and can interact with other agents and the environment through a set of protocols that limit their interaction (Macal and North, 2005). Agents are goal directed and heterogeneous with respect to their attributes and behavioral rules (Macal and North, 2005). An important outcome of agent-based models is the unexpected macroscopic behavior that is the result of individual interaction (Jorgensen and Fath, 2011). These macroscopic behaviors are the emergent patterns we seek to understand and predict. Agent based models are an appropriate tool that can help planners understand the

implications of spatial management measures, and they have already been used in many geographic applications.

2.6.2 Geographical Applications of Agent Based Modeling

Agent based modeling is not new for geographic applications and geographers routinely employ agent based models to describe pattern and process from micro- to macro-scales of behavior. The methodology has enjoyed a rich application history stretching from localized animal dispersal and migration studies to regional applications that study coupled human natural systems, land use change and urban dynamics. The local scale models tend to be sector based, whereas regional models tend to capture a more holistic view of dynamic system processes.

In the literature, local scale models tend to be calibrated for a single sector, whether it natural or socio economic in nature. Graniero and Robinson (2006) created an agent based squirrel dispersal model where landscape processes influenced individual interaction and movement decisions. Their work underscores the need for agents to respond to environmental forcing as well as individual interactions, as it provides behavior that is more realistic. Bennett and Tang (2006) developed a multi-agent model to simulate migratory behavior of elk on Yellowstone's northern range, where intelligent agents learned from their environment and experiences, which enabled them to mimic real-world behaviors and adapt to changing landscape metrics. Their approach was further refined in Tang and Bennett (2010) where agent's context-driven decision-making takes place within real dynamic spatial environments. Again, they applied their approach to an agent-based model of elk movement, where individual agents are contextual decision makers, capable of learning optimal movement patterns from experience and reacting to a heterogeneous landscape. Their approach required an agent to repeatedly sample its environment before choosing their next move and to make utility maximizing decisions. Local scale ABMs have also been applied to human systems.

Batty, Desyllas, and Duxbury (2003) proposed that small-scale interactions (individual agent reaction) accumulate over space and time to form emergent behavior of interest to safety planners, including congestion, crowding and panic among others. Their research has implications for an agent-based model of ship behavior where individual ship-agents interact during collision detection and avoidance procedures, which might lead to erratic behavior, slower speeds, and increased traffic density. Arentze, Pelizaro and Timmermans (2010) implemented an agent-based model where pedestrians not only learned spatially optimal routes for their daily routines, but they also adapted the timing of their activities for the most efficient travel. Torrens (2012) developed an approach for agent movement that relied less on particle physics and more on path dependence, where agents perceive and sort objects, plan routes, steer around obstructions, and interact with other agents, which all affects individual movement decisions. Torrens approach is similar to the approach applied herein, rather than physical dispersion physics or network flow models; movement is based on individual perception and utility maximizing decision rules. Torrens and McDaniel (2013) modeled riotous crowds. Their simulation architecture gave agents spatial perception, cognition, and the ability to act on their decisions on where, when and how to move across the study area. Contrary to local scale models, sectors should not be modeled in isolation for applications that encompass regional landscapes.

An, *et al.* (2005) developed, implemented and validated an agent based spatial model that simulates the impact of growing rural population on the forests and panda habitat adjacent to the Wolong Nature Reserve in China. Their model coupled human forcing with environmental responses, and it informed land use decision makers on how to regulate further development. On the regional scale, agent based models are used traditionally for land use change studies and research into urban dynamics and sprawl. Crooks (2010) expanded beyond the raster cell, and represented the urban environment as vector data to study residential segregation. This vector representation of space was one of the few approaches to expand beyond a square discrete grid and into continuous space. Although it can produce models that approach real world accuracy, their application remains a challenge due to computational requirements.

Chen, *et al.* (2012) relied upon economic theory that suggested the formation of urban structure results from interaction among individual actors, and they coupled an ABM with GIS and urban economic models to simulate residential dynamics. Their validated model had traditional economic theories driving agent behavior, an approach closely followed herein. Aside from coupling human-agent models with landscape response models, geographers have taken these coupled approaches and used them to inform resource management directives.

Bone, Dragicevic, and White (2011) integrated top down and bottom-up approaches for enhancing land use change modeling to support management directives. Their results suggest that bridging bottom-up (ABM) and top down models leads to negotiated land-use patterns in which the desires and objectives of all individuals are constrained by behaviors of others. This study provides the logical next step for marine spatial planning objectives, from plan creation to sustainability assessment, coupling bottom up with top down approaches can allow resource managers to meet in the middle without having to experiment with real life systems first. Sengupta and Bennett (2003) coupled an agent-based model for spatial decision support, where their model evaluated the ecological and economic impacts of agricultural policy for the Cache River watershed in Southern Illinois. Their effort assessed the sustainability of a resource management plan, which informed the next round of resource management evaluations. By coupling an ABM with traditional spatial decision support systems, Sengupta and Bennett (2003) validated the use of an ABM to assess the sustainability of a spatial resource management plan. Chen, *et al.* (2010) applied an agent based model directly towards a land use optimization problem for the Pearl River Delta in China. This is different from Sengupta and Bennett's (2003) because the ABM assesses current land use regimes to inform future implementations, while the former is a direct optimization routine. In a similar approach, the ABM developed by Bone and Dragićević (2010) learns through repetitive simulation on how to make decisions regarding natural resource extraction in an approach similar to evolutionary programming, where resource management regimes are tested against each other and better performing agents remain in future iterations.

Researchers have also constructed ABMs of the marine trade industry. Moon and Tudhope (2006) created a marine system simulator that utilizes ship agents for training purposes and investigates the potential of agent-based systems to maintain realistic behaviors. Their agents perform collision avoidance in much the same was as a human navigator would; if a dangerous situation is detected then rules are passed to determine what if any action an agent should take to avoid collision (Moon and Tudhope 2006). Their research demonstrated that an agent directed architecture can be used to build a simulator with reasonably realistic target ship motion, including track keeping and collision avoidance maneuvers. They also found that the interaction of relatively simple autonomous agents helps to produce reasonably realistic complex simulations. Moon and Tudhope's (2006) application shows that an ABM can develop realistic scenarios of marine trade, if an agent based architecture is good enough for a trainer simulation than it should be applicable to understand the ramifications of altering navigable space. Xiao, *et al.* (2012) developed an agent based model to assess collision risk in China's internal waterways. Their agents simulated movement with numerical models incorporating realistic vessel physics while collision avoidance procedures relied upon artificial force fields to guide an agent to its destination. With these applications in mind, and research on navigation and maneuvering of autonomous surface water vessels, an agent based model of the marine trade and transport sector can be developed, validated with AIS data and tested against OREI development scenarios.

2.7 Producing an ABM of the Marine Trade Sector

Geographical applications of agent-based models are not new; however, few applications assess the impacts of increased congestion and risk of vessel collision, and none have tried to understand how these impacts affect the resiliency of the marine trade and transport sector. Not only does the maneuverability of the simulated vessels have to approach reality, but the decision-making capabilities of the mariners with regard to the navigation problem, namely collision avoidance in congested space and route planning must also be realistic for the results of the ABM to have any merit when assessing the sustainability of an

OREI project. While no one application incorporates every facet of this project, many have touched upon these various themes.

2.7.1 Modeling the Maneuverability of Marine Vessels

Having knowledge of the maneuvering capabilities of ships allows practitioners to simulate their path as a function of their control settings (Sutulo, Moreira and Soares 2002). The ability to simulate vessel movement allows an intelligent agent to interact with or respond to spatial management scenarios, other agents, and congestion. The fastest mathematical ship models are purely kinematic and are effective at short-term path prediction, but they cannot account for any control change (Sutulo, Moreira and Soares 2002). Therefore, a numerical method that incorporates realistic vessel physics into movement models that allow for agent directed control change is required.

Researchers have placed significant attention to developing mathematical models for guidance and control of marine vessels. From control systems for forward speed, autopilots for course keeping, turning controllers, and track keeping systems (Fossen 1994), researchers have formalized the mathematics of ship control allowing for an intelligent software agent to realistically maneuver a virtual vessel in a simulated environment. Specifically, guidance is the action of determining the course, attitude and speed of the vehicle, relative to some reference frame (usually the earth) (Fossen 1994). Input from an agent's navigational decision-making and collision avoidance procedures are the direct control inputs for guidance algorithms. It is through these formulae that an agent maneuvers their vessel. Control is the development and application of appropriate forces and moments for operating point control, tracking and stabilization of a vehicle (Fossen 1994). These algorithms help an agent maintain course and speed. Modeling marine vehicles incorporates static models that are concerned with the equilibrium of bodies at rest or moving with constant velocity, and dynamic models that are concerned with bodies that accelerate (Fossen 1994).

The movement of marine vehicles occurs with 6 degrees of freedom (DOF), (Figure 2.2) because 6 independent coordinates are necessary to determine the position and orientation of a rigid body (Fossen 1994). The first set of three coordinates correspond to X, Y and Z positions while their time derivative (linear velocity) describes motion along the *x* (surge), *y* (sway) and *z* (heave) axes. The last three coordinates (K, M, N) and their time derivatives (p: role, q: pitch, and r: yaw) describe orientation and rotational motion (angular velocity) (Fossen 1994).

The study of ship maneuvering and control is broken up into two parts; kinematics and kinetics, whose series of equations operate over each axis of movement. Kinematics describes

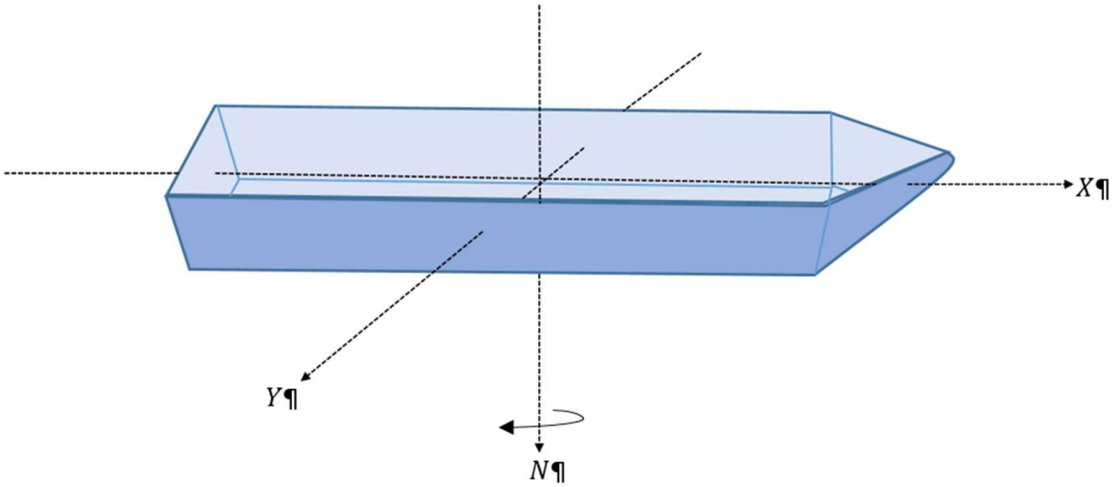

*Figure 2.2 a picture of a ship with movement forces of surge (**X**), sway (**Y**) and yaw (**N**).*

the geometrical aspects of motion (Fossen 1994). They describe the transfer of the ship from one location to another over the course of a time step. Kinetics analyze the forces causing this motion (Fossen 1994). For example, these forces could be in the form of a thrust (propeller RPM) or turning (rudder angle) control. Speed and ship steering equations for rigid body ship dynamics are based on the following assumptions; (1) that there is a homogenous mass distribution and the hull is symmetrical, and (2) that heave, roll, and pitch can be neglected (Fossen 1994). This gives us a series of equations describing a ship's maneuvering abilities:

$$m(\dot{u} - vr - x_G r^2) = X \tag{2.1}$$

$$m(\dot{v} + ur + x_G r^2) = Y \tag{2.2}$$

$$I_z \dot{r} + m x_G (\dot{v} + ur) = N \tag{2.3}$$

where X is motion in the x-direction (surge), Y is motion in the y-direction (sway), N is rotation about z-axis (yaw), u, v and r are linear and angular velocities for X, Y and N respectively, m is the object's mass, x_G is the center of the ship, and I_z is the moment of inertia about the Z axes. The perturbed equations of motion are based on an additional assumption that states sway velocity (v), the yaw rate (r) and the rudder angle (δ) are small (Fossen 1994). Further, the equation for surge can be decoupled from the sway and yaw equations if we assume that the mean forward speed u_0 is constant for constant thrust, and that the mean sway and yaw velocities are 0; $v_0 = r_0 = 0$ (Fossen 1994). After applying these assumptions, we find (Fossen 1994):

$$u = u_0 + \Delta u;\ v = \Delta v;\ \ r = \Delta r;\ \ X = X_0 + \Delta X; Y = \Delta Y; N = \Delta N \tag{2.4}$$

Each Δ represents small perturbations from nominal values. After assuming that higher order perturbations can be neglected, the nonlinear equations of motion can be expressed as (Fossen 1994):

Speed

$$m\dot{u} = X \tag{2.5}$$

Steering

$$m(\dot{v} + u_o r + x_G \dot{r}) = Y \tag{2.6}$$

$$I(_z \dot{r} + m x_G (\dot{v} + u_o r) = N \tag{2.7}$$

Thus, speed is controlled with the classic model of Newtonian motion where Surge force (X) is equal to mass (m) times acceleration ($\dot{u}$).

This implies that the surge mode can be decoupled from the sway and yaw modes by assuming that the mean forward speed $u_0$is constant for constant thrust (Fossen 1994). Equation 1 is commonly referred to as the speed equation or thrust, while equations 2 and 3 are commonly referred to as the steering equations. Aside from controlling their speed and maneuverability, our agents must also navigate their vessels in a manner that real world practitioners would.

2.7.2 Navigation

Navigation involves knowing the location of the vessel and controlling its movement towards a destination. It encompasses two important behaviors that act at different time scales. At the scale of a voyage, a ship captain will plan a general route that minimizes distance travelled while avoiding known obstacles (land, reefs, or infrastructure). At the scale of an individual time step, an agent must avoid other autonomous moving agents in such a manner that they comply with the COLREGs.

2.7.2.1 Collision Avoidance

Humans perform navigation to a satisfactory level, but their critical decisions are highly subjective, which can lead to error and increase collision potential (Statheros, Howells and Maier 2008). In 2002, 148 vessels suffered total losses with 1,274 lives lost, and 80 percent of these accidents occurred because of human error (Shi, Zhang and Peng 2007). An intelligent ship agent must avoid collision while maintaining a course towards their destination. Further, agent's behavior, especially collision avoidance procedures, must follow a strict set of behavioral rules set forth by the COLREGs. In 1977, the Convention on the International Regulations for Preventing Collision at Sea became effective thus applying a strict, codified protocol for collision avoidance for all flagged vessels upon the high seas and in all water connected by navigable seagoing vessels (USCG, Navigation Rules: International-Inland 2015). As such, collision avoidance is one of the major issues mariners face while at sea, and the model must take into consideration all of the human operations that are performed for collision avoidance

purposes. Researchers have developed a suite of applications for collision avoidance for autonomous vessels including potential fields, soft computing and methods incorporating fuzzy rules sets and expert systems. The most widely used, potential fields are also the method favored here.

Potential fields have traditionally been applied towards autonomous mobile robot navigation, however, they are well suited for agent based navigation. A potential field is a configuration of space that has a global minimum potential at the goal while all obstacles and walls are treated as high potential hills (Xue, et al. 2011). The robot is attracted to the goal position while simultaneously getting repelled from all obstacles (Xue, et al. 2011). Because of its mathematical elegance and simplicity, it allows for real time operation in a complex environment (Xue, et al. 2011). As humans approach an obstacle, they perceive the threat and assess a level of danger. The closer they are to the object; the more danger they feel. The perceived level of 'danger' is a function of distance, in much the same way potential is a function of distance. The closer an agent is to an obstacle, the more potential there is and the more extreme their evasive actions become. The simpler and more elegant the mathematical approach to the collision avoidance problem, the better suited it is for efficient computational modeling.

Since the method's inception, authors have iterated and improved upon potential fields with applications spanning autonomous robot navigation to ship maneuvering simulations. In 1991, Borenstein and Koren developed the vector field histogram (VFH) method, which permits detection of unknown objects and avoids collision while navigating through a two-dimensional Cartesian histogram grid world. In their application, mobile robots are navigating over raster space, where cell values represent collision potential. The robot navigates to the goal cell by choosing the path with lowest collision potential. Unfortunately, this method is inappropriate because an intelligent agent requires a fine scale for collision avoidance maneuvers, meaning each VFH cell would have to be very small. Determining collision potential and quantifying a least cost pathway at every time step would be computational inefficient and impractical to implement over a large area with many agents. Ge and Cui

(2002) proposed mobile robot planning in a dynamic environment where both the target and obstacles are moving. Their robot would chase the target while simultaneously avoiding moving obstacles. However, their methods have no mechanism to abide by the COLREGS. Lee, Kwon, and Joh (2004) expanded upon Ge and Cui (2002) so that a virtual ship can keep track or avoid collisions with a set of fuzzy rules designed to maintain COLREGs. In 2007, Shi, Zhang and Peng expanded upon the potential field approach with their harmonic potential field (HPF). Their approach, analogous to fluid dynamics, generates streamlines between initial and goal locations, where the gradient of the field constitutes the velocity field, which is then used to plan and control the ship's motion (Shi, Zhang and Peng 2007). In practice, the harmonic potential field causes ships to follow a path equidistant between boundaries while navigating a channel, an important consideration to take when exploring the application of gravity potential fields here.

While potential field methods enjoy wide adoption in the mobile autonomous robotics community, there are issues that will have to be addressed for our agents' behavior to approach that of mariners. Koren and Borenstein (1991) identified problems inherent to potential field methods. First, local minima may trap agents with negative potential in every direction. Local minima problems are resolved with simple heuristics or global recovery methods. In certain circumstances, Koren and Borenstein (1991) found no passage between closely spaced obstacles, which may lead to unnatural agent behavior when ships attempt to enter a navigational channel or constricted pathway. They also found oscillations in the presence of obstacles and narrow passageways (Koren and Borenstein 1991). However, (Xue, et al. 2011) found a simple solution for oscillations in narrow passageways by placing less vertices along the boundary of a corridor. Aside from potential fields, evolutionary computation has also been applied to collision avoidance.

Smierzchalski (1999) developed a method based on evolutionary computation to estimate safe and near optimal pathway. The application develops safe routing that avoids collision for ships at their

starting location. However, there may be real-time changes to system state that the evolutionary algorithm cannot account for because it is designing optimal collision free paths using starting conditions only. The procedure is also computationally expensive and would be prohibitive to repeat for all agents at all time steps. Expert rule based systems are another method used for collision avoidance.

Expert systems use rules to make deductions or choices. Nikitakos and Fikaris (2009) developed a collision avoidance method to select the best decision out of a set of existing decisions taking into account weather, loading, and ship type. Their approach uses Case Based Reasoning, which solves current problems or situations with the assistance of similar cases that were dealt with successfully in the past. The cases are stored in a library and retrieved by the system using indices. The retrieved cases are then ranked according to criteria and the system proposes the best solution to solve the current problem. The method unfortunately lacks mathematical rigor, and ranking of retrieved cases is arbitrary. The application mimics Bayesian decision making which makes use of prior data to reach a posterior conclusion on the best course of action to take, but does not use inductive reasoning, which may be more appropriate in the context given uncertainty in data. Expert rule based systems are one of the many decision methods that make use of prior information to choose the best course of action to take. Fuzzy logic is another one of these methods applied to the collision avoidance problem.

Fuzzy logic enables modelers to build a model that simulates approximate reasoning, where causal inferences drive decision making using linguistic variables (Bonissone 1980). Even though the models lack mathematical formalism, fuzzy control has been effectively used in the context of complex ill-defined processes, especially those that can be controlled by a skilled human operator without the knowledge of their underlying dynamics (Castro 1995). Castro notes that fuzzy logic controllers are universally capable of approximating any real continuous function on a compact set to arbitrary accuracy. Researchers have capitalized on the fact that fuzzy logic works well on ill-defined systems and that they can approximate any real function capable of directing behavior. Perera, Carvalho, and Soares (2009)

developed a fuzzy logic based decision making system to facilitate collision avoidance with respect to COLREGs rules and regulations. After collecting target vessel position and velocity and calculating relative and future positions, the data is "fuzzified" into membership functions that respect COLREGs (Perera, Carvalho and Soares 2009). These membership functions then inform the behavior of the agent. Kao, *et al.* (2007) proposed adding fuzzy collision avoidance capaiblity to vessel traffic systems that respect COLREGs. Fuzzy logic is fundamentally similar to Bayesian analysis, but it lacks the mathematical rigor and proof. Perera, Carvalho, and Soares' (2009) method is similar to the calculation of a Bayesian posterior, especially as it approximates real functions for decision analysis. Use of Bayesian estimation for robot or intelligent agent decision making is not new for vessel maneuverability applications.

Martins and Maturana (2013) used bayesian netwoks to evluate operational risks of a navigational system. They presented a methodology for human reliability analysis based on a bayesian belief network and applied this method to model the event of a tanker collision (Martins and Maturana 2013). Bayesian networks are graphic reasoning models based on uncertainty that can represent discrete and continuous variables with argches between nodes representing the direct connection between variables. They evaluated the operational risks of a system that considers all adverse effects that could occur (Martins and Maturana 2013). Not all of the potential events in their netowrk have the same probability of occurrence, and they state that for complex systems it is impractical to manipulate all of the hazard factors in operation. Instead a probabilistic study allows the analyst to classify events in terms of consequences and frequencies, with the selection of limits for these parameters guided by desired degree of operational safety. They used concept of probability as the analyst's (or in our case, the agent's) degree of belief allowing for expert judgements to be used as the information to fill conditional probability tables. While this method was not directly applicable to agent based decision making, the authors have developed an analogy that can "learn" from AIS data and develop a series of probabilistic rules that ship-agents will follow during collision avoidance procedures. From slowing down at certain traffic densities, to

identifying when it is safe for an agent to turn and by how much, a bayesian belief network can direct and agent's behavior in much the same way fuzzy logic does, but with a degree of mathematical formalism nor offered in the latter.

Due to their simplicity and mathematical elegance, collision avoidance procedures based on potential fields are the favored method. Methods that incorporate evolutionary computation would be inefficient to run for every agent at every time step in the simulation. Fuzzy logic and expert rule based systems lack the mathematical rigor of Bayesian networks. Bayesian methods can signal when an agent should take evasive action, however it is difficult to identify and quantify the collision avoidance procedures of real vessels from AIS data. For this reason, collision avoidance is performed with potential fields. Route planning is the last behavior our agents must reproduce for a simulation of industrial shipping.

2.7.2.2 Route Planning

Aside from maneuverability and collision avoidance, the agent-based model must also recreate the route planning procedures undertaken by real vessels. An agent's path towards the destination must encompass the shortest route while avoiding known obstacles. Route planning algorithms have been developed for continuous and discrete space. Hong and Murray (2013) state that the shortest route between two points in the presence of obstacles is comprised of one or more intermediate points along the convex hull of those obstacles. Measuring the Euclidean distance in the presence of obstacles has been referred to as the Euclidean shortest path (ESP), and most of the prominent approaches employ a visibility graph that connects all mutually visible vertices in a given area (Hong and Murray 2013). The visibility graph represents all line segments between every paired origin, destination, obstacle and boundary vertex that does not intersect another obstacle or boundary (Hong and Murray 2013). However, finding the shortest route within this visibility graph becomes inefficient when the size of the visibility graph increases (Hong and Murray 2013). Hong and Murray's (2013) implementation exploits spatial

knowledge by considering only relevant obstacles and the portions of the regional boundary that directly impede travel towards the destination. Other efficient algorithms have been developed for route selectin in discrete space

Smierzchalski (1999) developed an evolutionary method for estimating the safe and optimum path between an own ship's trajectory and the environment. They found that evolutionary algorithms can solve collision avoidance and find an optimum least cost pathway to the agent's destination. Lee, Kong, Kim, Kim, and Lee (2002) developed a network decision model that minimizes costs (sailing time, fuel consumption while considering weather conditions) and solved with a depth-first search algorithm (A*). In a similar method, Montes (2005) developed a ship router for the US Navy that used a binary heap version of Dijkstra's algorithm over a network graph of the Pacific Ocean with model generated wind and seas as input. Montes tested the model against recent weather data to verify performance and found that it avoided adverse weather and solved the least-time path to a destination. Prior to Montes application, naval officers formulated diversion routes and ocean voyages based on climatology, numerical weather forecasts, satellite products, and individual ship's sailing capabilities with manual techniques. A combination of Hong and Murray's (2013) convex path approach and Dijkstra's algorithm will provide efficient route finding for a population of agents.

2.7.3 The Rational Economic Actor; Utility Theory

A utility-based approach is most suitable for economic actors such as ship-agents. Utility theory is a treatment of normative approaches that evaluate an individual's preferences in a variety of decision situations (Fishburn 1970). For ship-agents, it simply states that individuals will seek to maximize their utility, in this case profits and safety. At any given time step, the agent chooses an optimal policy, which is the action from the set of all possible actions that an agent can do that leads to the highest expected utility (Salamon 2011). However, an ABM consisting of hundreds of agents over thousands of time steps cannot use exact optimization methods because of a lack of computational power and the realization that

ship captains are not performing continuous exact optimizations in real time. They may optimize their global route, but in real time, decision-making must be fast and computationally cheap. Therefore, a key challenge in designing a software agent that represents real decision-makers is determining the manner in which each agent solves problems (Manson 2006) while reaching their global objective. Agents do not have global information, nor have infinite computational power (Epstein 1999). They typically make use of simple rules based on local information (Epstein 1999). These simple rules are usually heuristics, which provide an adequate solution cheaply, where elaborate approaches would be expensive, time consuming and underutilized (Conlisk 1996). The optimizing, utility driven behavior of ship agents is bound with simple heuristics, which guide agent behavior and maintain the assumption of rational economic actors.

There are three major components regulating ship-agent behavior: physical, regulatory and economical. The first, physical, states that an agent can only travel so fast, that inertia affects the ability to decelerate, and that large vessels are not maneuverable. Agent movement is guided by numerical methods that incorporate vessel physics so that their simulated behavior approaches reality. Aside from the physical controls, agents are also rational actors in regards to regulations. The Convention on the International Regulations for Preventing Collisions at Sea (1972) produced a set of regulations, called the COLREGS, that bind all flagged vessels to a set of rules governing ship-ship interaction at sea (USCG, Navigation of Rules, International - Inland 2015). These set of rules affect all vessels operating on the high seas and all water connected to them that are navigable by sea going vessels (Benjamin and Curcio 2004). A ship captain cannot act in a manner that would put his vessel or cargo at risk of collision, and the COLREGS provide a manner in which to regulate. The last major component making up the ship-agent rule set ensures that individuals are rational, economic actors. The job of a ship captain is to get his vessel, crew and cargo to the destination as quickly and safely as possible. Time is money, and the longer the duration the less their profits. If rational, economic ship-agents are encoded with a strong desire to

minimize costs, then the choices they make concerning route selection would find individuals minimizing voyage duration.

2.8 Summary

The USCG recently ruled that creating routing measures where structures currently do not exist (i.e. displacing navigational channels), would more than likely result in an increase in risk due to vessel navigation in closer proximity to each other in than they would otherwise in an open ocean scenario (USCG, 2016). Thus, a potential conflict may arise between the marine offshore renewable energy industry and marine trade, and this application will seek to understand the interaction between the marine trade and transport industry and proposed wind farms along the continental shelf of the northeastern United States. Further, current MSP measures lack the ability to quantitatively understand displacement and/or anticipate the unintended consequences of foregone space, and this application seeks to develop a protocol that can be employed by MSP professionals when sighting their next project.

Impacts to the marine trade and transport industry will be assessed with an agent based model employed within an ecosystem based management framework. The ABM will simulate the marine trade and transport sector as it reacts to a proposed wind farm in New York Bight at the entrance to the third busiest marine terminal in the United States. The ABM will rely upon empirically derived and validated rigid hull ship movement models and collision avoidance procedures based upon gravitational potential. It is hypothesized that as long as the agents behave as rational actors, then their simulated behavior will approach reality. Therefore, the emergent behavior produced by the ABM will inform the marine spatial planner how and to what degree the proposed project will impact the industry.

Chapter 3

Methods

3.1 Introduction

This chapter presents the methodology for an agent based model of the commercial shipping industry. The agents in this simulation represent the individual ships of the marine trade and transport sector (henceforth known as the 'sector') as they interact with each other while competing for space within a constrained navigable waterway. Behavioral rules govern their interaction, which produce emergent properties of interest to resource management professionals. These properties can include everything from the location, heading and velocity of agents in time, to the location and number of

collision incidents, as well as calculated indices including time at sea and length of voyage. With an accurate simulation, spatial planners have the tools they need to anticipate impacts to navigation.

3.2 Overview

This agent-based model of commercial ship behavior is described with the Overview, Design Concepts, and Details (ODD) framework, meant to present ABMs in a hierarchical manner as an overview of model structure and processes followed by details on those processes (Heppenstall, *et al.*, 2012).

3.2.1 Objective

The ABM's objective is to simulate the sector and the socio-economic consequences of locating a WEA approximate to or within navigable space. WEAs are contiguous areas of the coastal ocean thought to hold high potential for the development of offshore wind farms. If WEAs are placed within navigable space, displacement will lead to a cascade of change within the system. As a consequence of the reduction in navigable space, the model estimates the increase in voyage length and duration over baseline conditions, as well as the frequency and severity of collision avoidance maneuvers. As more space is removed, the total distance travelled and voyage duration is likely to increase, individual vessel velocity will likely decrease, and the potential for collisions may increase; all of which will reduce profit margin. In other words, the model aims to quantify socio-economic impact. This model seeks to identify those thresholds (vessel density and the size and location of OREI) that disrupt the system and lead to novel emergent pattern.

A secondary objective is to implement the ABM in *Python 2.7,* an open source, object oriented programming language (Python 2016). Python is an ideal language for spatial planners familiar with industry standard GIS software (e.g. ESRI), which allow and encourage the open

source community to development new capabilities and implement them within a GIS environment.

3.2.2 Entities, State Variables and Scale:

The system entities (agents) represent individual ships that belong to more than one operational class. Modeled together, the agents represent the marine trade and transport sector (sector). The sector is comprised of multiple classes with different roles and capabilities. However, the current version of this ABM only simulates tankers and cargo vessels. Each agent is a separate Python class object, which allows for individualized method calls and the ability to store arbitrary data about the agent (Python 2016). During initialization, the simulation software creates a Python class object for every desired agent, and assigns them to one of two ship types (tanker or cargo vessel). Functions that identify navigational routes and control agent behavior are 'methods' bound to each class object. As the simulation progresses, the ABM iterates over each individual, calling methods that apply to the current agent only, thus ensuring their autonomy. Python class objects are also useful holders that describe agent parameters.

Python class objects are containers for arbitrary data (Python 2016). These containers are useful for storing variables including length (λ) (units: m, type: floating point), width (β) (units: m, type: floating point), draft (δ) (units: m, type: floating point), velocity (u) (units: m/s, type: floating point), and vessel type (type: string, 'cargo', 'tanker'). At initialization, the model draws these characteristics from statistical distributions of real vessel data. This application relied upon automatic information system (AIS) data for the calendar year 2014 provided by BOEM (2014). As the simulation progresses, the agents will use knowledge about themselves, their environment, and other agents as they move towards their destination and interact with each other.

The ship-agents are autonomous software objects interacting with each other over a simulated seascape. At every time step they must sample their environment and make decisions that maximize their well-being, all while interacting with other agents. Interactions only occur between two agents at a time,

the own-agent (Γ_o) and target-agent (Γ_t). One must view the own-agent (Γ_o) from a first-person perspective as it iterates over all target-agents within proximity ($\Gamma_1 \ldots \Gamma_n$). When interacting with the current (n^{th}) target-agent (Γ_n), the own-agent (Γ_o) knows the target's heading, velocity, and vessel parameters that are typically made available through AIS data, but it does not know the target's destination. With this information, the own-agent (Γ_o) can anticipate where the target (Γ_n) will most likely move during the current time step and can plan their own movement to minimize risk of collision. The population of agents are not only affected by each other, but state variables as well.

In real systems, there are a host of state variables that effect the navigability of a region, such as wind, waves and tide, but these are assumed to be negligible and have no effect on navigability. The main state variables that drive emergent behavior are the location of obstructions, other ship-agents, and the spatial plans that serve to displace the sector. At initiation, the agents are aware of the location of all navigational obstructions (including the proposed OREI), with their boundaries described by convex hulls (Figure 3.1).

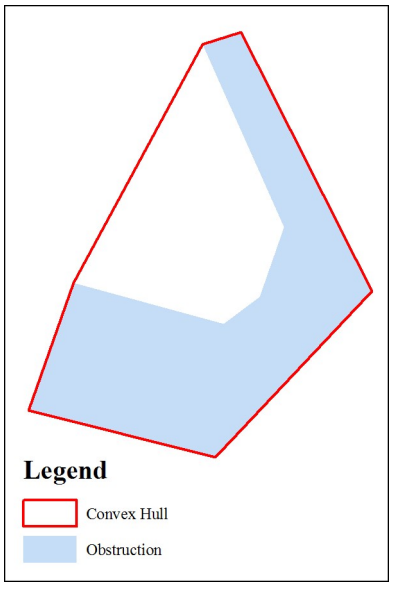

Figure 3.1 shows a crescent shaped navigation obstruction and its convex hull. The convex hulls of all obstructions are known to the agent at the start of the simulation.

The amount of space required to stop large sea-going vessels are a direct consequence of their size and the momentum. Therefore, ship-agents must plan out their interactions and route changes kilometers in advance, which consequently dictates a large study area. We chose the charted navigational approach to the port of New York and New Jersey, the third largest container port in North America (PANYNJ 2016), as our study area because the BOEM has located a WEA within the region (**Error! Reference source not found.**). All coordinates are within UTM Zone 18N. We also gave consideration to temporal scale. The model operates within continuous space at discrete one second time intervals, which are appropriate because large commercial vessels cannot move more than their length in one time-step.

3.2.3 Process overview and scheduling:

As the model initializes, it creates the number of agents (n) desired by the spatial planner. For each new agent, internal methods within the class object choose vessel characteristics from statistical distributions, and then finds the shortest route to its destination. Then, every agent executes the following actions once per time step until the simulation terminates. In an iterative fashion, an agent first assesses attraction towards its next waypoint, and then it quantifies the repulsive force generated by the other agents and obstacles around it. The agent uses attractive forces to orient itself towards its next way point and repulsive forces to keep it from danger. Aside from reacting to these navigational forces, the agent also regulates speed by controlling the engine's throttle. Finally, at the end of every time step, the agent resolves movement through a first order Nomoto model. When the model starts, agents are scattered throughout the study region, each with their own origin and destination. If agents are added during a simulation, then they can only enter from the sides.

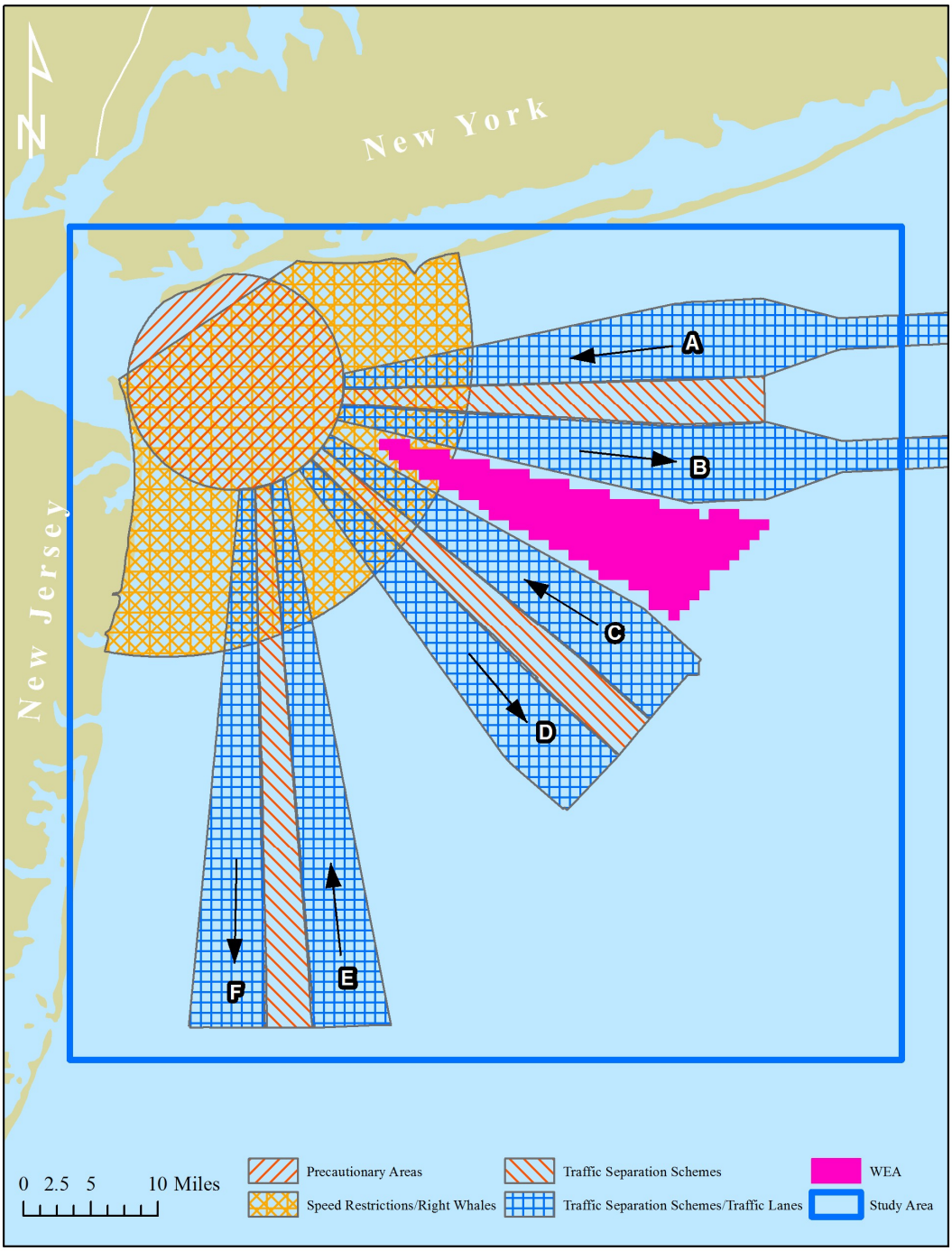

Figure 3.2 A depiction of the Entrance to the Port of New York and New Jersey, the Study Area for the Agent Based Model. The USCG has defined a traffic separation scheme designed to minimize congestion and the risk of collision into and out of the 3rd largest container port in the United States. The arrows indicate the direction of travel within each lane. Note the location of the WEA placed between two approaches. The labeled channels are as follows; A: Nantucket to Ambrose, B: Ambrose to Nantucket, C: Hudson Canyon to Ambrose, D: Ambrose to Hudson Canyon, E: Barnegat to Ambrose and F: Ambrose to Barnegat.

3.3 Design Concepts

The ABM aims to quantify key emergent properties, including aggregate measures of voyage duration and spatial behavior patterns in response to the planned construction of offshore renewable energy infrastructure. The model also exhibits adaptive behavior indicative of CAS: ship-agents react to their environment during initial routing, plan around obstructions and react to individual agents in real time. Initial routing consists of finding the shortest route to their destination that avoids known obstructions. During a voyage, a ship agent's only objective is to arrive at their destination while avoiding collisions.

3.3.1 Emergence

As traffic density within a constricted navigational corridor increases, traffic can form into ordered, laminar rows with reduced velocity indicative of traffic jams and form kinematic waves of low velocity that propagate through the population of agents. As vessel's come closer together they might have to implement emergency stopping procedures. It is the intent of the model to create abrupt changes in system state (i.e. traffic jams) as a response to spatial regulation. The system constraints under consideration are management decisions that remove navigable space and the number of agents within the system at any one time. Although complex systems tend not to be forwardly predictable (Abbott, 2007), repeated simulations demonstrating a propensity towards a singular emergent state (attractor) allows spatial planners to develop confidence when gauging impact. If there is an attractor, it can provide a means of assessing the sustainability of mutually exclusive economic activities, namely the offshore wind industry and the marine trade and transport sector. Aside from modeling emergence, this ABM also incorporates adaptation.

3.3.2 Adaptation

Agents alter their behavior due to external pressures from their environment and from interactions with other vessels because they are rational actors that must minimize risk of collision. Their initial route

is the shortest that avoids known obstructions. During a voyage agents steer from dangerous interactions and regulate their speed. When they are not interacting with other agents or in regulated navigational channels, the agents accelerate to their maximum cruising speed. The cruising speed is designed to maximize voyage profit, and is usually set at the onset of a voyage by the shipping company. Aside from adapting to present conditions, agents also have some predictive capabilities.

3.3.3 Prediction

In real systems, vessels are equipped with redundant and state- of- the- art safety systems including multiple radar and AIS technologies. Therefore, it is assumed that an agent knows where the locations of all obstacles exist, as well as the location, heading, velocity and characteristics of all vessels within proximity. The agent uses this information to minimize the risk of collision while navigating toward the next waypoint.

Collision avoidance requires the own agent (Γ_o) to anticipate the future location of itself and other vessels ($\Gamma_1 \ldots \Gamma_n$), which requires predictive capacity. Collision avoidance procedures use movement parameters (heading, forward and rotational velocity) of the own- (Γ_o) and target-agent (Γ_n) to anticipate where they and the target vessel are headed. The agent's predictive capabilities rely upon numerical methods of classical mechanics with two principle forces, drag and thrust, acting upon the hull of each vessel.

3.3.5 Stochasticity

The agents' classes and their starting locations, destinations, headings, and speeds are chosen randomly. The starting locations, although random, are constrained to be near the edge of the study area, as are the destinations. The software draws an agent's class from a multinomial probability distribution. The classes then define fundamental vessel shape and maneuvering characteristics such as length (λ), beam (β), draft (δ), and weight (μ) because it is assumed that different vessel types will have different shape characteristics.

3.3.6 Observation

The ABM creates a wealth of data as the simulation progresses, all of which are suitable for diagnostic purposes. From the locations and movement parameters of every agent in time, to their full decision making history, every interaction and resulting pattern can be accounted for and analyzed. During a simulation, the ABM logs data into an SQLite database, and after the simulation completes, diagnostics scripts analyze the event log and quantify emergent pattern. Because the location and internal state of each agent is tracked in time, it is possible to identify thresholds that drive a system towards a particular state.

3.3.7 Validation

There are two types of validation we aim to achieve in this application (system and micro simulation) with the hope that the ABM can reconstruct meaningful emergent states of use to spatial planners. For system validation purposes, the application will use AIS data for the study region provided in ESRI geodatabase format (BOEM 2014). This information contains the timestamped positions of actual vessels and their related characteristics (class, length, width, draft, and tonnage). The ABM was constructed to be realistic: the code was debugged by comparing simulated vessel tracks with actual tracks. Nonetheless, it is also stochastic, which precludes exact replication of the AIS data when running scenarios. So, with AIS data, we are not validating the positions of simulated vessels against actual scenarios, rather the emergent states within real system data. For example, do kinematic waves propagate through actual vessel traffic in the same manner it propagates through simulated traffic? The model provides researchers the means to create scenarios and to test them Monte-Carlo style to understand the threshold levels that drive emergent patterns (vessel density and plan configuration and size) rather than how well the simulation can reproduce traffic patterns on a specific day and time.

3.4 Details

The details section contains subsections on the ABM initialization routines, and on numerical models that guide navigation, route finding, collision avoidance, orienteering, throttle control, and then forward and angular movement.

3.4.1 Model Initialization

The end user defines a population of agents $\Gamma_1 \ldots \Gamma_n$, of length n, and the values for basic ship parameters (tonnage (μ), length (λ), beam (β) and draft (δ)), the vessel class (cargo or tanker), and their origin ($\boldsymbol{A}$) and destination ($\boldsymbol{B}$). Positions must be given in rectangular coordinates (i.e., not longitude and latitude). For this project, the origin and destination are *XY* coordinate pairs $\{\boldsymbol{A} = (x_A, y_A), \boldsymbol{B} = (x_B, y_B)\}$. Given $\boldsymbol{A}$,$\boldsymbol{B}$ and set of obstacles O, the software creates each agent's route and stores the waypoints within each ship-agent object as a list of XY coordinate pairs. The last initialization step rotates the agent so that it is oriented towards its first waypoint.

3.4.2 Submodules

Numerical submodules control agent behavior and are designed in such a manner that after calibration and validation, they mimic the behavior of individual actors in the system we are trying to emulate. The first set of submodules controls an agent's ability to navigate through the study area.

3.4.2.1 Navigation

Navigation involves knowing the location of the vessel and controlling its movement towards the destination. Reproducing the ability to navigate requires submodules for route planning, orienteering, collision avoidance and throttle control. Route planning only occurs once, while orienteering, collision avoidance and throttle control occur at every time step.

3.4.2.1.1 Route Finding

We developed a modified Hong and Murray's (2013) Euclidean shortest path (ESP) route finding algorithm. The ESP identifies the shortest pathway between two locations that avoid all obstacles to travel (Hong and Murray 2013). If the ESP finds no obstacles between the origin and destination, then the Euclidean distance is the shortest length path (Hong and Murray 2013). However, if there are obstacles, then the shortest path that avoids them requires a route comprised of one or more intermediate waypoints (Hong and Murray 2013). Their ESP algorithm finds those points.

Identifying the intermediate points that minimize path length is not trivial because we must locate an indeterminate number of points in continuous space while satisfying several conditions (Hong and Murray 2013). Hong and Murray (2013) also state that constraining conditions are challenging to impose because all intermediate points have to be located such that connected line segments avoid all obstacles.

The shortest path algorithm finds the number and location of an indeterminate number of waypoints (W) of length z. and their location through which the path is routed (Hong and Murray 2013). Each element (w) of W is stored as an *XY* coordinate pair (x_w, y_w).

Formally, the algorithm minimizes (Hong and Murray 2013):

$$Minimize \sum_{j=1}^{z+1} \sqrt{\left(\tilde{x}_{j-1} - \tilde{x}_j\right)^2 + \left(\tilde{y}_{j-1} - \tilde{y}_j\right)^2} \quad \textbf{3.1}$$

where $(\tilde{x}_0, \tilde{y}_0) = (x_A, y_A)$ and $(\tilde{x}_{z+1}, \tilde{y}_{z+1}) = (x_B, y_B)$ (Hong and Murray 2013). The straight line between two consecutive points w and $w + 1$ within W must not cross any obstacle (Hong and Murray 2013).

Hong and Murray (2013) use polygons to describe obstacles within the study area. Each obstacle Ω_i belongs to the set of all obstacles $O = \{\Omega_1 \dots \Omega_k\}$. Each obstacle is constructed of a set of vertices stored as a list of *XY* coordinate pair: $\Omega_k = \left\{(\hat{x}_{k1}, \hat{y}_{k1}), \dots, \left(\hat{x}_{kn_k}, \hat{y}_{kn_k}\right)\right\}$, where n_k is the number of vertices in the k_{th} obstacle.

With an agent's (Γ_n) origin $\boldsymbol{A}$ and destination $\boldsymbol{B}$ known, and the locations of all obstacle vertices also known (O), we can define Φ as the set of all obstacle vertices and points $\boldsymbol{A}$ and $\boldsymbol{B}$: $\Phi = O \cup (x_A, y_A) \cup (x_B, y_B)$. Hong and Murray (2013) show that this set (Φ) is important for two reasons. First, it reduces the number of points within the problem from potentially infinite to a more manageable amount. Second, they proved that the shortest path will consist of points in Φ, therefore, the search for intermediate points that make up the shortest path is limited to Φ (Hong and Murray 2013). The difficult task is to filter out those line segments between members of Φ that do not intersect the interior of Ω_k for any obstacle k (Hong and Murray 2013). That is, $i, j \in \Phi \mid \overline{ij} \cap int(\Omega_k) \neq \emptyset$ for any k, where $int(\Omega_k)$ is the interior of the k^{th} obstacle Ω_k $\overline{ij}$ is the line segment connecting vertex i to j, and $\emptyset$ means the empty set (Hong and Murray 2013).

For problems where travel is inhibited by a regional boundary, H is the set of all vertices of length g representing the boundary of the study region: $H = \{(\bar{x}_1, \bar{y}_1), \ldots, (\bar{x}_g, \bar{y}_g)\}$. When travel is restricted by a regional boundary, Φ is expanded to also include H: $\Phi = H \cup O \cup (x_A, y_A) \cup (x_B, y_B)$ (Hong and Murray 2013).

To derive the shortest path, Hong and Murray (2013) create a graph G of the vertices in Φ, by linking each vertex to members of the set N. The set N is contained within Φ ($\Phi \subset N$) and consists of vertices that can be connected without intersecting the interior of obstacles or outside of the regional boundary (Hong and Murray 2013). Thus G represents all of the feasible path segments to travel from A to B. However, G can be very large, therefore Hong and Murray (2013) were interested in finding an efficient graph G^* within G where $G^* \in G$. Hong and Murray (2013) state that the formulation of the ESP can be structured based on the graph G (or G^*)for the origin and destination locations $\boldsymbol{A}$ and $\boldsymbol{B}$.

Hong and Murray (2013) proved two theorems that allow us to implement an algorithm that derives G^* and solves the shortest path problem for a population of agents in real time. The first of these theorems stated that the 'optimal ESP between two points separated by single continuous obstacle will be

on the convex hull boundary.' With this proof, an algorithm (*Convexpath*) is possible for selectively identifying the vertices and arcs in G^*that contains the ESP (Hong and Murray 2013). Hong and Murray also prove that G^* contains the optimal ESP between two points with multiple obstacles inhibiting travel. With Hong and Murray's work, identifying the shortest route for our agents is simple. We only need to supply the algorithm with the convex hulls of all known obstacles and the agent's origin and destination.

Rather than implement Hong and Murray's (2013) *convexpath*, we developed an algorithm (*route)* that relies upon an iterative testing procedure to gradually build G^* from the origin ($\boldsymbol{A}$) by always working towards the destination ($\boldsymbol{B}$). Hong and Murray (2013) constrained the shortest path network problem to ensure G^* flows from the origin ($\boldsymbol{A}$) towards the destination ($\boldsymbol{B}$). Therefore, $G^*$is a directed graph consisting of nodes for the origin ($\boldsymbol{A}$), destination ($\boldsymbol{B}$), and all intermediate waypoint nodes (W), with edges connecting them in such a manner that they conserve the direction of flow towards the destination. The origin ($\boldsymbol{A}$) and destination ($\boldsymbol{B}$) are supplied to the algorithm as *XY* coordinate pairs, $(x_A, y_A), (x_B, y_B)$. Each element ($\boldsymbol{w}$) of W is stored as an *XY* coordinate pair (x_w, y_w). To identify the intermediate vertices ($\boldsymbol{w}$), *route* also needs to know the location of all obstacles within the study area.

The obstacles that ship-agents will need to avoid include wind farms, shipping lanes that guide opposing traffic, and the shoreline. A GIS preprocesses the convex hull of each obstacle within the study area and buffers them by one kilometer, 200 more than that required in the UK (MCA 2008). The set of all obstacles (O) within the study area is of length k ($O \in \Omega_k$). The k^{th} polygon (Ω_k) consists of a set of vertices ($\{(\hat{x}_1, \hat{y}_1), \dots, (\hat{x}_{n_k}, \hat{y}_{n_k})\}$) of length n_k. The agent stores each obstacle Ω_i as a *Shapely* polygon object (Gillies 2013). With the origin ($\boldsymbol{A}$), destination ($\boldsymbol{B}$), and set of obstacle vertices (Φ) known, we can derive G^*, a directed graph with edge weights measured as the Euclidean distance between connected nodes.

During initialization, an agent's *route* method finds the shortest path to the destination. The method starts by creating an empty *NetworkX* graph object G^* (Hagberg, Schult and Swart 2008) and adds the origin ($\boldsymbol{A}$) and destination ($\boldsymbol{B}$) as nodes. The iterative graph building procedure begins with the

creation of a *Shapely* line segment (Gillies 2013) connecting the origin and destination $\overline{\boldsymbol{AB}}$. The algorithm then iterates over each obstacle polygon ($O \in \Omega_k$), and uses *Shapely* functions (Gillies 2013) to determine if $\overline{\boldsymbol{AB}}$ `intersects` or is `within` the k^{th} obstacle Ω_k. If $\overline{\boldsymbol{AB}}$ does not cross any polygon, an edge connecting the nodes $\boldsymbol{A}$ and $\boldsymbol{B}$ and edge (AB)is added to G^* and the *route* algorithm terminates as the shortest route to the destination is found. However, if either function returns true, then the n_k vertices of k^{th} intersecting polygon $\Omega_k = \{(\hat{x}_1, \hat{y}_1), \dots, (\hat{x}_{n_k}, \hat{y}_{n_k})\}$ are added to a list of test vertices Υ (Figure 3.3). The algorithm then iterates over each vertex $\boldsymbol{i}$ in the test list Υ, and creates a *Shapely* line segment between $\boldsymbol{A}$ and the current vertex $\boldsymbol{i}$, $\overline{\boldsymbol{A\iota}}$,. Then, route iterates over all polygons in O. If the line segment $\overline{\boldsymbol{A\iota}}$, `crosses` or is `within` the k^{th} obstacle polygon (Ω_k), route removes $\boldsymbol{i}$ from Υ. If the segment is without spatial conflict, *route* adds $\boldsymbol{i}$ and Ai to G^*as a node and edge, adds $\boldsymbol{i}$ to a list of new nodes χ, and removes $\boldsymbol{i}$ from Υ (Figure 3.4). After the algorithm iterates over all vertices $\boldsymbol{i}$ in Υ, it then iterates over all of the new nodes $\boldsymbol{j}$ in χ. The algorithm creates a *Shapely* line segment between each $\boldsymbol{j}$ and the destination $\boldsymbol{B}$, $\overline{\boldsymbol{JB}}$. Then, $route$ tests for spatial conflict with every obstacle polygon in O with the *Shapely* functions `crosses` and `within`. If $\overline{\boldsymbol{JB}}$ does not conflict with any polygon, *route* adds $\overline{\boldsymbol{JB}}$ to G^* as an edge and removes $\boldsymbol{j}$ from χ. We do not add the node $\boldsymbol{B}$ to G^*, because it was added when the graph was created. If there is conflict with $\overline{\boldsymbol{JB}}$, then the n_k vertices of k^{th} intersecting polygon $\Omega_k = \{(\hat{x}_1, \hat{y}_1), \dots, (\hat{x}_{n_k}, \hat{y}_{n_k})\}$ are added to the list of test vertices Υ and ξ is removed from χ. The algorithm repeats this iterative test procedure until there are no more vertices in χ to test and add to G^*, or when it discovers all edges that connect to the destination node B (Figure 3.5). When $G^*$is complete, `networkx.dijkstra_path` implements Dijkstra's algorithm (Dijkstra 1959) to find the shortest path to the destination. The function call incorporates edge weights, which represent the Euclidean distance between nodes (Figure 3.6).

What differentiates this implementation of the ESP from Hong and Murray's, is that this algorithm requires an extra preprocessing step. By creating convex hulls of all navigational obstructions,

the algorithm does not use computational resources to determine if a potential edge is on the convex hull or not. We are already insured it does. In addition, by forcing the algorithm to always attempt a segment towards the destination, it only encounters polygons that happen to lie in its path. Therefore, the resulting edges in the directed graph are always headed towards the destination (B), and the size of G^* is greatly reduced making the implementation of Dijkstra's even more efficient. *Route* was implemented in Python 2.7.5 as a method of an agent (Python class object), and is called during initialization (see pseudo code). The algorithm is supported by *Shapely* 1.5.1 (Gillies 2013) for all applied geometrical operations and spatial data management, while *Networkx* 1.10-2 (Hagberg, Schult and Swart 2008) provided graph theoretical operations.

```
Route:
       create G*,
       add nodes A,B to G*
       create line segment AB
       for Ω_k in O:
           if AB crosses or is within Ω_k:
              add Ω_k to cross list
       if cross list is empty:
           add the edge AB to G*
       else:
           for Ω_k in cross list:
              for i in Ω_k:
                     create Ai
                     feasible = 1
                     for Ω_{k+1} in O:
                          if Ai crosses or is contained by Ω_{k+1}:
                              feasible = 0
                     if feasible is equal to 1:
                            add i to K
                            add i and Ai to G*
              while K is not empty:
                     for i in K
                            create iB
                            for Ω_k in O:
                                if iB crosses or is contained by Ω_k:
                                     add Ω_k to cross list
                                else:
                                     add iB to G*
                            for Ω_k in cross list:
                                  for j in Ω_k:
                                       create ij
                                       feasible = 1
                                       for Ω_{k+1} in O:
```

```
                                        if ij crosses or is contained by Ω_{k+1}:
                                            feasible = 0
                                    if feasible is equal to 1:
                                        if j not in M:
                                            add j to test list
                                            add j and ij to G*
                        remove i from K
                        add i to list of M
        Apply Dijkstra's on G* with distance weights, return list of waypoints
end;
```

After all agents identify their initial route, the simulation begins. During each time step, the agents rely upon the remaining navigation submodules (collision avoidance, orienteering and throttle control). At the beginning of each time step, the agent samples their environment and implement collision avoidance procedures.

3.4.2.1.2 Collision Avoidance

Under normal operating conditions, the own agent (Γ_o) sets its heading $\{\psi \in \mathbb{R} | 0 \leq \psi < 360\}$ and propeller speed in revolutions per second (RPS) ($\{r \in \mathbb{Z} | -5 \leq r \leq 60$) to their optimal settings (see: section 3.4.2.4 Orienteering). However, in the presence of obstacles (O) and other target-agents within range ($\Gamma_1 \ldots \Gamma_n$), the own-agent (Γ_o) must take evasive action. Agents minimize risk of collision with potential fields, which calculate the repulsive force generated by other agents and obstacles, and that serve to push the own-agent (Γ_o) away from danger. The method, *F_rep_agn* quantifies the repulsive force generated by the n^{th} target-agent Γ_n, while the method *F_rep_obs* quantifies the repulsive force generated by the k^{th} obstacle Ω_k.

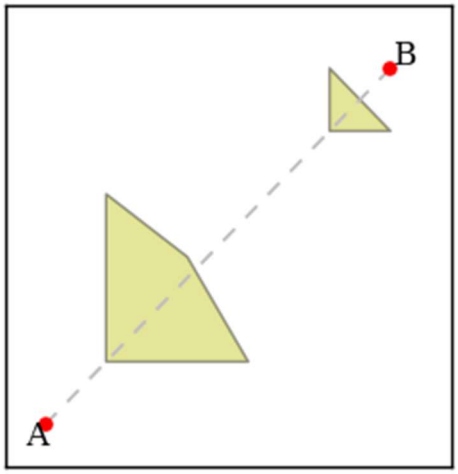

Figure 3.3 A depiction of the first step of ESP that creates a line segment $\overline{\boldsymbol{AB}}$ between the origin (A) and destination (B). Note, the line segment $\overline{\boldsymbol{AB}}$ will intersect both obstacle polygons

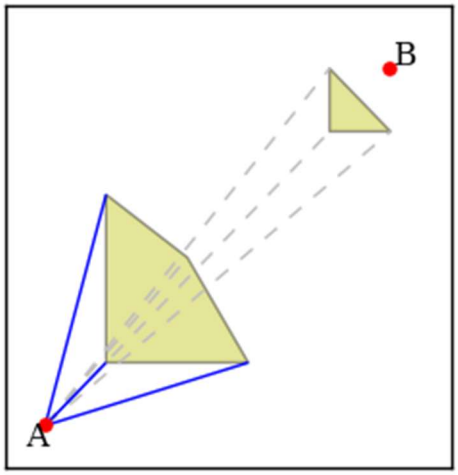

Figure 3.4 a depiction of the second step of the ESP algorithm. If the line segment $\overline{\boldsymbol{AB}}$ intersects any polygon, line segments are drawn from A to each intersecting polygon vertex $\boldsymbol{v}$. Only those segments that do not cross or are not contained by a polygon are kept.

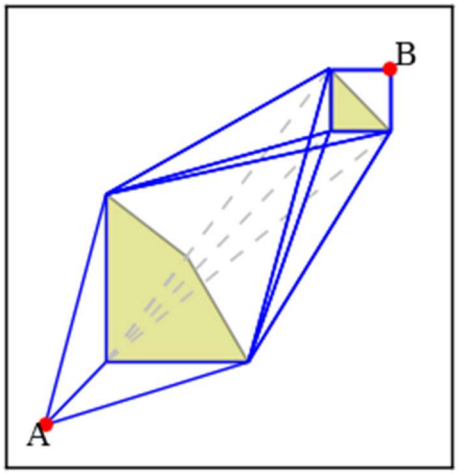

Figure 3.5 a depiction of the ESP edge testing procedure. The algorithm repeats in this manner until there are no more line segments to add, or all edges connecting with the destination B have been found.

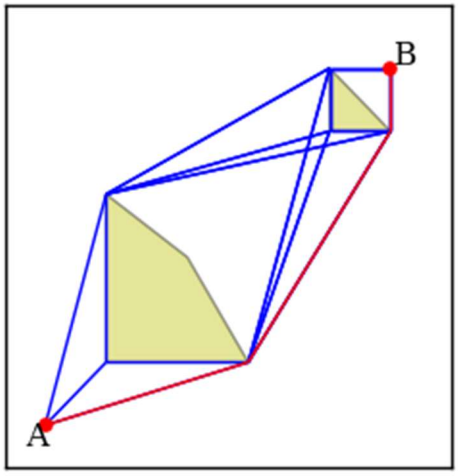

Figure 3.6 depicts the solution to the ESP. Following the creation of $\boldsymbol{G}^*$, Dijkstra's algorithm finds the shortest path between A and B.

The method *F_rep_agn* is comprised of a series of Boolean logical operations designed to guide the own-agent (Γ_o) on how to react to the n^{th} target-agent (Γ_n). At the start of each time-step, the own-agent (Γ_o) iterates over all target agents within proximity $\Gamma_{t_1} \ldots \Gamma_n$. The own-agent ($\Gamma_o$) is at position $\boldsymbol{p_0} = (x_{\Gamma_o}, y_{\Gamma_o})$ in UTM Zone 18N and the n^{th} target (Γ_n) is at $\boldsymbol{q_0} = \left(x_{\Gamma_n}, y_{\Gamma_n}\right)$ also in UTM Zone 18N. The vector from $\boldsymbol{p_0}$ to $\boldsymbol{q_0}$, $\boldsymbol{v} = \boldsymbol{q_0} - \boldsymbol{p_0}$, is the position of the target (Γ_n) relative to the own-agent (Γ_o). The associated unit vector of $\boldsymbol{v}$ is $\hat{\boldsymbol{v}} = \boldsymbol{v}/|\boldsymbol{v}|$. Collision avoidance procedures also require the position of the own-agent (Γ_o) relative to the target agent (Γ_n), where $\boldsymbol{v'} = \boldsymbol{p_0} - \boldsymbol{q_0}$, and the associated unit vector is $\hat{\boldsymbol{v}}' = \boldsymbol{v}'/|\boldsymbol{v}'|$. The distance between agents is the norm of the vector $|\boldsymbol{v}|$. If $|\boldsymbol{v}| < 5{,}000$ m, then the own-agent computes $swath$. *Swath* determines if the n^{th} target-agent Γ_n has the potential to interact with the own-agent Γ_o with:

$$swath = \psi_o - 135 < \angle\hat{v} < \psi_o + 135 \qquad \textbf{3.2}$$

where ψ_o is the own-agent's heading measured in degrees, and $\angle\hat{v}$ is the angle of the target-agent relative to the own measured in degrees. In other words, the own agent only considers interactions that are within a 270° swath around it, split equally between 135° port and 135° starboard (Figure 3. 3.7). If the target-agent is not within this swath, no repulsive force is applied (Figure 3.8).

When the n^{th} target-agent (Γ_n) is within the 270° swath, the own-agent (Γ_o) creates trajectory polygons for itself Ψ_o and the target vessel Ψ_n. Trajectory polygons represent a rough approximation of the area an agent could traverse while under inertial stop. Inertial stop is when a vessel uses only drag to slow itself down. This scenario should be considered the worst case and represents the maximum stopping area of the vessel.

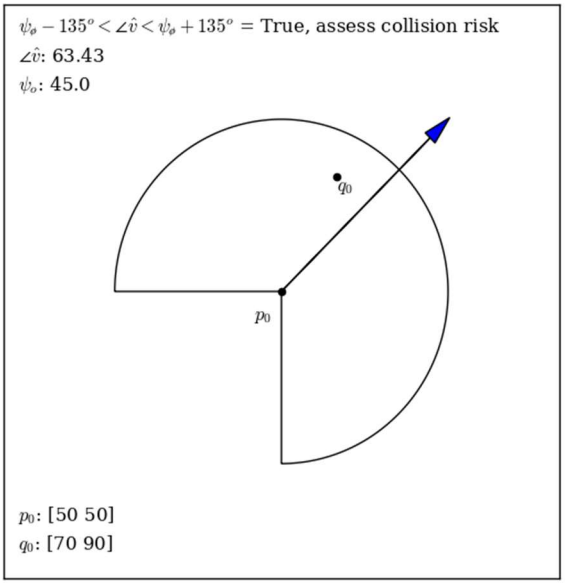

Figure 3.7 depicts a the $\boldsymbol{n^{th}}$ target-agent $\boldsymbol{\Gamma_n}$ within the collision risk swath of the own-agent $\boldsymbol{\Gamma_o}$. The own-agent $\boldsymbol{\Gamma_o}$ is located at $\boldsymbol{p_o}$ and traveling with a heading $\boldsymbol{\psi_o}$ of 45° as indicated by the arrow, while the $\boldsymbol{n^{th}}$ target-agent $\boldsymbol{\Gamma_n}$ is located at $\boldsymbol{q_0}$. Note the own-agent does not yet take into account the direction of travel of the $\boldsymbol{n^{th}}$ target-agent $\boldsymbol{\Gamma_n}$.

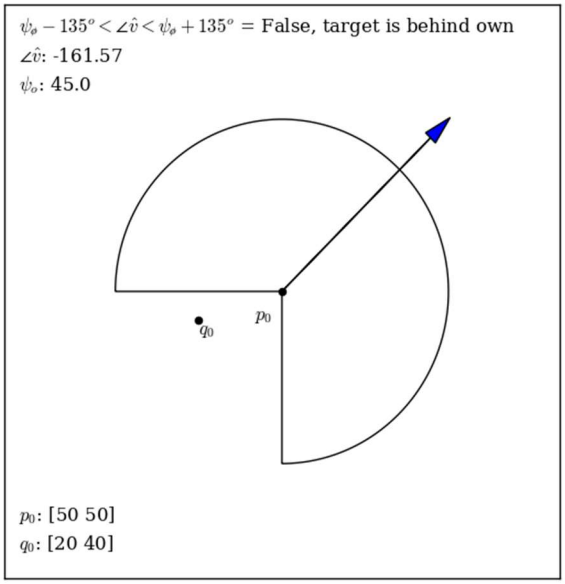

Figure 3.8 depicts a the $\boldsymbol{n^{th}}$ target-agent $\boldsymbol{\Gamma_n}$ outside of the collision risk swath of the own-agent $\boldsymbol{\Gamma_o}$. The own-agent $\boldsymbol{\Gamma_o}$ is located at $\boldsymbol{p_o}$ and traveling with a heading $\boldsymbol{\psi_o}$ of 45° as indicated by the arrow, while the $\boldsymbol{n^{th}}$ target-agent $\boldsymbol{\Gamma_n}$ is located at $\boldsymbol{q_0}$.

The first step in the creation of trajectory polygons quantifies the inertial stop displacement of the own s_o and target-agent s_t. This function only considers the resistance force generated by drag. There is no reverse thrust force acting on the hull of the ship because RPS (r) is set to zero. To find the stopping distance, we first calculate the velocity at time (t) with (Personal Comm. Meyer):

$$u_t = \frac{\mu\, u_0}{\mu + a\, C_D\, t\, u_0} \qquad \textbf{3.3}$$

Where t is the time in seconds, u_t is the velocity at time (t) in m/s, μ is the mass of the vessel in kilograms (kg), a is the cross-sectional area of the vessel measured in square meters (m^2), C_D is the drag coefficient, and u_0 is the initial velocity of the vessel measured in meters per second (m/s). At the start of every time step, the method *inertialStop* vectorizes equation (**3.3**) and solves for u_t over an array of time steps of length m=7200, ($\boldsymbol{\Delta} = [t_1 \ldots t_m]$ and $t_i \in \mathbb{Z}^m$) with `numpy.vectorize`. Numpy broadcasts a vectorized function over an input array ($\boldsymbol{\Delta}$) of length $m = 7200$ and returns an array of velocities ($\boldsymbol{U}$) of length $m = 7200$ by evaluating (3.2) over each element in $\boldsymbol{\Delta}$ (Van Der Walt, Colbert

and Varoquaux 2011). Displacement over each time step was calculated as the velocity ($\boldsymbol{U}$) multiplied by the change in time ($dt = 1$) where: $\boldsymbol{D} = \boldsymbol{U}dt$. The equation, which ignores friction, reveals that, under inertial stop, the vessel will never come to rest; therefore when the u < 0.1 m/s, the vessel is considered stopped. The function `numpy.where` (Van Der Walt, Colbert and Varoquaux 2011) returns the index (l) of the first velocity less than 0.1 m/s in $\boldsymbol{U}$, $d_l \leq 0.1\ m/s$. If the vessel does not slow down to $\leq 0.1\ m/s$, then $l = 7200$. The inertial stop displacement (s_n) of the n^{th} agent is the sum of all displacements where $\boldsymbol{D} \subset d_1 \ldots d_l$ and $s_n = \sum_{i=1}^{l} d_i$.

With the inertial stopping distance of the own s_o and target-agent s_t known, the position of the own (Γ_o) and n^{th} target-agent (Γ_n) at the inertial stop displacement is computed with 3.4 and 3.5 respectively:

$$\boldsymbol{p}_s = \boldsymbol{p_0} + s_o\, \widehat{\boldsymbol{\psi}}_o \qquad \textbf{3.4}$$

$$\boldsymbol{q}_s = \boldsymbol{q_0} + s_{t_n}\, \widehat{\boldsymbol{\psi}}_n \qquad \textbf{3.5}$$

Where $\boldsymbol{p_0}$ and $\boldsymbol{q_0}$ are the current positions of the own (Γ_o) and the n^{th} target-agent (Γ_n) in UTM Zone 18N, s_o and s_n are the inertial stop displacements of the own (Γ_o) and the n^{th} target-agent (Γ_n), and $\widehat{\boldsymbol{\psi}}_o$ and $\widehat{\boldsymbol{\psi}}_n$ are the unit vectors given with 3.6and **3.7**

$$\widehat{\boldsymbol{\psi}}_o = \boldsymbol{\psi}_o / |\boldsymbol{\psi}_o| \qquad \textbf{3.6}$$

$$\widehat{\boldsymbol{\psi}}_n = \boldsymbol{\psi}_n / |\boldsymbol{\psi}_n| \qquad \textbf{3.7}$$

where $\boldsymbol{\psi}_o$ is the vector $\boldsymbol{\psi}_o = \boldsymbol{p_{-1}} - \boldsymbol{p_0}$ and $\boldsymbol{\psi}_n$ is the vector $\boldsymbol{\psi}_n = \boldsymbol{q_{-1}} - \boldsymbol{q_0}$. The positions, $\boldsymbol{p_{-1}}, \boldsymbol{p_0}, \boldsymbol{q_{-1}}, \boldsymbol{q_0}$ are the previous and current positions of the own (Γ_o) and n^{th} target-agent (Γ_n) respectively.

To finish the trajectory polygons of the own (Γ_n) and the n^{th} target-agent (Γ_n), Ψ_o and Ψ_n, *F_rep_agn* rotates $\boldsymbol{p}_s$ and $\boldsymbol{q}_s$ to port and starboard by the maximum rudder deflection angle of each vessel (τ_o and τ_n) with equation **3.8** through **3.11**:

$$\boldsymbol{p}_s^{\tau} = \boldsymbol{p}_0 + s_o\left(\begin{bmatrix}\cos\tau_o & -\sin\tau_o\\ \sin\tau_o & \cos\tau_o\end{bmatrix}\cdot\begin{bmatrix}\widehat{\boldsymbol{\psi}}_{o_{1,1}}\\ \widehat{\boldsymbol{\psi}}_{o_{2,1}}\end{bmatrix}\right) \quad \textbf{3.8}$$

$$\boldsymbol{p}_s^{-\tau} = \boldsymbol{p}_0 + s_o\left(\begin{bmatrix}\cos-\tau_o & -\sin-\tau_o\\ \sin-\tau_o & \cos-\tau_o\end{bmatrix}\cdot\begin{bmatrix}\widehat{\boldsymbol{\psi}}_{o_{1,1}}\\ \widehat{\boldsymbol{\psi}}_{o_{2,1}}\end{bmatrix}\right) \quad \textbf{3.9}$$

$$\boldsymbol{q}_s^{\tau} = \boldsymbol{q}_0 + s_n\left(\begin{bmatrix}\cos\tau_n & -\sin\tau_n\\ \sin\tau_n & \cos\tau_n\end{bmatrix}\cdot\begin{bmatrix}\widehat{\boldsymbol{\psi}}_{n_{1,1}}\\ \widehat{\boldsymbol{\psi}}_{n_{2,1}}\end{bmatrix}\right) \quad \textbf{3.10}$$

$$\boldsymbol{q}_s^{-\tau} = \boldsymbol{q}_0 + s_n\left(\begin{bmatrix}\cos-\tau_n & -\sin-\tau_n\\ \sin-\tau_n & \cos-\tau_n\end{bmatrix}\cdot\begin{bmatrix}\widehat{\boldsymbol{\psi}}_{n_{1,1}}\\ \widehat{\boldsymbol{\psi}}_{n_{2,1}}\end{bmatrix}\right) \quad \textbf{3.11}$$

where the positions $\boldsymbol{p}_s^{\tau_o}$,$\boldsymbol{p}_s^{-\tau_o}$,$\boldsymbol{q}_s^{\tau_n}$, and $\boldsymbol{q}_s^{-\tau_n}$ are the inertial-displaced and rotated-positions of the own (Γ_o) and n^{th} target agent (Γ_n), $\boldsymbol{p}_0$ and $\boldsymbol{q}_0$. The superscript τ refers to rudder deflection to port, while $-\tau$ refers to rudder deflection starboard. Thus τ_o and $-\tau_o$ are the maximum rudder deflections to port and starboard for the own-agent (Γ_o), while τ_n and $-\tau_n$ are the maximum rudder deflections for the n^{th} target-agent (Γ_n). Equations **3.8** through **3.11** also have the unit vectors $\widehat{\boldsymbol{\psi}}_o$ (**3.6**) and $\widehat{\boldsymbol{\psi}}_t$(**3.7**) written in matrix form.

The positions $(\boldsymbol{p}_0, \boldsymbol{p}_s^{\tau_o}, \boldsymbol{p}_s, \boldsymbol{p}_s^{-\tau_o})$ form the trajectory polygon (Ψ_o) of the own-agent (Γ_o), while $(\boldsymbol{q}_0, \boldsymbol{q}_s^{\tau_{t_n}}, \boldsymbol{q}_s, \boldsymbol{q}_s^{-\tau_{t_n}})$ form the trajectory polygon (Ψ_n) of the n^{th} target-agent (Γ_n). The method *F_rep_agn* creates *Shapely* polygons (Gillies 2013) for both trajectory polygons, Ψ_o and Ψ_n, and tests for overlap with the function `shapely.intersects`. If the trajectory polygons (Ψ_o and Ψ_n) intersect ($\Psi_o \cap \Psi_n = \Psi_c$), then the interaction between the own (Γ_o) and the n^{th} target-agent (Γ_n) warrants further inspection (Figure 3.9), if they don't ($\Psi_o \cap \Psi_n = \emptyset$) then the own-agent Γ_o assesses the potential for collision with the next target-agent within range Γ_{n+1} (Figure 3. 3.10). When trajectory polygons intersect, *F_rep_agn* creates the intersection (Ψ_c) of Ψ_o and Ψ_n with `shapely.intersection` (Gillies 2013) and measures the minimum collision distance (c) from $\boldsymbol{p}_0$ to the intersection (Ψ_c) of Ψ_o and Ψ_n with `shapely.distance` (Gillies 2013).

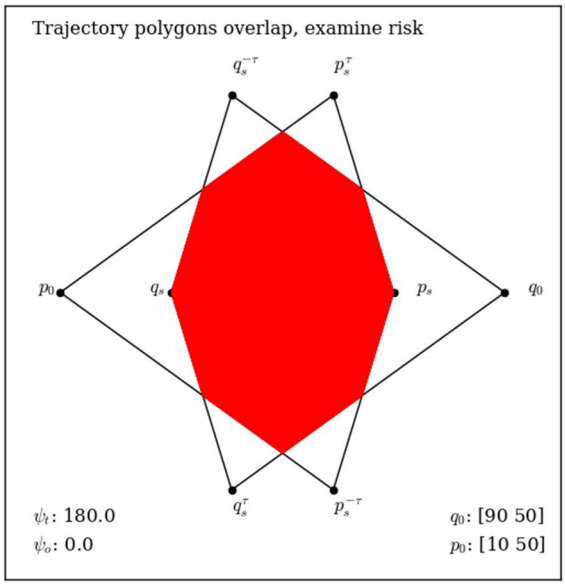

Figure 3.9 depicts the trajectory polygon $\boldsymbol{\Psi_o}$ of the own agent $\boldsymbol{\Gamma_o}$ with a heading of $\boldsymbol{\psi_o}$formed by the points $\{\boldsymbol{p_0}, \boldsymbol{p_s^{\tau}}, \boldsymbol{p_s}, \boldsymbol{p_s^{-\tau}}, \}$ intersecting the trajectory polygon $\boldsymbol{\Psi_{t_n}}$ of the $\boldsymbol{n^{th}}$ target agent $\boldsymbol{\Gamma_{t_n}}$ with a heading of $\boldsymbol{\psi_t}$ formed by the points $\{\boldsymbol{q_0}, \boldsymbol{q_s^{\tau}}, \boldsymbol{q_s}, \boldsymbol{q_s^{-\tau}}\}$. If the trajectory polygons overlap, there is potential for collision within the shaded area and the own-agent $\boldsymbol{\Gamma_o}$ continues assessing risk.

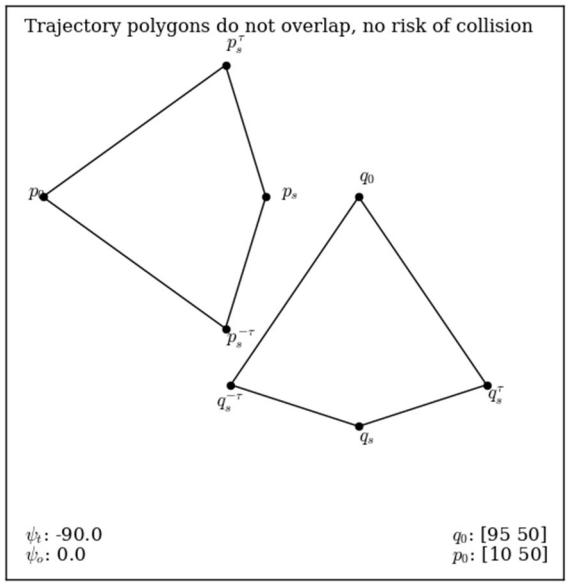

Figure 3.10 depicts the trajectory polygon $\boldsymbol{\Psi_o}$ of the own agent $\boldsymbol{\Gamma_o}$ with a heading of $\boldsymbol{\psi_o}$formed by the points $\{\boldsymbol{p_0}, \boldsymbol{p_s^{\tau}}, \boldsymbol{p_s}, \boldsymbol{p_s^{-\tau}}, \}$ not intersecting the trajectory polygon $\boldsymbol{\Psi_{t_n}}$ of the $\boldsymbol{n^{th}}$ target agent $\boldsymbol{\Gamma_{t_n}}$ with a heading of $\boldsymbol{\psi_t}$ formed by the points $\{\boldsymbol{q_0}, \boldsymbol{q_s^{\tau}}, \boldsymbol{q_s}, \boldsymbol{q_s^{-\tau}}\}$. If the trajectory polygons do not overlap, there is no potential for collision and the own-agent $\boldsymbol{\Gamma_o}$ assesses risk of collision with the next target-agent $\boldsymbol{\Gamma_{t_{n+1}}}$ within range.

Interactions between the own (Γ_o) and the n^{th} target-agent (Γ_n) with overlapping trajectory polygons belong to one of five categories: (I) the current position of the n^{th} target-agent Γ_n is within the trajectory polygon Ψ_o of the own-agent Γ_o, (II) the agents (Γ_o, Γ_n) are approaching head on, (III) the own agent (Γ_o) is in-line with but behind the n^{th} target-agent Γ_n , (IV) the own-agent (Γ_o) is approaching the port side of the n^{th} target-agent Γ_n, or (V) the own-agent (Γ_o) is approaching the starboard side of the n^{th} target-agent Γ_n. The method *F_rep_agn* classifies each interaction, and depending upon the interaction type and collision distance c, enacts different collision-avoidance protocols.

After finding that trajectory polygons intersect, *F_rep_agn* classifies the interaction between the own-agent Γ_o and n^{th} target-agent Γ_{t_n} with a series of Boolean operations. The first of which,

wit , looks for the presence of Type I interactions, where the n^{th} target-agent Γ_n is *within* the trajectory polygon $\Psi_o$of the own-agent Γ_o (**3.12**):

$$within = int(\Psi_o) \ni \boldsymbol{q}_0 \quad \textbf{3.12}$$

where $int(\Psi_o)$ is the interior of the own-agent's (Γ_o) trajectory polygon (Ψ_o) formed by the vertices $\{\boldsymbol{p}_0, \boldsymbol{p}_s^{\tau_o}, \boldsymbol{p}_s, \boldsymbol{p}_s^{-\tau_o}\}$ and $\boldsymbol{q}_0$ is the current position of the n^{th} target-agent (Γ_n). Type I interactions are the worst-case scenario and occur when the Shapely function `within` returns true. When this occurs, *F_rep_agn* enacts collision avoidance procedures, including setting the propeller speed (r) in revolutions per second (RPS) to maximum reverse $r = -5$ and quantifying repulsive force. If `within` is false, *F_rep_agn* tests for the presence of head on interactions.

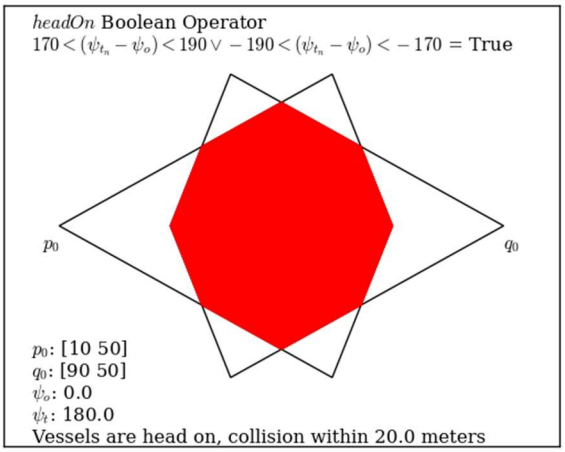

Figure 3.11 shows an example of a head on interaction between two agents, the own ($\boldsymbol{\Gamma_o}$) and $\boldsymbol{n^{th}}$ target ($\boldsymbol{\Gamma_{t_n}}$). The own-agent ($\boldsymbol{\Gamma_o}$) has a heading ($\boldsymbol{\psi_o}$) of 0.0° while the $\boldsymbol{n^{th}}$ target-agent ($\boldsymbol{\Gamma_{t_n}}$) has a heading ($\boldsymbol{\psi_{t_n}}$) of 180°.

Type II interactions (**3.13**), occur when the difference between the n^{th} target's heading (ψ_n) and own-agent's heading (ψ_o) range between -190° and -170° or between 170° and 190° as with the Boolean operation $headOn$:

$$headOn = 170 < \psi_n - \psi_0 < 190 \ \vee \ -190 < \psi_n - \psi_0 < -170 \quad \textbf{3.13}$$

where ψ_n is the heading of the n^{th} target-agent $\Gamma_n$heading and ψ_0 is heading of the own-agent Γ_o. When the agents are head on, the Boolean operator evaluates to true as depicted with (Figure 3.11), and protocol requires the own-agent (Γ_o) to implement collision avoidance procedures.

If the agents are not approaching each other head on, then F_rep_agn assesses for conditions where the own- (Γ_o) and (n^{th}) target-agent (Γ_n) are in-line, with the own-agent behind the target-agent (Type III). The Boolean operation $inLineBehind$ (Equation 3.14) tests for the presence of this scenario with the heading of the own -agent (ψ_o), the angle of the n^{th} target-agent (Γ_n) relative to the own (Γ_o) in degrees ($\angle\hat{v}$), the own-agent's unit heading-vector ($\widehat{\boldsymbol{\psi}}_o$), and target-agent's unit heading-vector ($\widehat{\boldsymbol{\psi}}_n$):

$$inLineBehind = (\psi_o - 22.5^o) < \angle\hat{v} < (\psi_0 + 22.5^o) \wedge sign(\widehat{\boldsymbol{\psi}}_o) \equiv sign(\widehat{\boldsymbol{\psi}}_n) \qquad \textbf{3.14}$$

Note the use of the 'and' operator ($\wedge$), which requires both Boolean operations to return true. The first logic operator ensures and n^{th} target-agent (Γ_n) is within a narrow 44.5° arc in front of own-agent (Γ_o). The second operator requires that the sign of the own-agent's unit heading-vector ($\widehat{\boldsymbol{\psi}}_o$) and n^{th} target-agent's (Γ_n) unit heading-vector ($\widehat{\boldsymbol{\psi}}_n$) are equivalent. Use of the equivalence operator ($\equiv$) requires that the sign of the first and second element in $\widehat{\boldsymbol{\psi}}_o$ must match their corresponding pair in $\widehat{\boldsymbol{\psi}}_n$. In other words, $sign(\widehat{\boldsymbol{\psi}}_o) \equiv sign(\widehat{\boldsymbol{\psi}}_n)$, means that the heading of the own (Γ_o) and n^{th} target-agent (Γ_n) must be within the same quadrant bearing. The function `numpy.sign` returns an element-wise indication of the sign of a number within an array (Van Der Walt, Colbert and Varoquaux 2011). When $inLineBehind$ returns true, we are ensured that the n^{th} target-agent Γ_n is directly in front of the own-agent Γ_o, and that they are headed in the same relative direction (Figure 3.12). If $inLineBehind$ is true, then the own-agent must implement collision avoidance procedures, including quantifying repulsive force and suggested RPS settings (r).

When $inLineBehind$ is false, F_rep_agn determines if the own-agent Γ_o is approaching the n^{th} target-agent (Γ_n) from the left with $portApproach$ (Type IV). The COLREGs state that vessels must yield to

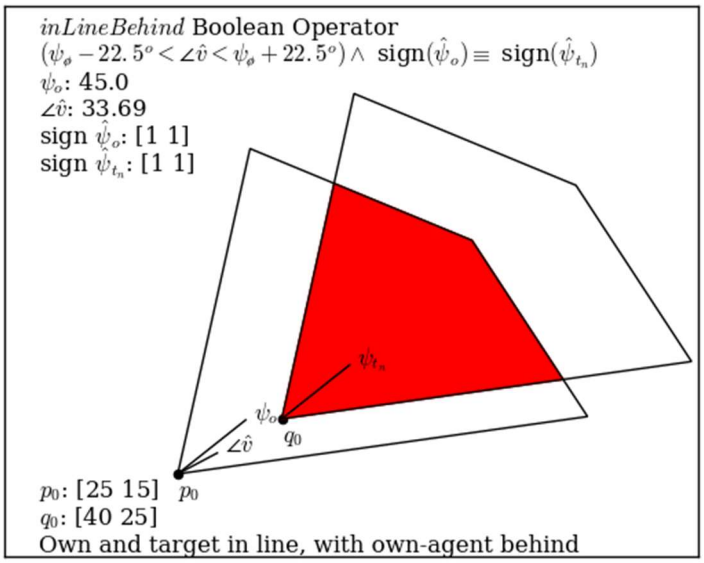

Figure 3.12 shows an example of the own-agent ($\boldsymbol{\Gamma_o}$) in line and behind the $\boldsymbol{n^{th}}$ target ($\boldsymbol{\Gamma_{t_n}}$).

those crossing from their starboard side (USCG 2015). If the target-agent (Γ_n) is performing a starboard cross, then own-agent Γ_o is approaching the port side of the target. The Boolean operation $portApproac$ is given with (Personal Comm. Meyer):

$$portApproach = sign\left(\widehat{\boldsymbol{\psi}}_{o\,(1,1)}\widehat{\boldsymbol{v}}_{(2,1)} - \widehat{\boldsymbol{v}}_{(1,1)}\widehat{\boldsymbol{\psi}}_{o\,(2,1)}\right) \equiv -1 \qquad \textbf{3.15}$$

where $\widehat{\boldsymbol{\psi}}_{(1,1)}$ and $\widehat{\boldsymbol{\psi}}_{(2,1)}$ are the *X* and *Y* components of the own agent's unit heading-vector $\widehat{\boldsymbol{\psi}}_{\boldsymbol{o}}$ and $\widehat{\boldsymbol{v}}_{(1,1)}$ and $\widehat{\boldsymbol{v}}_{(2,1)}$ are the *X* and *Y* components of the unit vector $\widehat{\boldsymbol{v}}$ that describes the position of the n^{th} target-agent (Γ_n) relative to the own agent (Γ_o). When the sign is negative, the target-agent (Γ_n) is on the right and the own agent (Γ_o) yields (Figure 3.13). When $portApproac$ is false, the own-agent approaches the starboard side of the target-agent, and does not yield (Type V) (Figure 3.14).

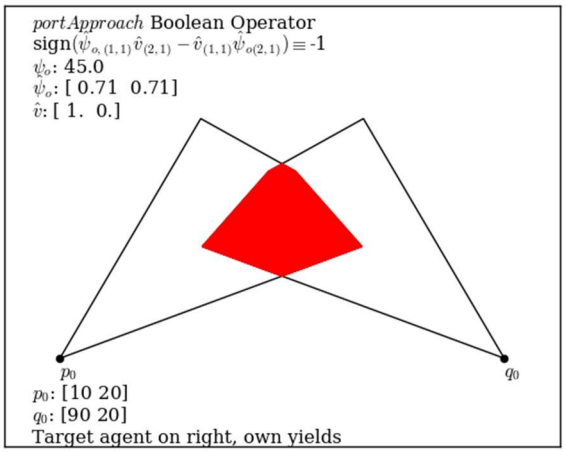

Figure 3.13 depicts the own-agent ($\boldsymbol{\Gamma_o}$) approaching the port side of the $\boldsymbol{n^{th}}$ target ($\boldsymbol{\Gamma_{t_n}}$). The own-agent ($\boldsymbol{\Gamma_o}$) must implement evasive maneuvers.

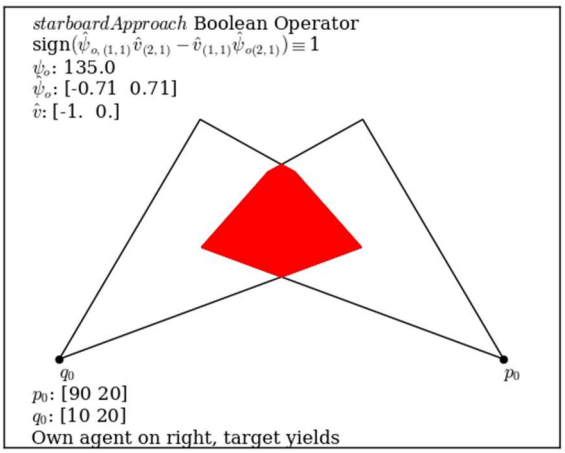

Figure 3.14 depicts the own-agent ($\boldsymbol{\Gamma_o}$) approaching the starboard side of the $\boldsymbol{n^{th}}$ target ($\boldsymbol{\Gamma_{t_n}}$). The own-agent ($\boldsymbol{\Gamma_o}$) is not required to implement evasive maneuvers.

If $swath$ is true, the trajectory polygons of the own Ψ_o and target-agent Ψ_{t_n} overlap, and the interaction is either a Type I, II, III or IV, then the own-agent (Γ_o) is at risk of collision with the n^{th} target-agent Γ_n and must implement evasive maneuvers. Evasive maneuvers include changes in heading and/or propeller speed (r) measured in RPS. These actions are designed to slow the agent down and minimize risk of collision. Not all interactions require an agent to change their course, the following pseudo code outlines how the own-agent Γ_o decides to react to the n^{th} target agent Γ_{t_n}:

```
If |v| < 5000:
    If ψ_o − 135 < ∠v̂ < ψ_o + 135:
        If Ψ_c ≠ ∅:
            If int(Ψ_o) ∋ q_0 (Type I):
                Calculate: R_{t_n,o}
                If s_o < (3/4)c then:
                    Suggested RPS: r = −5
                Else:
                    Suggested RPS: r = 0
            Else If 170 < ψ_{t_n} − ψ_0 < 190 ∨ −190 < ψ_{t_n} − ψ_0 < −170 (Type II):
                Calculate: R_{t_n,o}
                If s_o < (3/4)c then:
                    Suggested RPS: r = −5
                Else:
                    Suggested RPS: r = 0
            Else If (ψ_o − 22.5°) < ∠v̂ < (ψ_0 + 22.5°) ∧ sign(ψ̂_o) ≡ sign(^_{t_n}) (Type III):
                Do not calculate: R_{t_n,o} = [0,0]
                If s_o < (3/4)c then:
                    Suggested RPS: r = −5
```

```
                        Else:
                                Suggested RPS: r = 0
                Else If sign(ψ̂_o(1,1) v̂_(2,1) − v̂_(1,1) ψ̂_o(2,1)) ≡ −1 (Type IV):
                        Calculate: R_(t_n,o)
                        If s_o < (3/4)c then:
                                Suggested RPS: r = −5
                        Else:
                                Suggested RPS: r = 0
                Else If sign(ψ̂_o(1,1) v̂_(2,1) − v̂_(1,1) ψ̂_o(2,1)) ≡ 1 (Type V):
                        Do not calculate: R_(t_n,o) = [0,0]
                        Suggested RPS: r = r_opt
        Else:
                Do not calculate: R_(t_n,o) = [0,0]
                Suggested RPS: r = r_opt
Else:
        Do not calculate: R_(t_n,o) = [0,0]
        Suggested RPS: r = r_opt
```

where $\boldsymbol{\mathcal{R}}_{\Gamma_n}$ is the repulsive force generated by the n^{th} target-agent Γ_{t_n}, and r_{opt} is the optimal propeller speed (see section:3.4.2.5 Throttle Control). When required, the repulsive force, $\boldsymbol{\mathcal{R}}_{\Gamma_n}$, generated by the n^{th} target-agent Γ_n is given with equation (**3.16**):

$$\boldsymbol{\mathcal{R}}_{\Gamma_n} = \frac{G\mu_n\,\hat{\boldsymbol{v}}}{(|\boldsymbol{v}|/(\lambda_o+\lambda_n))^2} \qquad \textbf{3.16}$$

where $\boldsymbol{\mathcal{R}}_{\Gamma_n}$ is the repulsive force generated by the n^{th} target-agent Γ_n, G is the universal gravitational constant ($6.67408 * 10^{-11}\ m^3 kg^{-1} s^{-2}$), μ_n is the mass of the n^{th} target-agent (Γ_n) in kg, $\hat{\boldsymbol{v}}$ is the unit vector from the n^{th} target-agent Γ_n towards the own-agent (Γ_o), $|\boldsymbol{v}|$ is the norm of the position vector $\boldsymbol{v}$, λ_o is the length of the own-agent Γ_o in m, and λ_n is the length of the n^{th} target-agent Γ_n in m. The closer the own agent is to the target agent, the greater the repulsive force becomes. The direction of the repulsive force ($\hat{\boldsymbol{v}}$) acts pushing the own agent away from danger. The total repulsive force ($\boldsymbol{\mathcal{R}}_\Gamma$) exerted by the target-agents $\{\Gamma_1 \dots \Gamma_n\}$ as felt by the own-agent (Γ_o) is the sum of all proximate target-agent $\{\Gamma_1 \dots \Gamma_n\}$ repulsive forces, and is given with: $\boldsymbol{\mathcal{R}}_\Gamma = \sum_{i=n}^{n} \boldsymbol{\mathcal{R}}_{\Gamma_i}$. After calculating $\boldsymbol{\mathcal{R}}_\Gamma$, the ABM then calculates the repulsive force generated by all obstacles (O) with the agent class-method *F_rep_obs*.

The own-agent's (Γ_o) original route avoids known obstructions. However, interaction with other agents throughout the course of a simulation may push the own-agent (Γ_o) to within close proximity of an obstacle (Ω_k). The agent class-method, *F_rep_obs*, quantifies the repulsive force of obstacles that are within 5 km of the own-agent (Γ_o) and within the own-agent's (Γ_o) trajectory polygon (Ψ_o). The distance to the nearest point ($\boldsymbol{\omega}$) on the k^{th} obstacle Ω_k is the norm of the vector $\boldsymbol{\varsigma} = \boldsymbol{\omega} - \boldsymbol{p}_o$. To find $\boldsymbol{\omega}$, Shapley's linear referencing function `project` (Gillies 2013) returns the distance along the k^{th} obstacle's (Ω_k) boundary that is nearest to current position ($\boldsymbol{p}_o$) of the own-agent (Γ_o). Then, `shapely.interpolate` (Gillies 2013) returns the point at the specified distance ($\boldsymbol{\omega}$) along the boundary of Ω_k as calculated with `project`.

With the nearest obstacle point ($\boldsymbol{\omega}$) and distance $|\boldsymbol{\varsigma}|$ to the own- agent (Γ_o) known, Boolean logic (**3.17**) determines whether or not the own-agent Γ_o reacts to the k^{th} obstacle Ω_k with.:

$$|\boldsymbol{\varsigma}| < s_o \wedge \Psi_o \cap \Omega_k \neq \emptyset \qquad \textbf{3.17}$$

Where $|\boldsymbol{\varsigma}|$ is the distance from the own-agent (Γ_o) to the nearest point ($\boldsymbol{\omega}$) along the boundary of the k^{th} obstacle (Ω_k), s_o is the inertial stopping distance of the own-agent (Γ_o), and Ψ_o is the trajectory polygon of the own-agent (Γ_o). Use of the 'and' operator ($\wedge$) requires that the distance between the k^{th} obstacle (Ω_k) and own-agent (Γ_o) is less than the inertial stopping distance (s_o), and that the intersection ($\cap$) of the trajectory polygon (Ψ_o) and obstacle (Ω_k) is not empty ($\neq \emptyset$). The function `shapely.distance` (Gillies 2013) measures the distance between the own-agent (Γ_o) and obstacle polygon (Ω_k) boundary point ($\boldsymbol{\omega}$), while `shapely.intersection` (Gillies 2013) finds the intersection of the k^{th} obstacle Ω_k and trajectory polygon (Ψ_o). The pseudo code in outlines the own-agent's (Γ_o) decision logic when reacting to an obstacle (Ω_k).

```
If |ς| < s_o ∧ Ψ_o ∩ Ω_k ≠ ∅ then:
    Calculate: R_Ω_k
    If s_o < (3/4)|ς| then:
```

```
            Suggested RPS: r = −5
      Else:
            Suggested RPS: r = 0
Else:
      Do not calculate: R_Ωk = [0,0]
      Suggested RPS: r = r_opt
```

where $\boldsymbol{\mathcal{R}}_{\Omega_k}$ is the repulsive force generated by the k^{th} obstacle Ω_k in the direction of $\hat{\boldsymbol{\varsigma}}$ where $\hat{\boldsymbol{\varsigma}} = \boldsymbol{\varsigma}/|\boldsymbol{\varsigma}|$, Ψ_o is the trajectory polygon of the own-agent (Γ_o), and s_o is the stopping distance of the own-agent (Γ_o). The repulsive force generated by the k^{th} obstacle Ω_k, $\boldsymbol{\mathcal{R}}_{\Omega_k}$ is given with equation **3.18**:

$$\boldsymbol{\mathcal{R}}_{\Omega_k} = \frac{G\mu_{\Omega_k}\,\hat{\boldsymbol{\varsigma}}}{(|\boldsymbol{\varsigma}|/s_o)^2} \qquad \textbf{3.18}$$

where μ_{Ω_k} is the mass of the k^{th} navigational obstruction Ω_k measured in kg, $\hat{\boldsymbol{\varsigma}}$ is the unit vector from the k^{th} navigational obstruction Ω_k to the own-agent Γ_o, and $|\boldsymbol{\varsigma}|$ is the norm of the vector $\boldsymbol{\varsigma}$. The total repulsive force ($\boldsymbol{\mathcal{R}}_{\Omega}$) exerted by the obstacles as felt by the own-agent (Γ_o) is the sum of the repulsive forces from all other agents in proximity $\{\Omega_1 \ldots \Omega_k\}$, and given with: $\sum_{i=k}^{k} \boldsymbol{\mathcal{R}}_{\Omega_i}$.

The ABM passes on the suggested RPS settings to the throttle control module (see section 3.4.2.5 Throttle Control), and passes on the repulsive forces ($\mathcal{R}_{\Gamma}, \mathcal{R}_{\Omega}$) to the orienteering module.

3.4.2.1.3 Orienteering

Aside from route finding and collision avoidance, the navigation submodule also has functions that orient the own-agent (Γ_o) towards the next waypoint ($\boldsymbol{w}_{i+1}$) while minimizing risk of collision. Attractive force ($\boldsymbol{\mathcal{A}}$) is the gravitational potential that exists between the own-agent Γ_o and the next waypoint $\boldsymbol{w}_{i+1}$. The attractive force $\boldsymbol{\mathcal{A}}$ acts to pull the own agent towards the next waypoint $\boldsymbol{w}_{i+1}$ in the direction of $\hat{\boldsymbol{\sigma}}$ and is given with (3.19): **3.19**

$$\boldsymbol{\mathcal{A}} = -G\mu_w\,\hat{\boldsymbol{\sigma}}$$

where G is the acceleration due to gravity 9.8 m/s^2, μ_w is the mass of the next waypoint $\boldsymbol{w}_{i+1}$ measured in kg, and $\hat{\boldsymbol{\sigma}}$ is the unit vector of $\boldsymbol{\sigma} = \boldsymbol{p}_o - \boldsymbol{w}_{i+1}$. Note that the attractive potential force $\boldsymbol{\mathcal{A}}$ is not affected by the inverse-square law, meaning the attractive potential towards the next waypoint ($\boldsymbol{w}_{i+1}$) has the same magnitude throughout the study region. If the inverse distance squared term remained within the attractive force equation, the own-agent (Γ_o) becomes too sensitive to repulsive forces ($\boldsymbol{\mathcal{R}}_\Gamma, \boldsymbol{\mathcal{R}}_\Omega$) far from the next waypoint ($\boldsymbol{w}_{i+1}$), and can potentially ignore critical collision scenarios close to $\boldsymbol{w}_{i+1}$.

After resolving repulsive ($\boldsymbol{\mathcal{R}}_\Gamma, \boldsymbol{\mathcal{R}}_\Omega$) and attractive forces ($\boldsymbol{\mathcal{A}}$), the own-agent (Γ_o) then sums all steering forces with (**3.20**):

$$\boldsymbol{\mathcal{F}} = \boldsymbol{\mathcal{R}}_\Gamma + \boldsymbol{\mathcal{R}}_\Omega + \boldsymbol{\mathcal{A}} \qquad \textbf{3.20}$$

where $\boldsymbol{\mathcal{F}}$ is the steering force vector, $\boldsymbol{\mathcal{R}}_\Gamma$ is the repulsive force generated by all target-agents within proximity $\{\Gamma_{t_1} \dots \Gamma_n\}$, $\boldsymbol{\mathcal{R}}_\Omega$ is the repulsive force generated by all obstacles in proximity $\{\Omega_1 \dots \Omega_k\}$, and $\boldsymbol{\mathcal{A}}$ is the attractive force of the next waypoint ($\boldsymbol{w}_{i+1}$). The repulsive forces ($\boldsymbol{\mathcal{R}}_\Gamma$, $\boldsymbol{\mathcal{R}}_\Omega$) are a function of the inverse distance squared between objects. While very low and inconsequential at long distances ($\boldsymbol{\mathcal{R}}_\Gamma + \boldsymbol{\mathcal{R}}_\Omega \ll \boldsymbol{\mathcal{A}}$), the repulsive force will outweigh the attractive force the closer the own-agent (Γ_o) gets to an object ($\boldsymbol{\mathcal{R}}_\Gamma + \boldsymbol{\mathcal{R}}_\Omega \gg \boldsymbol{\mathcal{A}}$), eventually prompting a change in course. Equations (3.17 and 3.18) have measures in the inverse distance term that ensure the repulsive force is large enough to implement a change in course far enough in advance so that the own-agent has enough space to maneuver out of the way. For example, when the distance between the own (Γ_o) and n^{th} target-agent (Γ_{t_n}) are within 2 vessel lengths, the denominator in equation **3.17** is < 1, thus amplifying the repulsive force and causing the own-agent to implement emergency maneuvers with enough time for a commercial shipping vessel to escape.

The unit vector of $\hat{\boldsymbol{\mathcal{F}}}$, given with $\hat{\boldsymbol{\mathcal{F}}} = \boldsymbol{\mathcal{F}}/|\boldsymbol{\mathcal{F}}|$, describes the direction that resolves all steering forces, striking a balance between the desire to reach the destination and the need for self-

preservation. After converting the unit vector $\widehat{\boldsymbol{\mathcal{F}}}$ to degrees ($\angle \mathcal{F}$), the own-agent (Γ_o) then calculates the change in heading command with 3.21:

$$\Delta\psi_o = \angle \mathcal{F} - \psi_o \quad \textbf{3.21}$$

where $\Delta\psi_o$ is the change in heading command, ψ_o is the current heading in degrees and $\angle \mathcal{F}$ is the optimal heading. Change in heading is restricted by the maximum rudder deflection angle τ with (**3.22**):

$$\Delta\psi_o > \tau_o \vee \Delta\psi_o < -\tau_o \rightarrow \tau_o * sign(\Delta\psi_o) \quad \textbf{3.22}$$

which restricts the change in heading to be within the range $\pm\tau_o$.

Figure 3. graphically depicts the collision avoidance and orienteering navigational submodules. Here, the own-agent (Γ_o) interacts with two target-agents (Γ_1 and Γ_2) and reacts to the k^{th} obstacle (Ω_k) while navigating towards the next waypoint ($\boldsymbol{w}_{i+1}$). The gravitational potential ($\boldsymbol{\mathcal{A}}$) that exists between the own-agent Γ_o and the next waypoint $\boldsymbol{w}_{i+1}$ serves to pull the agent through the study area, while inverse gravitational forces ($\boldsymbol{\mathcal{R}}_{\Gamma_1}, \boldsymbol{\mathcal{R}}_{\Gamma_2}$, and $\boldsymbol{\mathcal{R}}_{\Omega_k}$) push the agent away from navigational obstructions (Ω_k) and other agents (Γ_1 and Γ_2). Given the current location ($\boldsymbol{q}_0^1, \boldsymbol{q}_0^2$), heading ($\psi_1, \psi_2$) and inertial displacement (s_1, s_2) of each target-agent (Γ_1, Γ_2), and the point of impact ($\boldsymbol{\omega}$) along the boundary of Ω_k, the own-agent resolves all repulsive forces acting upon its hull and computes the steering force vector ($\boldsymbol{\mathcal{F}}$).

Figure 3.15 also displays the trajectory polygons of the own Ψ_o and target-agents Ψ_1, Ψ_2, and we find that the interaction with target-agent 1 (Γ_1) is a Type II, while the interaction with target-agent 2 (Γ_2) is a Type IV. Both instances require the own-agent to compute repulsive force ($\boldsymbol{\mathcal{R}}_{\Gamma_1}, \boldsymbol{\mathcal{R}}_{\Gamma_2}$).

We also find the trajectory polygon (Ψ_o) of the own-agent (Γ_o) intersecting the k^{th} obstacle (Ω_k), which prompts the own-agent (Γ_o) to calculate the repulsive force ($\boldsymbol{\mathcal{R}}_{\Omega_k}$) of the k^{th} obstacle (Ω_k). The own-agent Γ_o then sums the steering force $\boldsymbol{\mathcal{F}}$, and calculates the change in heading $\Delta\psi_o$ with equation

3.22. Given overwhelming repulsive forces ($\boldsymbol{\mathcal{R}_\Gamma + \mathcal{R}_\Omega \gg \mathcal{A}}$), the own-agent ($\Gamma_o$) reverses course with a heading command for full starboard rudder ($\Delta\psi_o = -35^o$).

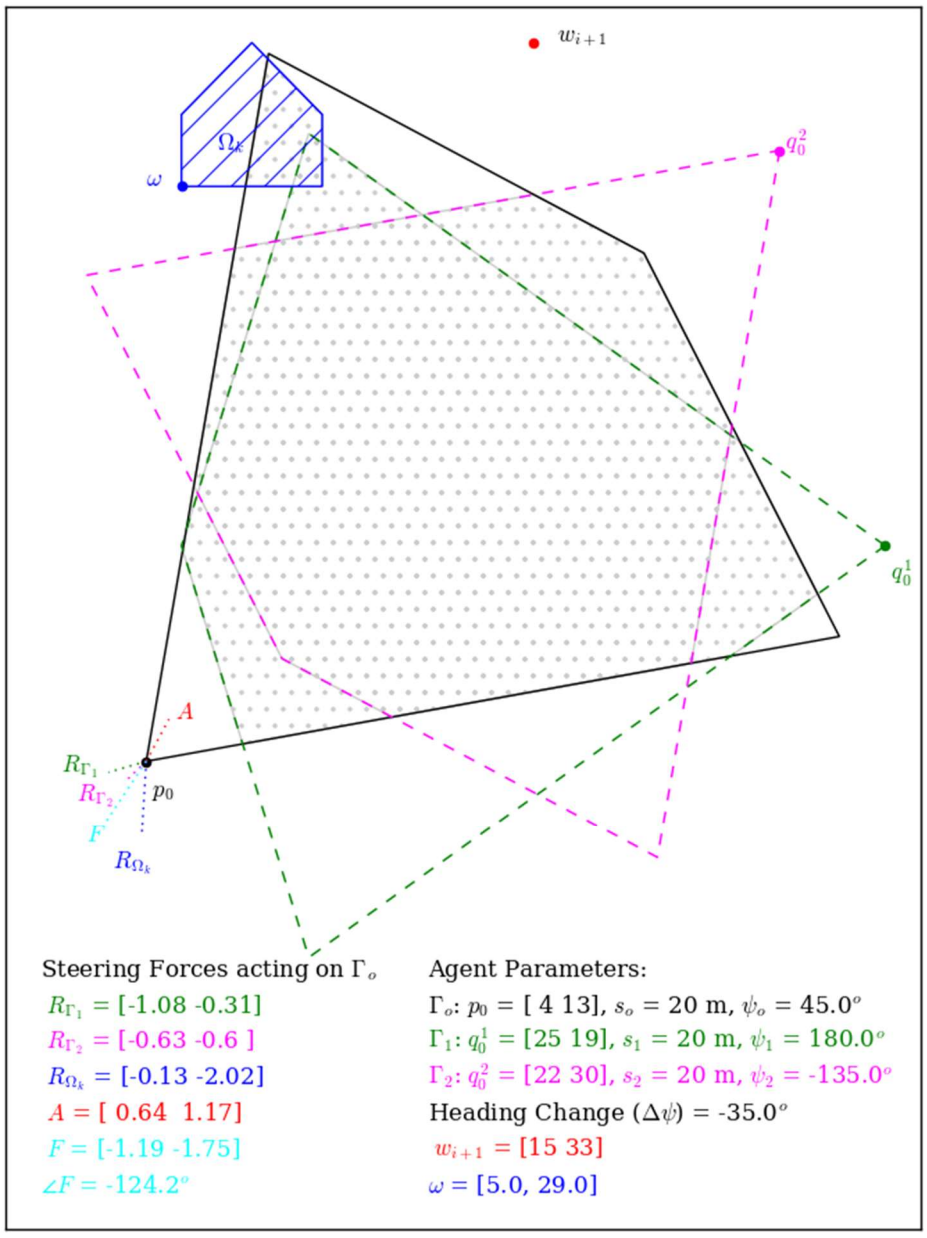

Figure 3.15 depicts the collision avoidance and orienteering submodules. The trajectory polygon and parameters of each agent $\boldsymbol{\Gamma_o, \Gamma_1, \Gamma_2}$ and obstruction $\boldsymbol{\Omega_k}$ have been color coded to aid the reader. Note, that the gravitational potentials have been scaled by a factor of 10^5 for illustrative purposes, however the relative length of each force vector is indicative of the weight of the obstruction or agent and the distance to the own agent $\boldsymbol{\Gamma_o}$. The steering force is $\boldsymbol{\mathcal{F} = \mathcal{R}_{\Gamma_1} + \mathcal{R}_{\Gamma_2} + \mathcal{R}_{\Omega_k} + \mathcal{A}}$. This situation depicts overwhelming force pushing on the own-agent causing it to change course as it gives the command for maximum starboard rudder deflection.

3.4.2.1.4 Throttle Control

During collision avoidance procedures, the own-agent (Γ_o) classifies the severity of each interaction, and the suggested RPS setting r can take 1 of 3 values: $\{-5,0,r_{opt}\}$. Most interactions do not warrant emergency stopping protocols, meaning the own-agent (Γ_o) finds the propeller speed (r_{opt}) that accelerates to the desired cruising velocity (u'). However, some interactions come with greater collision risk, and the own-agent (Γ_o) must slow down. If any of the interactions are severe enough to warrant full astern thrust, then the own-agent sets $r = -5$. If any of the interactions are severe enough to warrant inertial stop, then the agent sets $r = 0$. If the interaction does not warrant either emergency action, then the own-agent (Γ_o) finds the optimal propeller speed r_{opt} with 3.23:

$$\lfloor r_{opt} \rceil = \sqrt{\frac{m\dot{u}' + \mathcal{D}}{K_t \rho \kappa^4}} \quad \textbf{3.23}$$

where $\lfloor r_{opt} \rceil$ is the nearest integer optimal propeller setting in RPS, m is the mass of the ship in kg, $\dot{u}'$ is the acceleration required to reach the desired velocity in 1 minute (see equation 3.24) given in m/s^2, $\mathcal{D}$ is the force of drag on the own-agent's (Γ_o) hull (**3.253.24**), K_t is the dimensionless propeller thrust coefficient ($K_t = 1.2$), ρ is the density of seawater (1029 kg/m^3), and κ is the diameter of the propeller measured in m. When not in corridors that regulate speed, the own-agent (Γ_o) attempts to reach the desired cruising velocity (u') as set by the shipping firm at the onset of the voyage. The own-agent regulates their velocity by adjusting propeller speed (r), but must first calculate the acceleration ($\dot{u}'$) required to reach the desired velocity (u') within 1 minute with 3.24:

$$\dot{u}' = \frac{u' - u}{60} \quad \textbf{3.24}$$

where u' is the desired velocity (m/s) and u is the current velocity (m/s). The ship is limited to a maximum RPS of 60. The desired acceleration will push most r_{opt} well over the design capacity of the engines, therefore for most acceleration scenarios the agent will set the vessel to full throttle (60 RPS).

3.4.2.2 Movement

Following collision avoidance, orienteering and throttle control, the own-agent (Γ_o) now resolves movement by passing on the commands for RPS (r) and heading change ($\Delta\psi_o$). These movement submodules control an agent's movement over the course of a time step. They conserve forward and angular momentum while incorporating navigation commands ($\Delta\psi_o, r$) and approximating the movement of real commercial vessels. As previously discussed, researchers have decoupled movement equations for speed (2.5) and steering (2.6 and 2.7). Forward movement, or surge, is modeled with classical mechanics, while angular movement is modeled with a first order Nomoto model.

3.4.2.2.1 Forward Movement: Surge

Newton's second law of motion ($F = m\dot{u}$) states that the acceleration ($\dot{u}$) of an object is caused by a force F that is inversely proportional to its mass m (Meyer 2010). The own-agent (Γ_o) must resolve thrust ($\mathcal{T}$) and drag ($\mathcal{D}$) to solve the *surge* component of movement ($\mathcal{X}$). Thrust ($\mathcal{T}$) pushes the own-agent forward, while drag ($\mathcal{D}$) acts in the direction opposite of travel pulling the own-agent (Γ_o) to a stop. When $\mathcal{T} > \mathcal{D}$ the vessel accelerates, and when $\mathcal{T} < \mathcal{D}$ the agent slows down. If $\mathcal{T} = \mathcal{D}$, there is no net force in either direction and the own-agent (Γ_o) maintains velocity. The force of drag ($\mathcal{D}$) is proportional to the square of the agent's speed (u^2) and the ship's wetted area (α) (Ueng, Lin, & Liu, 2008), and is given with equation **3.25**:

$$\mathcal{D} = \frac{1}{2}\rho\, C_D\, \alpha\, u^2 \qquad \textbf{3.25}$$

where drag ($\mathcal{D}$) is the resistive force of the water along the hull, ρ is the density of seawater (1029 kg/m^3), C_D is the drag coefficient, α is the wetted area of the hull m^2, and u^2 is the square of the velocity (m/s). The drag coefficient (C_D) is a dimensionless quantity used to quantify the drag or resistance of an object in a fluid environment (Zubaly 1996). The current ABM employs a standard C_D of 0.04 for streamlined

bodies. Wetted area (α) is the area of the own-agent's (Γ_o) hull submerged in water, and is estimated with:

$$\alpha = C_B\ (\lambda\beta + 2\lambda\delta + 2\beta\delta) \quad \textbf{3.26}$$

where C_B is the vessel's block coefficient, λ, β, and δ are the typical ship dimensions of length (λ), beam (β), and draft (δ) in meters. The block coefficient (C_B) is the ratio of a vessel's displacement to the product of its ship dimensions (Zubaly 1996). The closer the block coefficient (C_B) is to 1, the closer the hull is to a perfect block shape.

Thrust ($\mathcal{T}$) is the other surge force ($\mathcal{X}$) acting on the hull of the own-agent (Γ_o), and it is controlled by the rotational speed (r) of the propeller as measured in RPS. When the propeller speed (r) remains stable over the course of a time step, so does thrust $\mathcal{T}$. Thrust is computed with (Ueng, Lin, & Liu, 2008):

$$\mathcal{T} = K_t\ \rho\ r^2 \kappa^4 \quad \textbf{3.27}$$

where $\mathcal{T}$ is thrust, ρ is the density of seawater (1029 kg/m^3), K_t is the propeller thrust coefficient (Zubaly 1996), r is the propeller speed measured in revolutions per second (RPS), and κ is the diameter of the propeller (m). The version of this ABM used a standard K_t of 1.2.

After resolving drag ($\mathcal{D}$) and thrust ($\mathcal{T}$), the own agent calculates the total surge force $\mathcal{X}$ with:

$$\mathcal{X} = \mathcal{T} - \mathcal{D} \quad \textbf{3.28}$$

where $\mathcal{X}$ is the total surge force in the positive x direction in a body fixed coordinate system, $\mathcal{T}$ is thrust (**3.27**) and $\mathcal{D}$ is the drag or resistance force applied to the hull (**3.25**). Rearranging Newton's second law of motion, the own-agent Γ_o then solves for acceleration ($\dot{u}$) with:

$$\dot{u} = \frac{\mathcal{X}}{m} \quad \textbf{3.29}$$

Where $\mathcal{X}$ is the surge force, m is the mass of a vessel in kg and $\dot{u}$ is the acceleration of the own-agent Γ_o over time step t in m/s^2. With acceleration over the time step known, the own-agent Γ_o computes velocity at $t + 1$ with:

$$u_1 = u_0 + \dot{u}\, dt \quad \textbf{3.30}$$

Where u_1 is the velocity of the own-agent at time $t + 1$, u_o is velocity at time t, $\dot{u}$ is acceleration over time t, and dt is the change in time over a time step t. After solving for velocity, the model solves for movement.

3.4.2.2.2 Angular Movement

With forward movement solved, the agent now incorporates the steering command $\Delta\psi$ (from 3.21) and completes the movement modules ($turn$). The position at the start of the next time step $\boldsymbol{p}_1$ is solved with 3.31 and 3.32. The new heading ψ_1 is given with 3.33 and the rate of turn η with 3.34 as in (Kawaguchi 2004):

$$x_{\boldsymbol{p}_1} = x_{\boldsymbol{p}_0} + u \cos\psi_0\, dt \quad \textbf{3.31}$$

$$y_{\boldsymbol{p}_1} = y_{\boldsymbol{p}_0} + u \sin\psi_0\, dt \quad \textbf{3.32}$$

$$\psi_1 = \psi_0 + \eta\, dt \quad \textbf{3.33}$$

$$\eta_1 = \eta + \frac{K\Delta\psi - \eta}{T}\, dt \quad \textbf{3.34}$$

where $(x_{\boldsymbol{p}_0}, y_{\boldsymbol{p}_0})$ and $(x_{\boldsymbol{p}_1}, y_{\boldsymbol{p}_1})$ are the own-agents Γ_o current $\boldsymbol{p}_0$ and next $\boldsymbol{p}_1$ positions, u is the own-agent's (Γ_o) current velocity measured in m/s at the beginning of the time step, ψ_0 is the vessel's current heading in degrees, η is the vessels current rate of rotation in degrees per second, $\Delta\psi$ is the command rudder angle, and K and T are first order Nomoto indices.

The T and K indices are simplified characteristic constants of a ship (Journee 2001) and are often called the K-T indices. A large time constant T is necessary for vessels with a large moment of inertia, which defines the torque needed for a desired angular acceleration (Journee 2001). Long, heavy vessels like tanker vessels will have a large T. As K increases, so does the steady state turning ability of the ship, while a smaller T provides quicker response to helm (Journee 2001). Poor turning, slow response or bad course stability is associated with a small K and large T. Table 3.1 lists the range of the K-T indices used by this ABM. Currently, we only have K-T indices for cargo and tanker vessels.

Table 3.1 typical ship parameters used in this simulation

Ship Type	K	T_N	C_D	C_B
Cargo	1.5 – 2.5	1.5 – 2.0	0.04	0.60
Tanker	3.0 – 6.0	1.7 – 3.0	0.04	0.80

After each agent solves resolves movement, the simulation proceeds to the next timestamp, iterates over each agent and repeats these methods until all agents have reached their destination or until the simulation has reached the desired number of time steps. The following pseudo code outlines the entire ABM

```
Initialize simulation:
     Create event log file
     Import obstacles: O
     Create population of agents: {Γ_1 … Γ_n}
For Γ_i in {Γ_1 … Γ_n}
     Run route(A, B):
For t in Δ
     For Γ_o in {Γ_1 … Γ_n}:
          Calculate: s_o
     For Γ_o in {Γ_1 … Γ_n}:
          Calculate: 𝒜
          Run F_rep_agn():
               For Γ_i in Γ_o ∉ {Γ_1 … Γ_n}:
                    Calculate ℛ_Γi
               ℛ_Γ = Σ_{i=n−1}^{n} ℛ_Γi
          Run F_rep_obs():
               For Ω_k in O:
                    Calculate ℛ_Ωk
               ℛ_Ω = Σ_{i=k}^{k} ℛ_Ωi
```

```
Calculate: 𝓕 = ℛΓ + ℛΩ + 𝒜
Run surge(r):
Run turn(Δψ):
Write interaction and decision details to event log
```

3.5 Calibration

Kawaguchi (2004) provided the only published values of K-T indices found during literature review, and they were only for cargo and tanker vessels. As a result of this data gap, we experimented with a calibration method designed to identify K-T indices from empirical data.

During sea trials, a vessel's maneuverability under load is tested with a turning circle test. A procedure for identifying K-T indices from turning circle data was outlined in NTNU (2009). Data obtained from turning circle tests provides the necessary calibration data, and allows for realistic vessel maneuverability. The NTNU (2009) procedure employs a nonlinear least squares regression technique to solve for two unknowns (K and T). The Nomoto gain (K) and time constants (T) are computed from a turning test using non-linear least-squares curve fitting via the SciPy function `curve_fit` (Jones, et al. 2001). During a turning test, the rudder angle τ is held constant, usually at τ', the initial rate of turn η and rate of turn at time $\eta(t)$ are also known. Our equation to solve for K and T is given with (NTNU 2009):

$$\eta(t) = \exp\left(-\frac{t}{T}\right)\eta + \left[1 - \exp\left(-\frac{t}{T}\right)\right]K\tau \qquad \textbf{3.35}$$

The method requires that the rate of turn over time $\eta(t)$, initial rate of turn η, and rudder deflection angle τ are known.

Data from the turning circle test is typically displayed on the 'wheelhouse poster' found at the helm of all commercial vessels, which provides local vessel pilots with the necessary information to safely navigate a vessel to berth. A number of consulting firms, pilot associations and shipyards were asked to provide data from wheelhouse posters. Following ABM calibration, numerical experiments were conducted testing the model's ability to reproduce chaotic behavior.

3.6 Numerical Experiments

Prior to running a simulation of the approach to the Port of New York and New Jersey, a series of numerical experiments were conducted to understand how the vessel physics work, as well as testing whether or not the model is capable of simulating a complex adaptive system. For the first series of experiments, we tested the inertial stopping capabilities, acceleration, maneuverability, and route finding capabilities by altering specific vessel parameters and study area configuration.

3.6.1 Inertial Stop

For the inertial stopping capabilities (s_o), it is hypothesized that a vessel's tonnage (μ), hull dimensions (λ, β, δ), shape (C_B) and drag (C_D) affect its ability to stop. In each experiment, the initial velocity (u) was set at 8 m/s or 15.56 knots and fluid density (ρ) remained constant at 1029 kg/m^3 while calculating the inertial stopping distance (s_o) of a reference vessel (Γ_o) after altering a single vessel parameter. Table 3.2 lists the experiments, the first varied tonnage (μ), the second vessel size (λ, β, δ), the third block coefficient (C_B) and the fourth the drag coefficient (C_D).

Table 3.2 Numerical experiments designed to assess inertial stop capabilities of a reference vessel. Variable indicates the parameter the parameter that is incrementally changed to understand how a vessel would react to small changes.

Parameter	Units	Experiment 1	Experiment 2	Experiment 3	Experiment 4
Weight μ	kg	variable	90,000	90,000	90,000
Length (λ)	m	200	variable	200	200
Beam (β)	m	25	variable	25	25
Draft (δ)	m	15	variable	15	15
Block Coefficient (C_B)		0.8	0.8	variable	0.8
Drag Coefficient (C_D)		0.10	0.10	0.10	variable
Initial velocity (u)	m/s	8	8	8	8
Fluid density (ρ)	kg/m3	1029	1029	1029	1029

3.6.2 Acceleration

The second set of experiments aims to understand how an agent determines r_{opt}, and how it accelerates from a velocity (u) of 0 m/s up to its optimal velocity (u'). The parameters hypothesized to affect propeller speed (r_{opt}) and acceleration ($\dot{u}$) are propeller diameter (κ), the vessel's size (λ, β, δ), block coefficient C_B, and drag coefficient (C_D). Propeller diameter (κ) affects thrust ($\mathcal{T}$), while the vessel's size affects wetted area (α) and thus drag ($\mathcal{D}$). In all experiments, the initial velocity (u) is 0 m/s and the desired velocity (u') is 15 m/s. Table 3.3 contains the parameter settings for each experiment, with the first altering weight (μ), the second altering size (λ, β, δ), the third altering the block coefficient (C_B) and the fourth altering the drag coefficient (C_D).

Table 3.3 Numerical experiments designed to show how certain vessel parameters effect the number of propeller revolutions per second (RPS) required to obtain a desired acceleration.

Parameter	Units	Experiment 1	Experiment 2	Experiment 3	Experiment 4
Weight μ	tonnage	150,000	150,000	150,000	150,000
Length (λ)	m	200	200	Variable	Variable
Beam (β)	m	25	25	Variable	Variable
Draft (δ)	m	15	15	15	Variable
Block Coefficient (C_B)		0.8	0.8	0.8	0.8
Drag Coefficient (C_D)		0.04	0.04	0.04	0.04
Fluid density (ρ)	kg/m3	1029	1029	1029	1029
Thrust Coefficient (K_t)		1.2	1.2	1.2	1.2
Propeller Diameter (κ)	m	9.75	variable	9.75	variable
Initial velocity (u)	m/s	0	0	0	0
Desired velocity (u')	m/s	15	15	15	15

3.6.3 Maneuverability

The next set of experiments examined the maneuverability of vessels and incrementally altered a reference vessel's K and T index. In each experiment, the vessels maintained a velocity of 15 m/s. The

first reference vessel was a 250,000 DWT (μ) tanker, which was 330 m long (λ), 60 m wide (β) and 20 m deep (δ) with a block coefficient (C_B) of 0.8 and drag coefficient (C_D) of 0.004. The second reference vessel was a 40,000 DWT cargo vessel that was 226 m long (λ), 24 m wide (β) and 7 m deep (δ) with a block coefficient (C_B) of 0.6 and drag coefficient (C_D) of 0.004. Table 3.4 lists each maneuvering experiment:

Table 3.4 Numerical experiments showing the effect of K and T on a vessel's maneuverability. Each experiment employed a standard vessel while manipulating K and T.

Experiment	Vessel Type	K	T	Velocity (m/s)
1	Tanker	1.7	3.0	15
2	Tanker	1.7	6.0	15
3	Tanker	3.0	3.0	15
4	Tanker	3.0	6.0	15
5	Cargo	1.5	1.5	15
6	Cargo	1.5	2.5	15
7	Cargo	2.0	1.5	15
8	Cargo	2.0	2.5	15
9	Tanker	1.7	3.0	5
10	Tanker	1.7	6.0	5
11	Tanker	3.0	3.0	5
12	Tanker	3.0	6.0	5
13	Cargo	1.5	1.5	5
14	Cargo	1.5	2.5	5
15	Cargo	2.0	1.5	5
16	Cargo	2.0	2.5	5

3.6.4 Routing

The next set of numerical experiments examines route selection for a population of agents $\{\Gamma_1 \ldots \Gamma_n\}$ and navigational obstructions will affect the route of each agent. A population of 20 agents are created, with 10 in the southwest corner of the study area travelling northeast, and 10 in the northwest corner of the study area traveling southeast. We tested three configurations (including one without any obstructions) and noted the change in routing configuration.

3.6.5 Chaos

Charles Ruelle (1991) discussed the properties of chaotic systems and noted that they are: (1) deterministic, (2) sensitive to initial conditions, and that (3) individual interaction within the modeled system results in emergent properties of interest. For the first two experiments, an input file created *a priori* is loaded into the simulation in repeated trials so that initial conditions match exactly, and parameters of interest are easily altered by small amounts. The initial model run is henceforth known as the 'reference model', and will serve as the standard by which the first two sets of chaos-experiments are assessed against. Each experiment occurred within a rectangular study area 10 km wide by 20 km long with vessels starting in the northwest quadrant and traveling southeast and vessels starting in the southwest quadrant and travelling northeast.

The first of these experiments determines whether or not the system is deterministic. If the model is truly deterministic, it is hypothesized that there will be no difference in position across model runs. The second set of experiments incrementally alter a single vessel parameter ($\Delta\beta, \Delta\delta, \Delta\mu$) on a logarithmic scale (Table 3.). Each experiment contains the same 20 agents, meaning they could be paired and followed in time allowing for an exact measurement of the error (e) in position across model runs in time with:

$$\varepsilon = \sqrt{\left(x^1_{\boldsymbol{p}_0} - x^0_{\boldsymbol{p}_0}\right)^2 + \left(y^1_{\boldsymbol{p}_0} - y^0_{\boldsymbol{p}_0}\right)^2} \qquad \textbf{3.36}$$

Where $(x^0_{\boldsymbol{p}_0}, y^0_{\boldsymbol{p}_0})$ is the position of the agent Γ_o within the reference model at time t, and $(x^1_{\boldsymbol{p}_0}, y^1_{\boldsymbol{p}_0})$ is the position of the agent Γ_o at time t within the current experiment iteration. Table 3.5 lists the change in vessel parameter for each set of experiments (β, δ, μ)

Table 3.5 Numerical experiments designed to test for the presence of chaos. Is the ABM deterministic yet sensitive initial conditions?

Model Run	Beam ($\Delta\beta$)	Draft ($\Delta\delta$)	Mass ($\Delta\mu$)
Reference	0	0	0
1	0	0	0
2	0.001	0.001	1
3	0.002	0.002	2
4	0.003	0.003	3
5	0.004	0.004	4
6	0.005	0.005	5
7	0.006	0.006	6
8	0.007	0.007	7
9	0.008	0.008	8
10	0.009	0.009	9
11	0.010	0.010	10
12	0.020	0.020	20
13	0.030	0.030	30
14	0.040	0.040	40
15	0.050	0.050	50
16	0.060	0.060	60
17	0.070	0.070	70
18	0.080	0.080	80
19	0.090	0.090	90
20	0.100	0.100	100
21	0.200	0.200	200
22	0.300	0.300	300
23	0.400	0.400	400
24	0.500	0.500	500
25	0.600	0.600	600
26	0.700	0.700	700
27	0.800	0.800	800
28	0.900	0.900	900
29	1.000	1.000	1000

The final chaos experiment assesses whether or not the simulation is capable of producing complex emergent phenomena of interest to the marine spatial planner. In a seminal paper on traffic jams, Lighthill and Whitham (1955) describe a jam as a 'hump or region of increased concentration' that propagates along a crowded main road, and coined the phenomena 'kinematic waves'. This simulation seeks to produce those waves as described by Lighthill and Whitham (1955). The experiment purposefully set up a navigational bottle neck and forced a population of agents through the narrow pass (Figure 3.16). Following the experiment, the agents speed and location along the x-axis were plotted and assessed for kinematic waves.

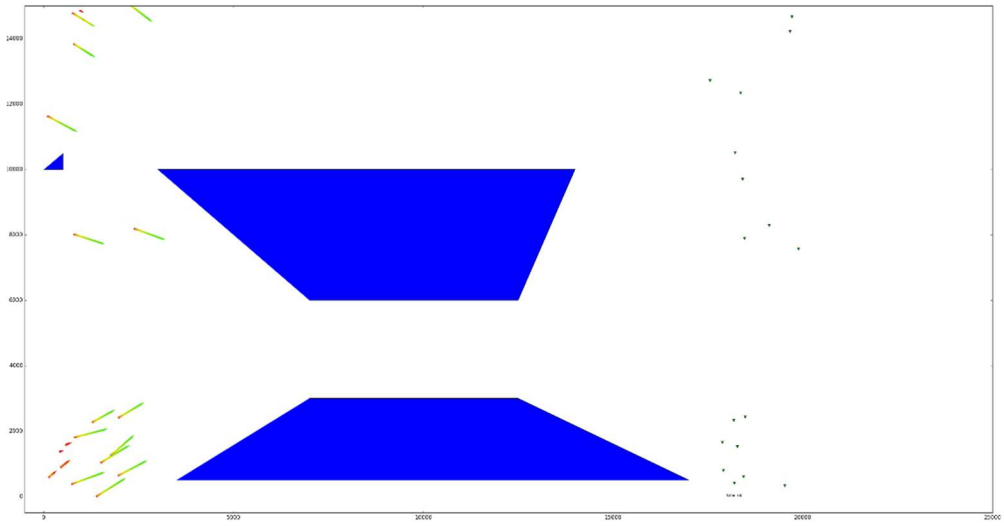

Figure 3.16 depicts a screen shot of the simulation purpose built to produce kinematics waves. The study area forces all agents through a bottle neck on their way towards the destination. In all cases, vessels either start in the northwest with destinations in the southeast, or from the south west with destinations in the northeast. The vessel track lines are present and are shaded according to their velocity. As vessels approach their desired velocity, they turn green, while stopped vessels appear read.

3.7 Application

The Bureau of Ocean Energy Management (BOEM) has located a wind energy area (WEA) between two shipping channels within the approach to the Port of New York and New Jersey (**Error! Reference source not found.**). The WEA represents foregone space that commercial shipping could have once occupied. The USCG fears that displacement can result in an increase in risk due to vessels navigating in closer proximity to each other than they would otherwise in an open ocean scenarios, and they have recommended creating modeling and analysis tools that are capable of predicting changes in vessel traffic patterns (USCG, 2016). Our ABM of commercial shipping simulated the sector's response to the planned wind energy area, and attempted to identify emergent pattern resulting from displacement. However, before we could proceed with the simulation, we need to generate an input file that is reflective of the sector as it operates within the project area to inform the model's input parameters.

During ABM initialization, we pass along an input file that is designed to reproduce conditions of the study area, including the relative proportion of each vessel type, their maneuvering characteristics, direction of movement, origins, destinations and basic vessel parameters. Input data for the ABM relies upon statistics generated from AIS data of the study region (BOEM 2014). To generate the input file, we first generate a list of agent vessel classes of length n with `numpy.random.choice` (Van Der Walt, Colbert and Varoquaux 2011). The vessel class can have one of two values: 'cargo' or 'tanker'. The probability of either vessel-class is not uniform, but rather is represented as the relative proportion of each vessel type as given with AIS data.

Next, we assign the agents K-T indices. Kawaguchi et al. (2004) provided the only published range of K-T indices for cargo and tanker vessels. Therefore, the K-T indices for the agents in this application are not representative of the regional sector, but instead are generated with draws from uniform random probability distributions (Table 3.6).

Table 3.6 *Uniform random probability distributions for K and T indices by vessel type.*

Vessel Type	K	T
Cargo	$\mathcal{U}(1.5,2.0)$	$\mathcal{U}(1.5,2.5)$
Tanker	$\mathcal{U}(1.7,3.0)$	$\mathcal{U}(3.0,6.0)$

Vessel traffic within the study region is bidirectional with incoming and outgoing traffic. The input file generation procedure chooses direction randomly with draws from a multinomial probability distribution with the proportion of incoming traffic at 0.75 and outgoing at 0.25. Incoming traffic may originate from one of three channels, the Nantucket to Ambrose, Hudson Canyon to Ambrose or Barnegat to Ambrose (Figure 3.2). All incoming traffic is destined for one of two locations, Port Jersey or Port Elizabeth (Figure 3.2). Outgoing traffic may originate from either Port Elizabeth or Port Jersey (Figure 3.2) and is destined for either the Ambrose to Nantuket, the Ambrose to Hudson Canyon or the Ambrose

to Barnegat channel (Figure 3.2). The assignment of origins and destinations is uniform and random. Following the assignment of origins and destinations, we then generate vessel parameters.

After implementing the input data generation procedure and ensuring that it approximates the regional sector, we can proceed to the ABM itself. The application was not just one model run, but rather a series of simulations that altered the number of agents (n) at each iteration. We ran 100 simulations with the WEA present, and 100 without it. After each simulation, we analyzed the event log and calculated the the average time agents spent repulsed by other agents or obstacles, the number of crashes that occurred and when and where they occurred, the average duration of the first voyage, the average distance travelled per agent, and the average velocity per agent. We designed the indicator statistics in such a manner that we could assess the socio-economic well-being of the system following change, either through an increase in the number of agents or the presence of the wind farm. When agents feel repulsive forces, they are at risk of collision. The more time they are at risk, the greater the likelihood that they will crash. Also, shipping companies make profit by minimizing travel costs, the longer their duration or greater the distance travelled, the more their profit is reduced.

3.8 Summary

We described the ABM of the navigational approach to the Port of New York and New Jersey within the Overview, Design Concepts, and Details (ODD) framework. We presented ABM in a hierarchical manner as an overview of model structure and processes followed by details on those processes. The ABM incorporates route finding, collision avoidance, throttle control and movement modules based on classical mechanics to control the behavior ship-agents. We also implemented a calibration procedure that is capable of identifying K-T indices from vessel parameters commonly found and displayed within the bridge of every ship. Following calibration, we designed a series of experiments to assess whether or not the model is capable of simulating a complex adaptive system. After validating

the model, we finally simulated the approach to the Port of New York and New Jersey, and modeled the impact to the sector with and without the proposed WEA.

Chapter 4

Results

4.1 Introduction

This chapter presents the results of the ABM of commercial shipping, which was designed to quantify displacement related effects from the location of an offshore wind farm within close proximity to a navigational channel. The first section contains a set of numerical experiments that show how vessel parameters effect an agent's maneuverability and behavior. The next set of experiments look for signals evident of complex interaction. Following this section, are the results of the numerical calibration and validation procedures. Then, we describe the study area and spatial patterns of shipping. The final

section discusses the results of the ABM and identifies the impacts, if any, of the proposed wind farm on the navigability of the entrance to the Port of New York and New Jersey.

4.2 Numerical Models

We designed a series of experiments to understand how the agents move (stop, accelerate, and turn) and find their way within the study area. With each experiment, we incrementally vary a few key parameters in the model and study how an agent responds. This broadens our understanding of how agents navigate through their virtual environment and allows us to explain and eventually validate their behavior. The first set of these experiments examines the inertial stopping capabilities of large commercial ships with great momentum.

4.2.1 Inertial Stop

When $r = 0$, the propeller is not producing any thrust and the force of drag slows the vessel down. With the velocity at time (t) given with eqn 3.3, we assume that an agent's tonnage, hull size, shape and drag coefficient affect its ability to stop. In all experiments, the initial velocity was set at 8 m/s or 15.5508 knots and the fluid density (ρ) remained constant at 1029 kg/m^3. The first experiment varied tonnage, while the second increased the size of the hull, the third varied the shape of the hull, and the fourth varied the reference hull's drag coefficient.

Table 4.1 Results of the first inertial stop microsimulation varying vessel tonnage (DWT). The noted velocity and displacement occurred at 7200 seconds.

Agent	DWT	Velocity at 7200s (m/s)	Displacement at 7200s (m)
1	20000	0.01	546.67
2	40000	0.02	977.37
3	60000	0.03	1,364.52
4	80000	0.05	1,723.55
5	100000	0.06	2,061.70
6	120000	0.07	2,383.27
7	140000	0.08	2,691.09
8	160000	0.09	2,987.16
9	180000	0.10	3,273.00
10	200000	0.11	3,549.78

The first experiment incrementally increased tonnage (μ) while holding wetted area (α) and block coefficient (C_B) constant. The heavier a vessel becomes, the more momentum it has, and the lower the rate at which it slows down under inertial stopping conditions (Table 4.1). Therefore, a lighter vessel will travel much shorter distances during inertial stop than a heavier vessel. At 7200 seconds, a 20,000 DWT vessel is displaced by 546.67 m, while a 200,000 DWT vessel will travel over 3 km (3,549.78 m). Figure 4.1 contains the results of the first numerical experiment, note as the vessel tonnage (DWT) increases, so does the velocity at 7200 s and its subsequent displacement. The top panel of Figure 4.1 shows velocity over time while the bottom panel displays displacement at time *t*.

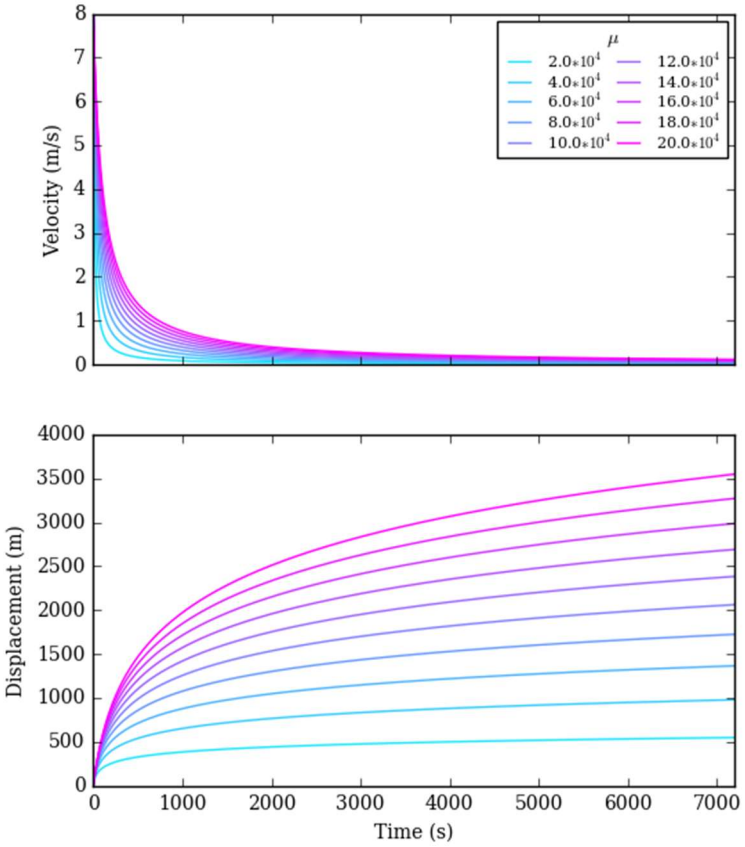

Figure 4.1 is a graphical depiction of velocity (top) and displacement (bottom) over time during the first inertial stop simulation. Colors represent increasing vessel tonnage as noted in the legend.

The second experiment increased the size of the hull (and subsequently wetted area, α) while holding tonnage (μ) and the block coefficient (C_B) constant (Table 4.2). As the wetted area becomes larger, resistance increases and the vessel will decelerate faster. This experiment incrementally decreased the basic hull dimensions of length (λ), width or beam (β) and depth or draft (δ), thus decreasing the wetted area (α). At 7200s, a 10,550 m^2 vessel would slow down to 0.05 m/s covering a distance of 1,894 m while a 1583.49 m^2 vessel slows to 0.33 m/s and covers 7961.57 m (Table 4.). Figure 4.2 displays velocity (top) and displacement (bottom) at time (t).

Table 4.2 *Results of the second inertial stop microsimulation varying wetted area. As wetted area increases the vessel will slow down more quickly than a smaller vessel because it has more resistance.*

Agent	L (m)	B (m)	T (m)	Wetted Area (A)	Velocity (m/s)	Displacement (m)
1	200.0	25.0	15.0	10,550	0.05	1,894.92
2	180.0	22.5	13.5	8,545.50	0.06	2,242.20
3	162.0	20.25	12.15	6,921.86	0.08	2,648.35
4	145.8	18.23	10.94	5,606.70	0.10	3,122.35
5	131.22	16.40	9.84	4,541.43	0.12	3,672.64
6	118.10	14.76	8.86	3,678.56	0.15	4,310.54
7	106.28	13.29	7.97	2,979.63	0.18	5,046.72
8	95.66	11.96	7.17	2,413.50	0.22	5,892.74
9	86.10	10.76	6.46	1,954.94	0.27	6,860.44
10	77.48	9.69	5.81	1,583.50	0.33	7,961.57

The third experiment decreased the block coefficient (C_B) while holding wetted area (α) and tonnage (μ) constant. The block coefficient (C_B) effects the hull's wetted area (3.26). The larger the coefficient, the more "brick-like" the hull. Thus, a small coefficient equates to a very streamlined hull with a smaller wetted area. As the block coefficient increases, so does wetted area, which increases resistance allowing a vessel to decelerate faster (Table 4.3). While this relationship holds, velocity is not affected much by the change in block coefficient (Figure 4.3). For a 61% reduction in a hull's block coefficient (0.8 - 0.31), the velocity at 7200 seconds only decreases by 38%.

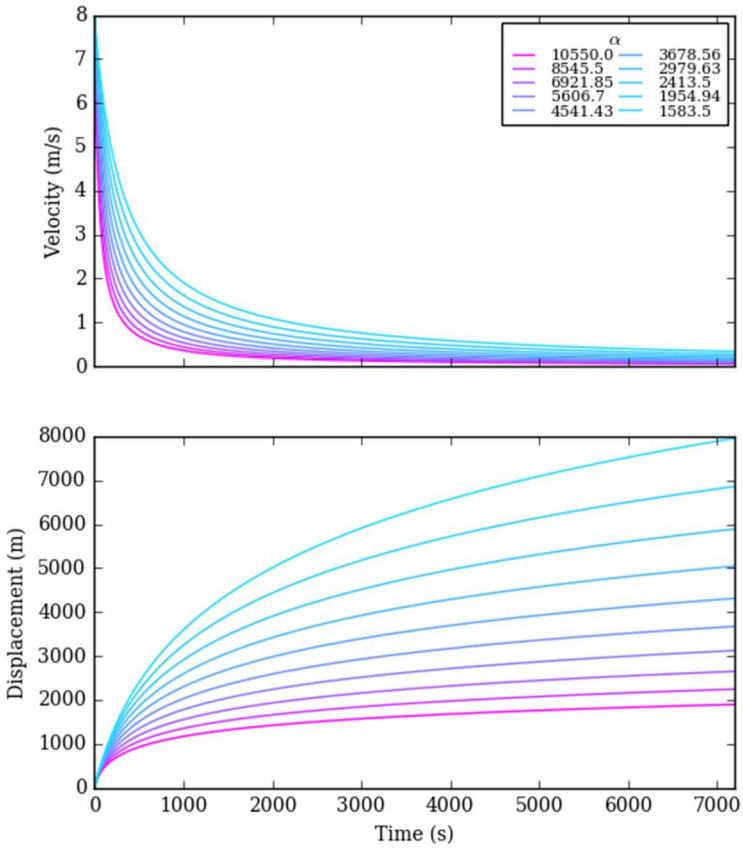

Figure 4.2 Graphical depiction of velocity (top) and displacement (bottom) over time during the second inertial stop simulation varying the size of the hull. Colors represent increasing hull size (m2) as noted in the legend.

Table 4.3 *results of the third inertial stop microsimulation that alters the block coefficient of a vessel's hull. As the block coefficient decreases, the hull becomes more streamlined and displacement and velocity at 7200 seconds increases.*

Agent	Block Coefficient (C_B)	Velocity (m/s)	Displacement (m)
1	0.8	0.05	1,894.92
2	0.72	0.05	1,967.00
3	0.65	0.06	2,037.23
4	0.58	0.06	2,105.32
5	0.53	0.06	2,171.02
6	0.47	0.06	2,234.13
7	0.42	0.07	2,294.48
8	0.38	0.07	2,351.95
9	0.34	0.07	2,406.46
10	0.31	0.07	2,457.95

The fourth inertial stop experiment increased drag coefficient (C_D) while holding wetted area (α), tonnage (μ), and block coefficient (C_B) constant. As the drag coefficient increases, the rate at which an agent decelerates is greater (Table 4.4). From Figure 4.4, velocity over time appears similar across increasing drag coefficients, however the hypothesized trend holds. A vessel with a higher drag coefficient has more deceleration than a vessel with a low drag coefficient.

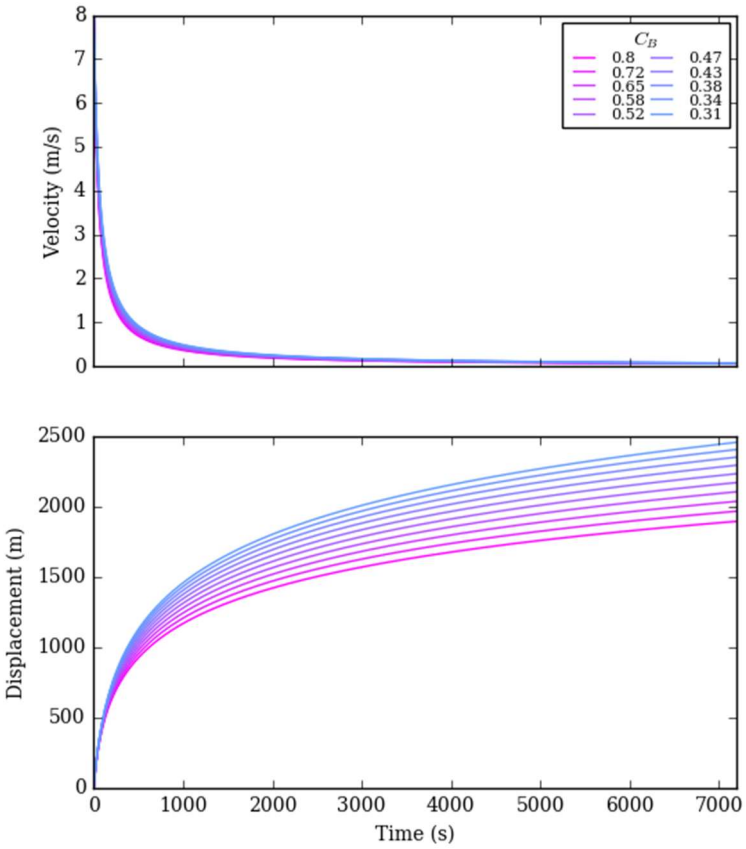

Figure 4.3 Graphical depiction of velocity (top) and displacement (bottom) over time during the third inertial stop simulation varying the block coefficient of a hull. Colors represent increasing block coefficient (CB) as noted in the legend.

Table 4.4 results of the fourth inertial stop microsimulation varying drag coefficient while holding wetted area, tonnage and block coefficient constant. As drag coefficient increased, so does resistance. Therefore, the velocity and displacement at 7200 seconds decreases.

Agent	Drag Coefficient (C_D)	Velocity (m/s)	Displacement (m)
1	0.04	0.05	1,894.92
2	0.04	0.05	1,755.07
3	0.05	0.04	1,625.01
4	0.05	0.04	1,504.11
5	0.06	0.04	1,391.77
6	0.06	0.03	1,287.45
7	0.07	0.03	1,190.59
8	0.08	0.03	1,100.72
9	0.09	0.02	1,017.36
10	0.09	0.02	9,40.06

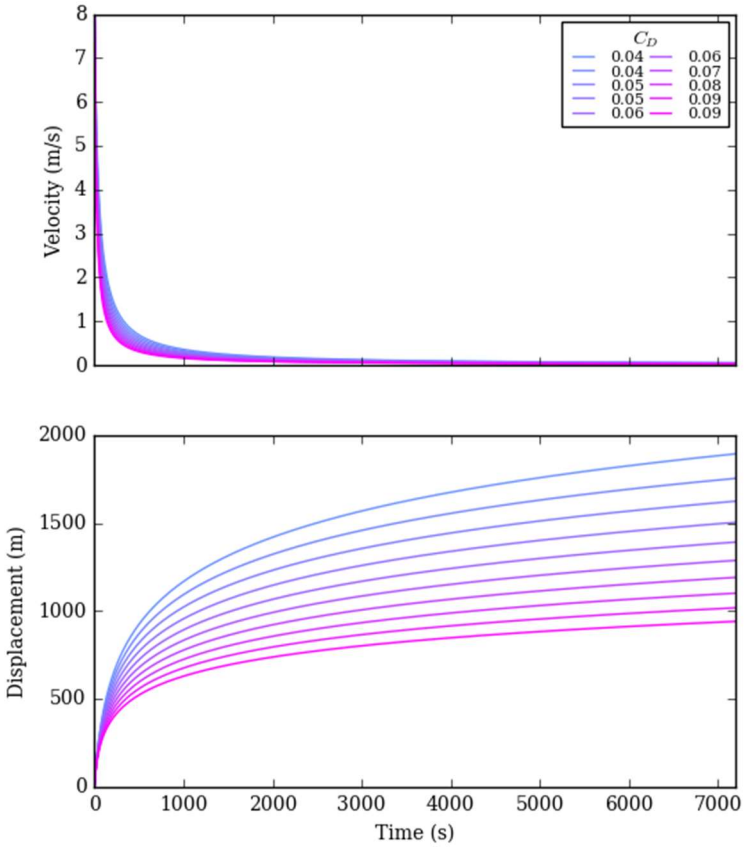

Figure 4.4 Graphical depiction of velocity (top) and displacement (bottom) over time during the fourth inertial stop simulation varying the drag coefficient of a hull. Colors represent increasing hull size (m2) as noted in the legend. As the coefficient increases, so does the rate of deceleration.

4.2.2 Acceleration

The next series of experiments uncovered how agents control their throttle and accelerate. In each experiment, an agent starts from a dead stop (0 m/s) and accelerates until it reaches the desired

velocity (15 m/s), all while continuously varying throttle (r) according to equation 3.23. The first experiment examines how the forces of thrust and resistance counterbalance as an agent accelerates, while the second incrementally varies propeller diameter, and the third varies size of the hull.

In each experiment, an agent starts from a dead stop and accelerates until it reaches its optimal velocity (15 m/s ≈ 30 knots). Initially, the velocity is low and RPS (r) high, meaning that there is little resistance and high rate of acceleration. As the agent approaches the optimal velocity, it throttles down by lowering r so as not to overshoot its goal. When the desired velocity is achieved, thrust counterbalances resistance and the agent maintains velocity.

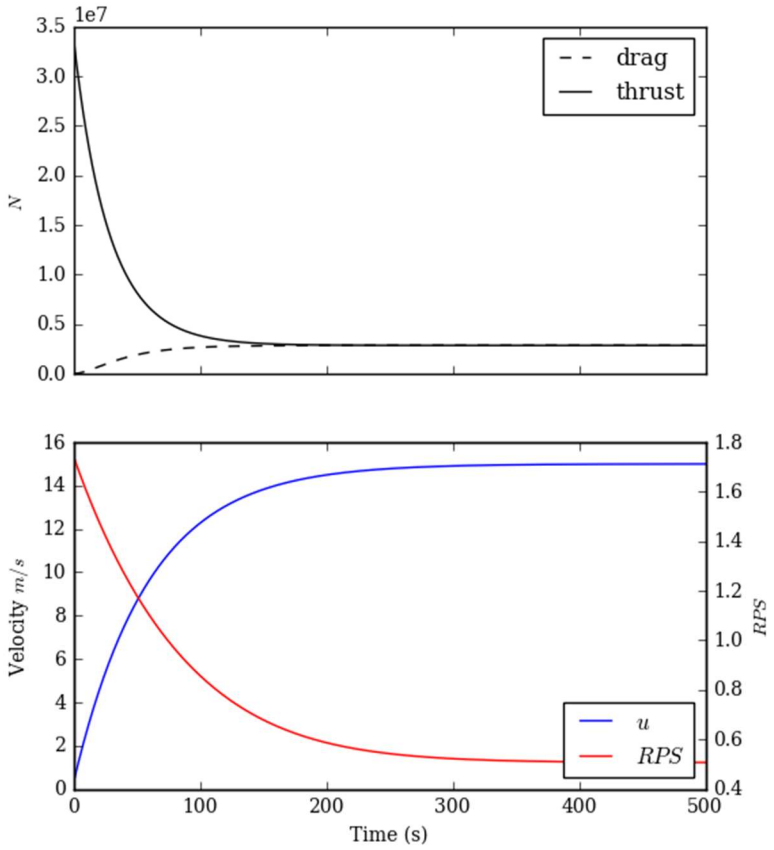

Figure 4.5 results of the first throttle experiment. The top panel shows the initial disparity between drag and thrust as the vessel accelerates towards the optimal velocity setting. Over time, as the vessel approaches 15 m/s, thrust is reduced until it equals drag and the vessel maintains speed. In the bottom panel, velocity in m/s is on the primary y-axis while RPS is on the secondary y-axis.

In the first experiment, a reference vessel (table 3.3) accelerates from 0 m/s until the desired velocity of 15 m/s is met. In the top panel of Figure 4.5, thrust (measured in newtons, N) is much greater than drag (also measured in N) and the vessel accelerates. As the desired velocity is met, thrust equals drag and the vessel maintains velocity. The lower panel displays velocity on the primary y-axis while r (RPS) is on the secondary y-axis. Note as the vessel accelerates, the agent will decrease r so it does not overshoot the desired velocity.

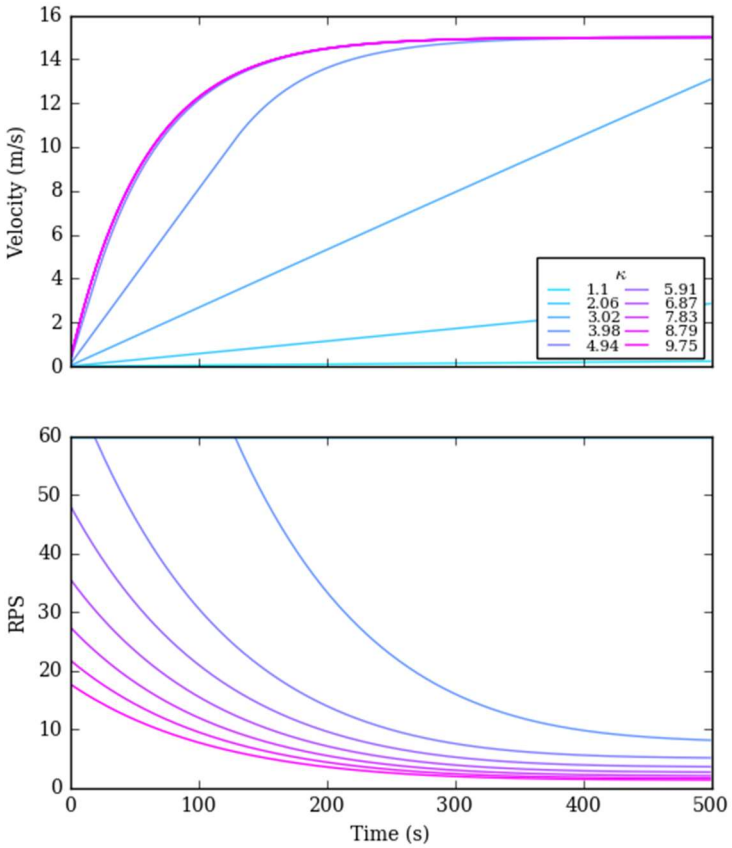

Figure 4.6 Results of the second set of thrust experiments altering propeller diameter. The top panel displays velocity over time while the bottom panel displays the RPS setting. Note the undersized propeller diameter of 1.1 m, the agent maximizes the RPS setting at 60 (3600 RPM) and the vessel takes much longer to reach the desired velocity. An undersized propeller means the engine must work harder to achieve the same velocity.

The second experiment incrementally reduced propeller diameter (κ) while holding wetted area (α) constant. As the propeller diameter is decreased, the number of revolutions per second (r) needed to

maintain the same rate of acceleration as larger propellers increases (Figure 4.6). The figure depicts a critical propeller diameter (1.1 m) where the number of revolutions required exceeds the capacity of the engine (60 RPS = 3600 RPM) and the engine cannot spin fast enough to maintain acceleration. However, at all other diameters tested, the propeller is able to produce the same amount of thrust, with smaller propellers requiring higher RPS.

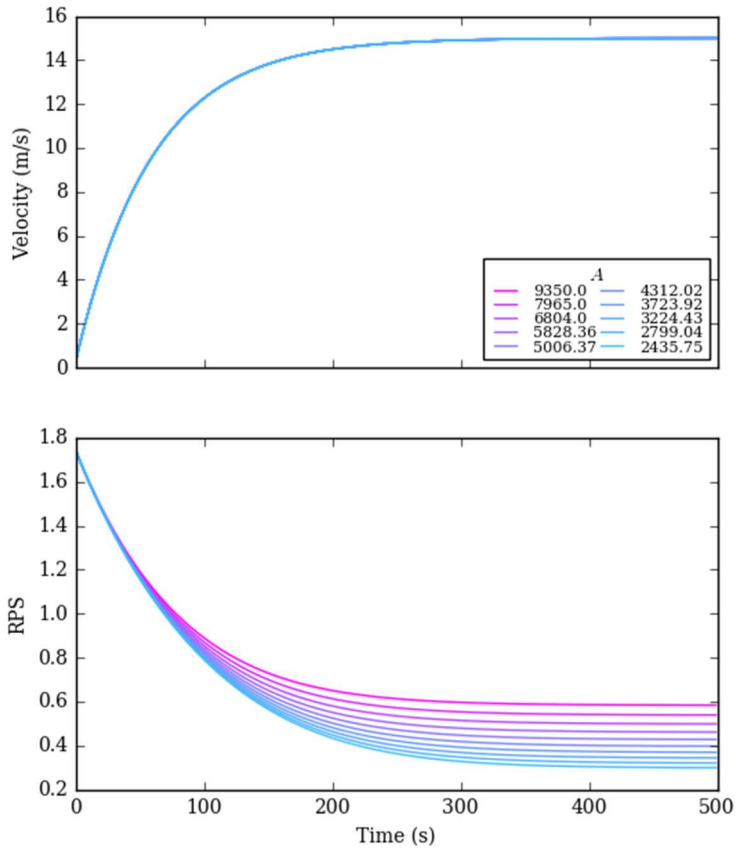

Figure 4.7 Results of the third thrust experiment altering the size of the hull. As the size of the hull increases, so does the resistance, therefore more RPS are required to produce more thrust to maintain the desired velocity.

The third thrust experiment varied the hull's cross sectional area. As cross sectional area increases the amount of revolutions required to sustain sufficient thrust over time also increases, because a larger hull (m^2) generates more drag (Figure 4.7). While we increase the size of the hull in this experiment, the propeller is never undersized and the same velocity profile is achieved with each iteration.

4.2.3 Vessel Maneuverability

The next set of numerical experiments assessed the maneuverability of vessels by altering their respective K and T indices (refer to Table 3.4). The experiments used a standard tanker (250,000 DWT, 330 L, 60 B, 20 T, 0.8 C_B, and 0.004 C_D) and cargo vessel (40,000 DWT, 226 L, 24 B, 7 T, 0.6 C_B, and 0.004 C_D) that incorporated the minimum and maximum published K-T indices (Table 3.1) while simulating a port side turn at low and high speeds (see Table 3.4). In each experiment, the test vessel maintains a straight course for 100 time steps, then it makes a turn to port and maintains a constant rudder angle for the next 400 time steps.

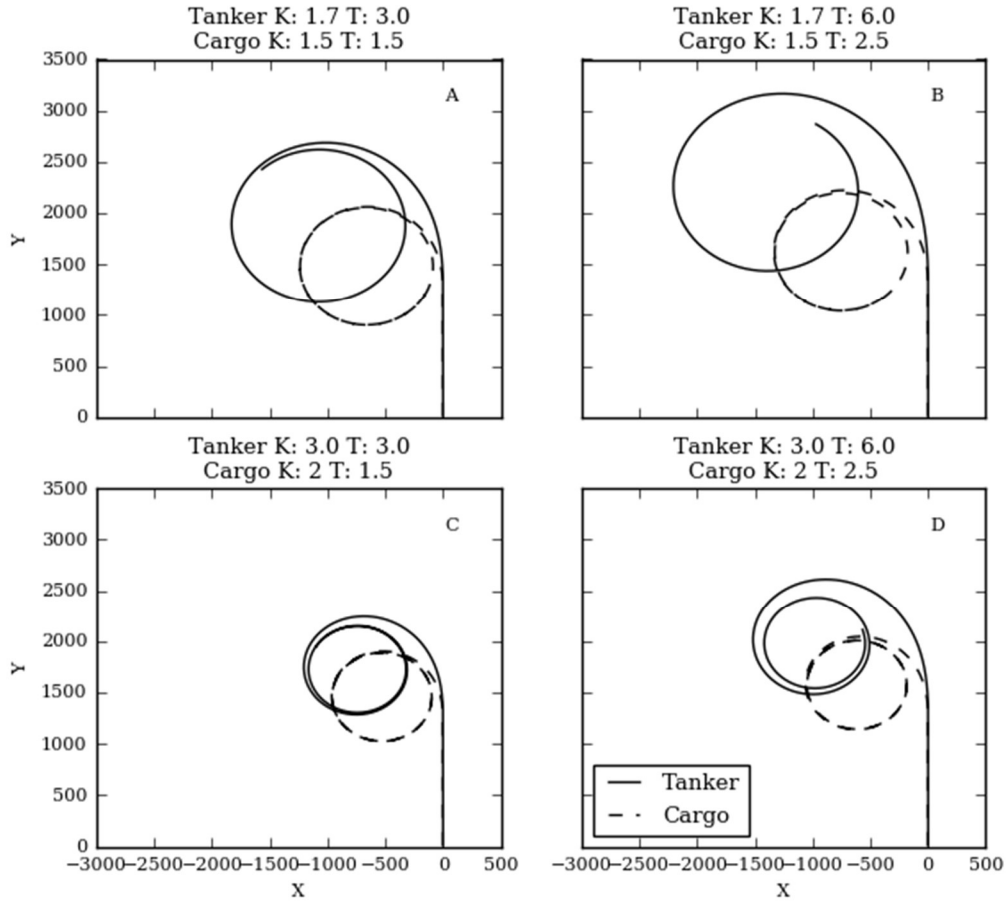

Figure 4.8 depicts the high velocity scenario turning radius tests. Refer to table 3.4 for K-T parameters. Plot A experiments 1 and 4, plot B experiments 2 and 5, plot C experiments 3 and 6 and plot D experiments 4 and 7. Note smaller K' values result in a larger turning radius.

Figure 4.8 displays the results of the high velocity (15 m/s) scenarios, with each subplot having the same X and Y scale. The first sub plot (A) simulates a left turn with minimum published K and T index for Tanker and Cargo vessels (experiments 1 and 5 on table 3.4). Note the cargo vessels (dashed lines) are able to make a much tighter turn than the tanker (solid line). Subplot B displays experiments 2 and 6, subplot C displays experiments 3 and 7 and subplot D shows experiments 4 and 8. Note, smaller K values (plots A and B) result in a larger turning radius. Similar results were obtained in Figure 4.9, however, due to the lower velocity the vessels were not capable of completing a full turn and the overall displacement was much lower.

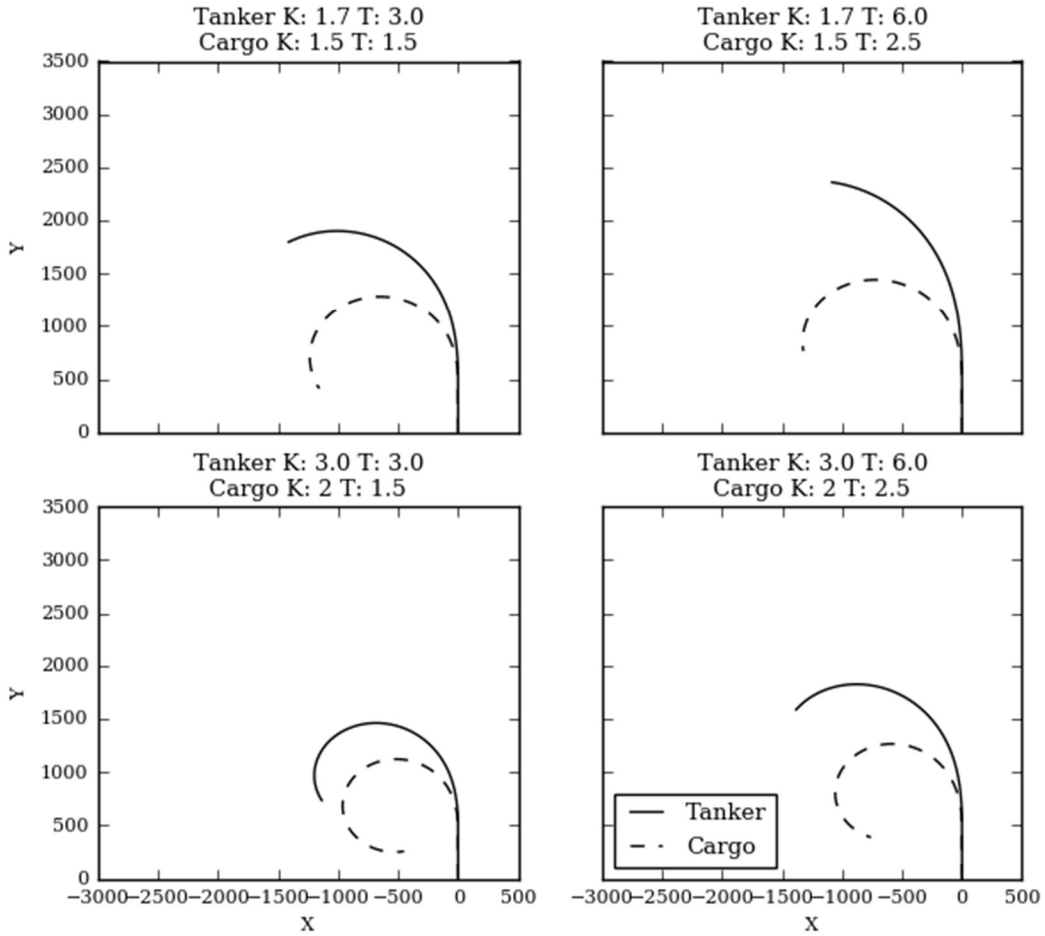

Figure 4.9 low velocity scenario turning radius tests. Refer to table 3.4 for K-T parameters. Plot A contain experiments 9 and 13, plot B experiments 10 and 14, plot C experiments 11 and 15 and plot D experiments 12 and 16. Note smaller K' values result in a larger turning radius.

The vessel with the worst turning performance was the tanker vessel with a K of 1.7 and T of 6.0. The turning radius was much larger than all other vessels, and it did not make it as far around the circle compared with others. The vessel with the tightest turning radius was the cargo vessel with a K of 2.0 and T of 1.5. When velocity is decreased, the vessel made tighter turns.

4.2.3 Route Planning

The Euclidean shortest path (ESP) algorithm created routes for each agent that depended on their initial location, destination, and all known obstacles. The study area was a simple 20 x 10 km rectangle. The initial locations and destinations of each agent were random within a quadrant with ten vessels starting in the northwest and ending in the southeast, and ten vessels starting in the southwest and end in the northeast. The first route planning experiment (Figure 4.10) did not have any obstacles, and the ESP algorithm identified the shortest path for each agent as a straight line. Note the ESP algorithm does not plan routes around other agents, rather each agent is responsible for collision avoidance within every time step.

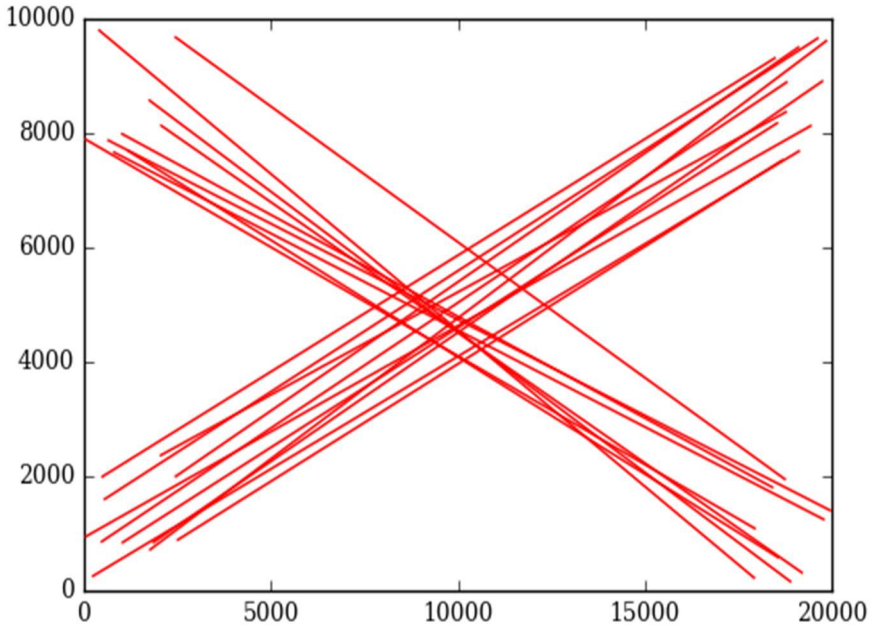

Figure 4.10 Result of 20 agents implementing the ESP algorithm from their starting locations without any obstacles present. Note the ESP algorithm does not plan around the route of other agents, rather it is up to each agent within each time step to avoid collision using the collision avoidance procedures identified in section 3.xx of the methods.

The next two figures, Figure 4.11 and Figure 4.12 show the results of the ESP algorithm with two obstacle configurations. The introduction of obstacles creates choke points where agent routes converge around the corners of obstructions. In these locations, agents will compete for space increasing the risk of interaction and possible collision. The COLREGs state that vessels on the left must yield, and give way, meaning the repulsive forces may push the agent towards an obstacle, force further interaction, and initiate obstacle collision avoidance procedures. These figures show an unintended consequence of locating a wind farm in navigable water, displacement will lead to routing scenarios where multiple ships aggregate into choke points around obstacles.

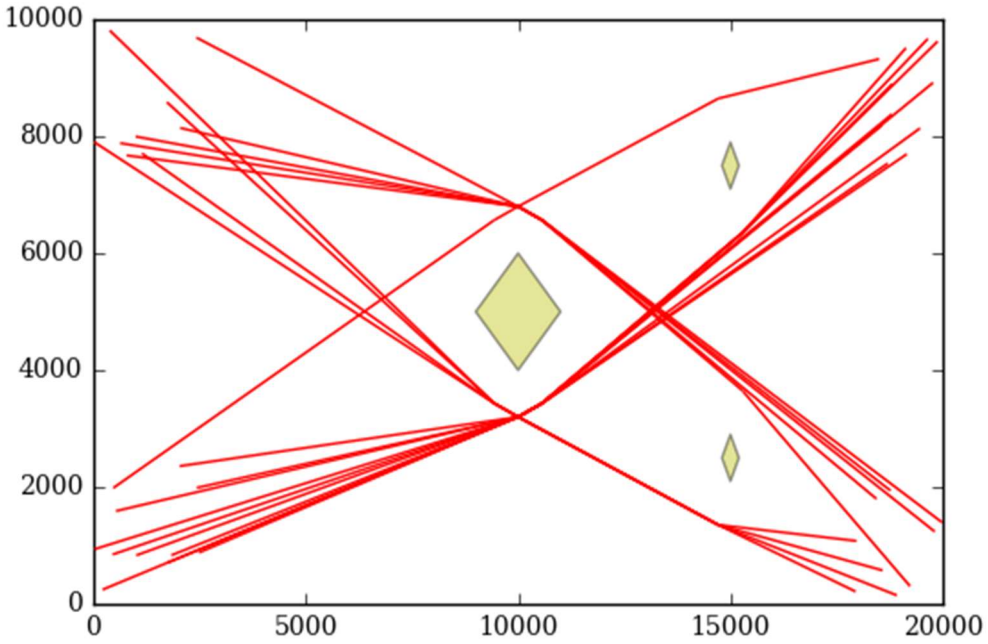

Figure 4.11 Results of the ESP algorithm with twenty agents and 3 obstacles. Note the convergence of routes around obstacles forming "choke points".

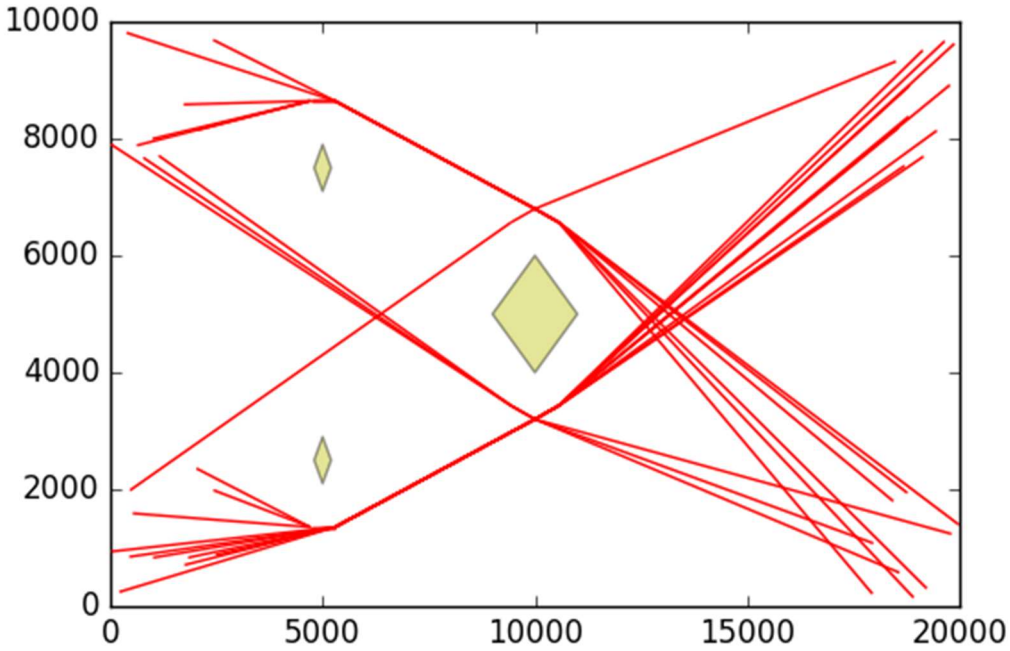

Figure 4.12 Results of the ESP algorithm with twenty agents and three obstacles. Note the convergence of routes around obstacles forming "choke points".

4.3 Chaos Experiments

The following experiments assessed whether or not the proposed agent based model is capable of exhibiting chaotic behavior. Charles Ruelle (1991) discussed the properties of chaotic systems and noted that they are (1) deterministic, are (2) sensitive to initial conditions, and that (3) individual interaction within the modeled system results in emergent properties of interest. For the first two experiments, an input file was created *a priori* allowing us to match initial conditions match exactly or alter specific parameters by small amounts. The initial model was the reference model, and serves as the standard by which the first two sets of chaos-experiments are assessed against. To determine whether or not the ABM was sensitive to initial conditions, we tested the same 20 agents in each iteration by incrementally changing the beam (β), draft (δ) and weight (μ) of each agent allowing for a measurement of error (ε) in position across model runs with equation 3.36. Each experiment occurred within a rectangular study area 10 km wide by 20 km long with vessels starting in the northwest quadrant and traveling southeast and vessels starting in the southwest quadrant and travelling northeast.

The first experiment tested whether or not the ABM was deterministic. For this experiment, we used the same input file from the reference model, meaning that there were no changes in vessel parameters. In each figure, we find no error in vessel position (Euclidean distance between positions in time) between model runs (Figure 4.13 - Figure 4.15) signaling that the model is deterministic. The next set of experiments incrementally varied beam, draft and weight according to Table 3.5.

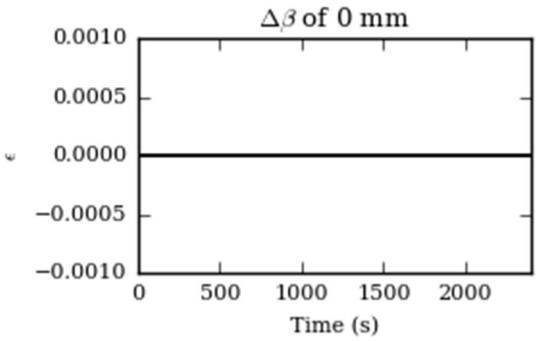

Figure 4.13 Two separate model runs with identical starting conditions and no change in beam (β)

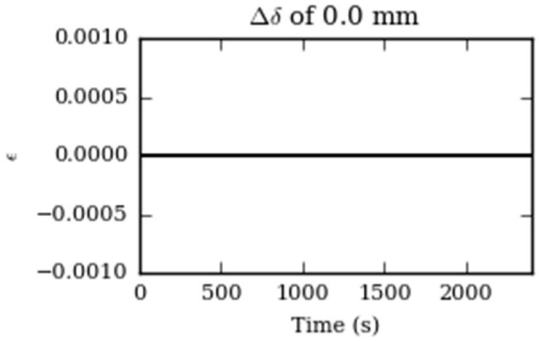

Figure 4.14 Two separate model runs with identical starting conditions and no change in draft (δ)

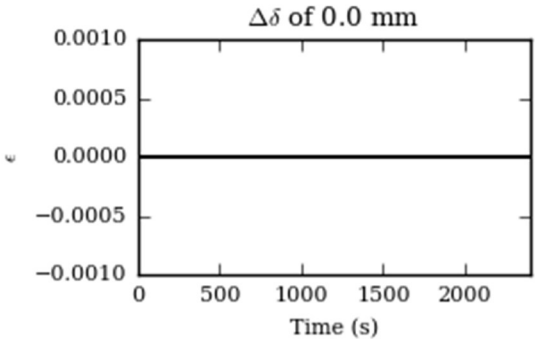

Figure 4.15 Two separate model runs with identical starting conditions and no change in tonnage (μ).

By incrementally altering beam (β), draft (δ) and tonnage (μ) by small amounts, the performance characteristics of an individual vessel changes, which affects the displacement of a vessel between time steps. This means the timing and location of vessel interactions change, which leads to unforeseen and profound (chaotic) changes in system state. Increasing beam (β) affects the wetted area of a hull, which changes resistance ($\mathcal{D}$, eqn 3.25). The more wetted area (α), the more resistance ($\mathcal{D}$). Increasing draft (δ)

also affects the wetted area (α), however there is also a design relationship between draft and propeller diameter (κ). Increasing the draft allows for a larger propeller diameter, the larger the propeller more thrust ($\mathcal{T}$, eqn 3.27). Lastly, tonnage (μ) effects acceleration, the heavier the vessel, the lower the rate of deceleration.

We found the ABM to be sensitive to changes in beam (β). A 1.0 mm change in beam leads to a 0.25 m error (ε) for an individual agent at 1000 seconds, while a change of 1,000 mm leads to an error in 10 km. Aside from the drastic error in position across simulations, no discernable pattern exists between simulations (Figure 4.16 - 4.19). We found displacement error (ε) between simulations chaotic and sensitive to small changes in beam.

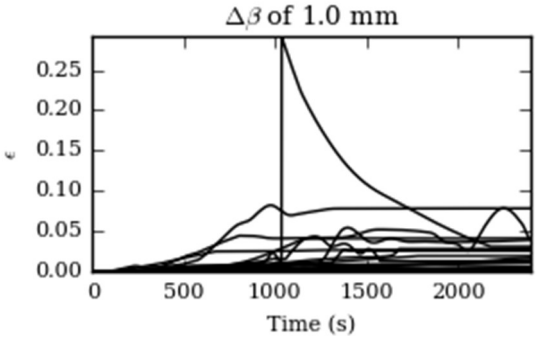

Figure 4.16 Results of experiment changing the beam of each agent by 1.0 mm. Note, each line is a separate agent.

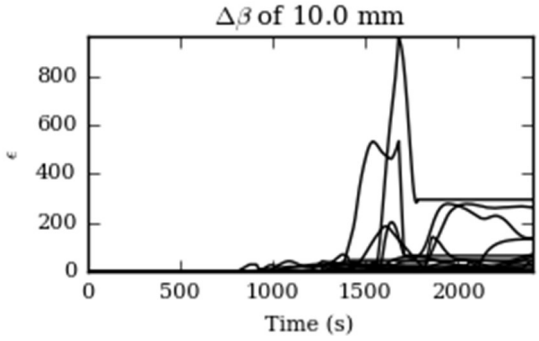

Figure 4.17 Results of experiment changing the beam of each agent by 10.0 mm. Note, each line is a separate agent.

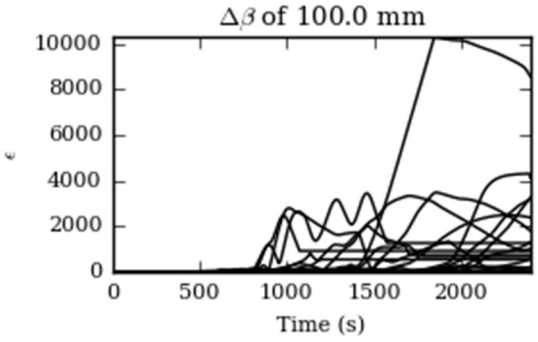

Figure 4.18 Results of experiment changing the beam of each agent by 100.0 mm. Note, each line is a separate agent.

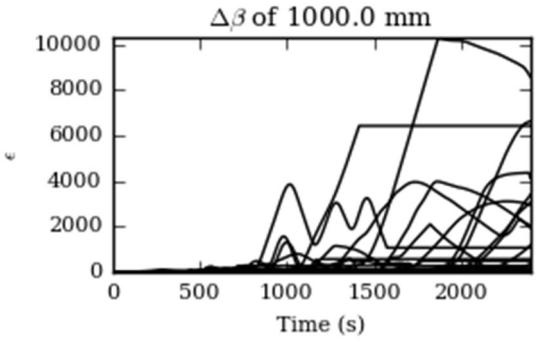

Figure 4.19 Results of experiment changing the beam of each agent by 1000.0 mm. Note, each line is a separate agent.

We also found the ABM sensitive to small changes in draft (δ). A 1.0 mm change in draft can cause an error in displacement of 10 km (Figure 4.20), while a change in 10.0 mm causes an error in 6 km (4.21). Further, there is no discernable pattern across experiments. This unpredictable nature in displacement error (ε) across simulations is a true signal of chaos.

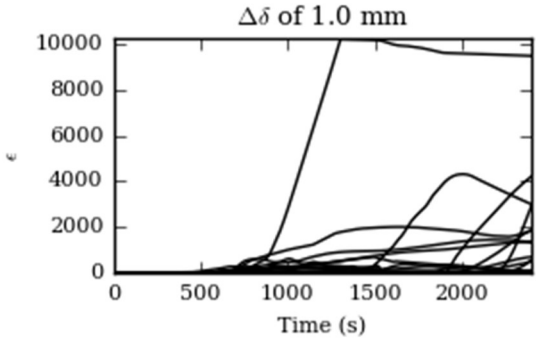

Figure 4.20 Results of experiment changing the draft of each agent by 1.0 mm. Note, each line is a separate agent.

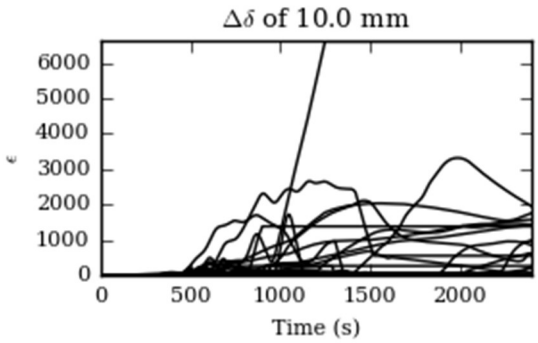

Figure 4.21 Results of experiment changing the draft of each agent by 10.0 mm. Note, each line is a separate agent.

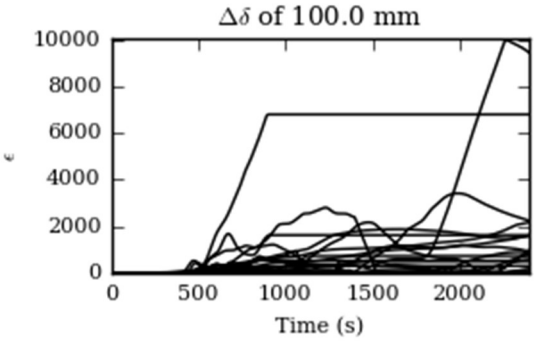

Figure 4.22 Results of experiment changing the draft of each agent by 100.0 mm. Note, each line is a separate agent.

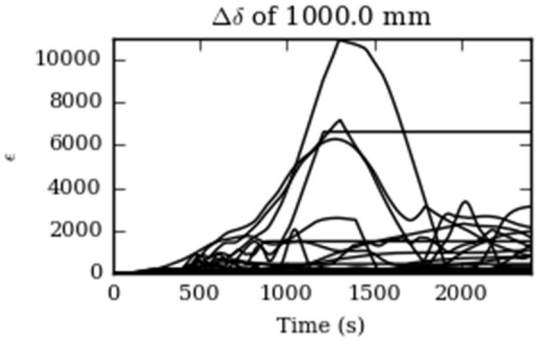

Figure 4.23 Results of experiment changing the draft of each agent by 100.0 mm. Note, each line is a separate agent.

The final experiment incrementally varied vessel tonnage (μ). Unlike beam (β) and draft (δ), the displacement error (ε) pattern after a 1-unit (Figure 4.24), 10-unit (Figure 4.24) and 100 DWT change (Figure 4.25) were similar, albeit orders of magnitude apart. It wasn't until a change in 1,000 DWT (Figure 4.27) where an unpredictable change in pattern occurred. However, significant and unpredictable changes from the reference model still occurred, and the ABM was still sensitive to changes in tonnage.

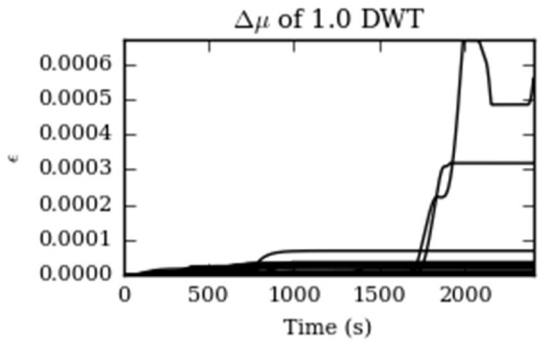

Figure 4.24 Results of experiment changing the tonnage of each agent by 1.0 DWT. Note, each line is a separate agent.

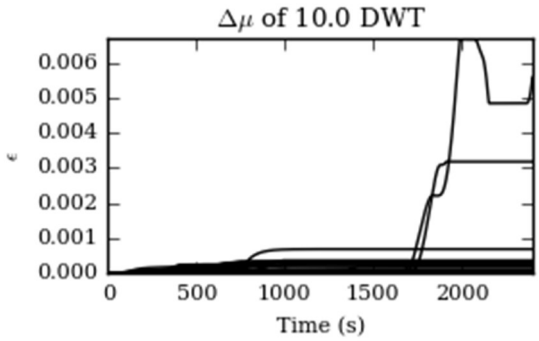

Figure 4.25 Results of experiment changing the tonnage of each agent by 10.0 DWT. Note, each line is a separate agent

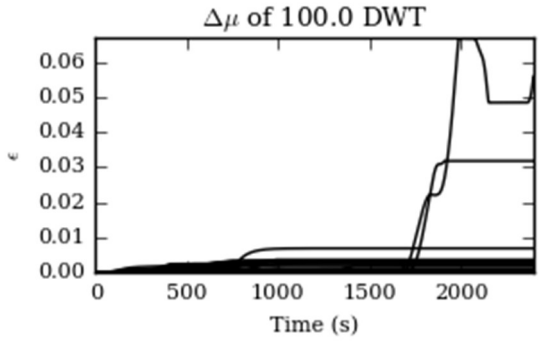

Figure 4.26 Results of experiment changing the tonnage of each agent by 100.0 DWT. Note, each line is a separate agent

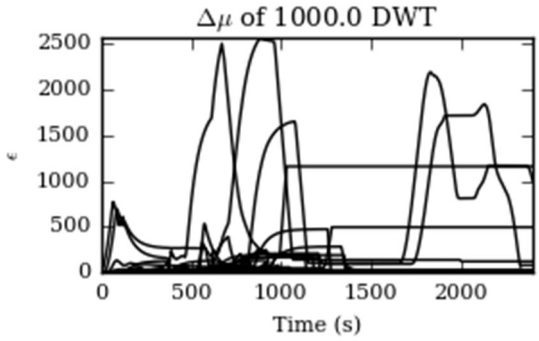

Figure 4.27. Results of experiment changing the tonnage of each agent by 1000.0 DWT. Note, each line is a separate agent.

The final experiment assessed if the ABM was capable of emergent properties of interest through individual interaction. Of interest to marine spatial planners is whether or not offshore renewable energy installations will create traffic related problems that lead to increased interaction and risk of collision. The experiment was designed to induce traffic jams by funneling 20 agents through a narrow passage. The presence of kinematic waves (Figure 4.28) demonstrate the ABM is capable of reproducing emergent behavior of interest to planners. The diagonal columns depicted in the figure represent individual agent tracks while the color hue represents velocity (left panel) or change in direction (right panel). Note a majority of the agents, with the exception of the first few, slow down prior to 10,000 m, which is the location of the bottleneck depicted on figure 3.19. Some agents are able to progress through the

bottleneck unscathed while the remaining agents compete for space and decelerate in order to minimize risk of collision. Further, as the simulation progresses, there is a contingent of slower moving agents close to their origins, indicating that they are at the back of the traffic jam throughout the entire simulation.

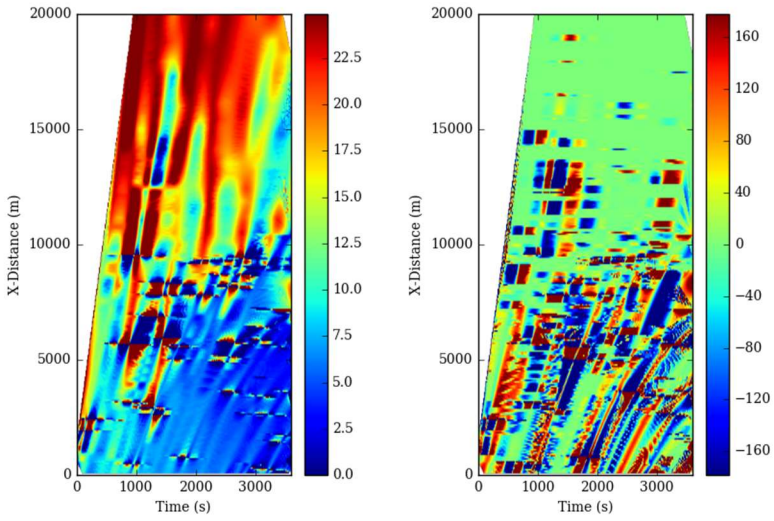

Figure 4.28 results of the simulation that intentionally causes traffic delays through the creation of a bottleneck that forces all agents through a narrow pass. Diagonal columns represent individual agent tracks. The left panel shows speed in m/s while the right panel displays changes in direction in degrees. Note, once agents pass through bottleneck, their speed generally increases as they are through the jam and their direction remains relatively unaffected.

4.4 Calibration and Validation

The researcher made multiple data requests to boat builders, pilot organizations, regulatory agencies and shipping companies, however, data on the turning capabilities of vessels was not forthcoming as most viewed this information to be sensitive in nature. A pilot on the Great Lakes was able to share information from a single bulk cargo carrier (Figure 4.29, name withheld). The vessel was 143 m in length, started the turning test at 15.7 knots and ended at 7.0 knots. Throughout the turning test, the vessel held its rudder angle constant at -35.0^{o}. The derived T and K were 2.25 and 1.72 respectively. Figure 4.30 contains a port turn validation simulation with parameters matching those of the calibration vessel. The simulated transfer closely matched that of the calibration vessel while the advance was slightly under estimated.

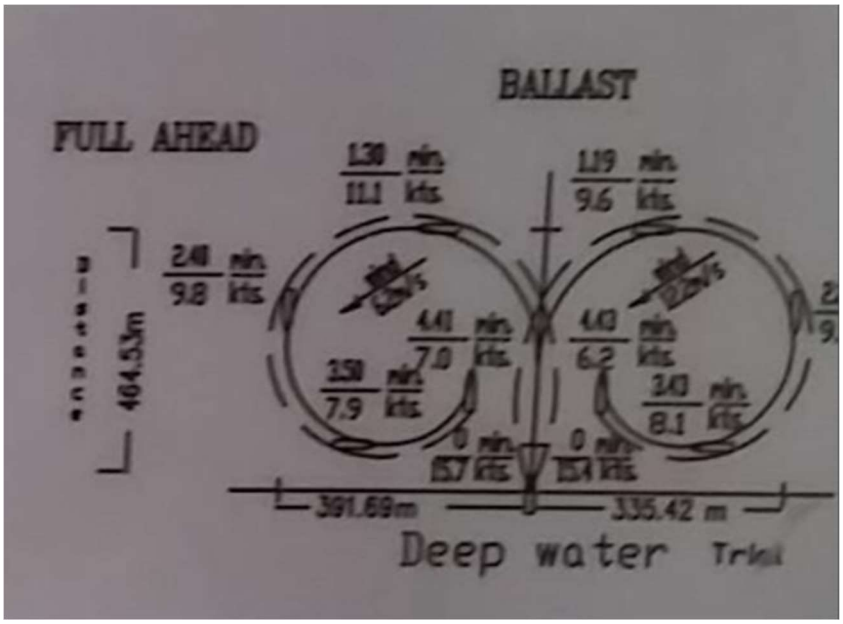

Figure 4.29 A picture of a wheelhouse poster taken from a bulk carrier operating on the great lakes. K-T indices were derived from the port side turning test, note advance was 404.53 m while transfer was 391.69 m.

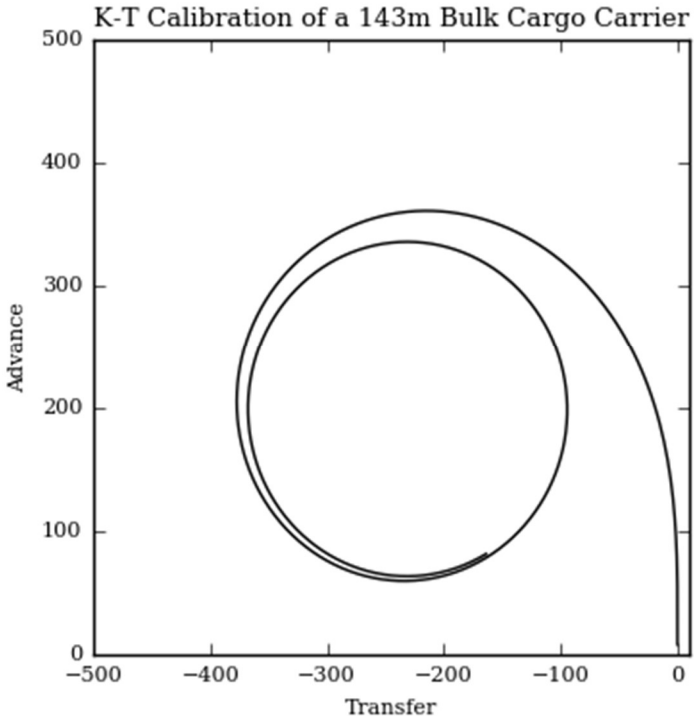

Figure 4.30 Validation simulation run of a port side turn with the same parameters as the calibration vessel. Note the advance obtained in the simulation run was slightly under that of the calibration vessel, however the transfer was validated.

4.5 The Port of New York and New Jersey

Prior to performing a simulation of the effect of an offshore renewable energy installation on the commercial shipping industry, an analysis of the traffic patterns into and out of the Port of New York and New Jersey (henceforth known as the Port) was required. The Port is the third busiest by cargo volume in the United States (PANYNJ, 2016) and receives considerable vessel traffic. Figure 4.31 - 4.42 contain a simple Poisson count of unique voyages per 100 m^2. Overall, the highest concentration of voyages occurred in June with one cell having 1,332 unique voyages. In total June 2014 had 2,034 unique voyages from 1,260 vessels. The highest concentration of vessel traffic occurs within the Ambrose Channel where the Nantucket, Hudson Canyon, and Barnegat traffic lanes converge at the entrance to the Port. June is by far the busiest month for commercial traffic in and around the Port, descriptive statistics were compiled describing the vessel traffic.

The study area contained a diverse assemblage of vessel traffic during the month of June 2014 (Table 4.5). Aside from cargo vessels and tankers, there is considerable traffic associated with port service vessels (tugs and pilot craft) as well as ferry and cruise ship traffic (passenger vessels).

Table 4.5 Unique voyages by vessel type found within the study region during the month of June, 2014

Vessel Type	Unique Voyages
Cargo	557
Tanker	226
Tugs	169
Towing	146
Passenger (ferry and cruise ship)	90
Pleasure Craft	57
Wing in Ground Effect	55
Pilot Vessel	35
Law Enforcement	23
Fishing	13
Dredging	9
Military	6
High Speed Craft	5
Search and Rescue	4
Sailing	4
Port Tender	1

The longest (λ) ships found within the study area were cargo ships at 352 m followed closely by passenger ships at 345 m (Table 4.6). The largest vessels by beam (β) are Passenger vessels with 51 m while cargo vessels and tankers are regulated at 46 m to fit within the new Panama Canal locks and are

considered New Panamax vessels (Table 4.7). The maximum reported draft for passenger ships, dredging vessels, towed barges and tugs appear to be suspect as they are all greater than the dredged depth of the Ambrose Channel at 50 feet (PANYNJ, 2016), however, the draft for cargo vessels and tankers appear to be correct (Table 4.8).

Table 4.6 Vessel type length summary statistics. Note AIS data did not report statistics for Port Tenders.

Vessel Type	Mean	St. Dev.	25%	50%	75%	max
Cargo Ships	233.7	76.56	195	261	294	352
Passenger Ships	167.13	124.06	63	104	294	345
Military	81.5	104.95	36	42	72	289
Tanker	184.21	39.67	180	183	186	256
Pilot Vessel	203.17	55.9	220	220	220	220
Towing	62.11	55.46	30	34	133.75	205
Tugs	32.6	30.6	21	29	33	200
Wing in ground effect	114.85	59.49	41	152	152	182
Dredging	81.22	22.71	68	84	86	121
Pleasure Craft	35.51	13.2	22	39	45	61
Law Enforcement	10.74	14.1	0	9	11	53
High Speed Craft	38.8	6.53	39	39	44	44
Sailing	25.25	6.85	20.75	23	27.5	35
Fishing	18.54	10.71	9	21	27	32
Search and Rescue	10.5	4.12	7.5	11	14	14

Table 4.7 Vessel type beam summary statistics. Note AIS data did not report statistics for Port Tenders.

Vessel Type	Mean	St. Dev.	25%	50%	75%	max
Passenger Ships	25.41	14.9	14	22	32	51
Tanker	30.54	6.84	30	32	32	46
Cargo Ships	31.32	6.95	31	32	32	46
Pilot Vessel	39.74	10.8	43	43	43	43
Military	12.33	10.8	7.5	12	12	32
Towing	12.97	7.35	9	10	23.8	27
Tugs	9.5	3.49	8	8	10	24
Dredging	17.22	4.38	16	17	20	24
Wing in ground effect	17.82	7.9	11	22	24	24
Law Enforcement	2.87	3.18	0	3	3.5	12
Pleasure Craft	7.72	2.02	6	8	10	12
High Speed Craft	9.6	3.29	10	10	12	12
Sailing	5.75	3.1	3.8	5	7	10
Fishing	6.54	2.18	6	7	8	9
Search and Rescue	3.75	0.96	3	3.5	4.25	5

Table 4.8 Vessel type draft summary statistics. Note AIS data did not report statistics for port tenders or pilot vessels and the maximum draft data for passenger ships, dredging vessels, towed barges and tugs appear suspect as they are greater than the maximum depth of the Ambrose Channel.

Vessel Type	Mean	St. Dev.	25%	50%	75%	max
Passenger Ships	5.31	4.91	0	4	8.4	25
Dredging	7.2	6.28	3.63	5.8	6.38	20
Towing	5.81	3.35	4	5.2	6.1	17
Tugs	3.66	2.44	2.6	3	4.53	16
Cargo Ships	10.08	2.82	8.5	11	12	15
Tanker	9.59	1.99	8.5	10	10.9	13
Military	4.9	5.41	2	4	7.35	11
Pleasure Craft	2.46	1.36	2	2.1	2.45	8
Wing in ground effect	5.72	1.17	4.5	6	6.8	7
Port Tender	6		6	6	6	6
Law Enforcement	1.3	1.86	0	0	2.5	4
Sailing	2.25	1.75	1.5	2.4	3.15	4
High Speed Craft	1.3	1.84	0.65	1.3	1.95	3
Fishing	0.82	1.37	0	0	1.2	3

The ABM attempted to model the worst-case traffic scenario, which was the highest travelled hour during the highest travelled month. An hourly assessment of vessel traffic during the month of June in the Ambrose channel showed the highest vessel traffic occurred during the hour of 8 PM (Figure 4.43) averaging upwards of 36 vessels per hour within the Ambrose Channel where the offshore traffic lanes converge at the point closest to the Port. Within this convergence area, traffic densities during the 8 PM hour ranged between less than 1 and 36 vessels per hour per 1 km^2 cell (Figure 4.44). When just cargo vessels and tankers are taken into account, the maximum average number of vessels per hour is only 27 within the Ambrose Channel. The Ambrose to Barnegat maxes out at 6 outgoing vessels per hour, while the Nantucket to Ambrose incoming traffic lane has only 5 vessels per hour (Figure 4.45).

4.6 ABM of the Entrance to the Port of New York and New Jersey

As stated, the purpose of the agent based model for the Port was to assess potential socio-economic impacts to marine trade, including navigability, from the construction of a proposed wind farm (Figure 3.1). The agent based model consisted of two sets of simulations. The first contained no wind farm and served to validate against current configurations, while the second located the wind farm as proposed. Each scenario had multiple iterations that increased the number of agents from 20 to 100 at 5 agent increments. Each simulation ran for 7200 seconds, which was enough time for agents to reach their destination. Once agents reached their destinations there were removed from the simulation. Each simulation employed a standard input dataset, meaning starting conditions would match between each scenario-agent pair with the exception of new agents added during each iteration. The simulations started with 20 agents, and each iteration added 5. However, results were only compiled for the original 20 agents so that simulation iterations could be compared.

The simulation consisted of 41 cargo vessels and 59 tanker vessels. The mean lengths for cargo and tanker respectively were 278.18 and 278.04 m respectively. While lengths were similar, their respective maneuvering indices were not (Table 4.9), cargo vessels were not as responsive to helm, but could turn faster. In total, there was 84 incoming vessels and only 16 outgoing. Of the outgoing vessels, three were headed to Barnegat, four along the coastal tug route, three to the Hudson Canyon and 6 were headed to Nantucket. Of the incoming vessels, 37 were headed to the Elizabeth container terminal adjacent to Newark International Airport, while 47 were headed to Port Jersey through the Verrazano Narrows. Following creation of the initial states, the first set of simulations modeled the system without the proposed wind farm.

Table 4.9 *Mean values for maneuvering indices of each vessel class used in the agent based model.*

Vessel Type	Mean K	Mean T
Cargo	1.77	2.00
Tanker	2.28	4.61

In general, as the number of agents increased, the percent of time agents felt repulsive forces increased, as did the duration of each voyage, while the average distance travelled and average velocity decreased (Figure 4.46 and Figure 4.48). However, at 30 and 35 agents, the percent of model time the original 20 agents felt repulsive forces increased dramatically (Figure 4.46) suggesting a threshold, but there was no increase in voyage duration or average velocity which paralleled these increases. Under these circumstances, it is hypothesized that the agent-agent interaction scenarios did not warrant a reduction in speed. Starting at 45 agents, accidents started occurring. The most vessel crashes to occurred in the simulation with 90 agents, the locations of which are found in (Figure 4.47). A majority of the crashes occurred within the USCG precautionary area that regulates vessel speed into the Ambrose Channel where all incoming and outgoing traffic lanes converge as vessels enter the Port. The location of the crash outside of the precautionary area was due to a traffic jam and a vessel that could not slowdown in time. Following the no-farm simulation, another agent based model assessed the impact to the shipping industry with the same agents only this time included the proposed WEA (Figure 3.2).

However, there was no difference between either simulation (Figure 4.48), including the positions and times of each crash which suggests the placement of this WEA has no effect on the industry.

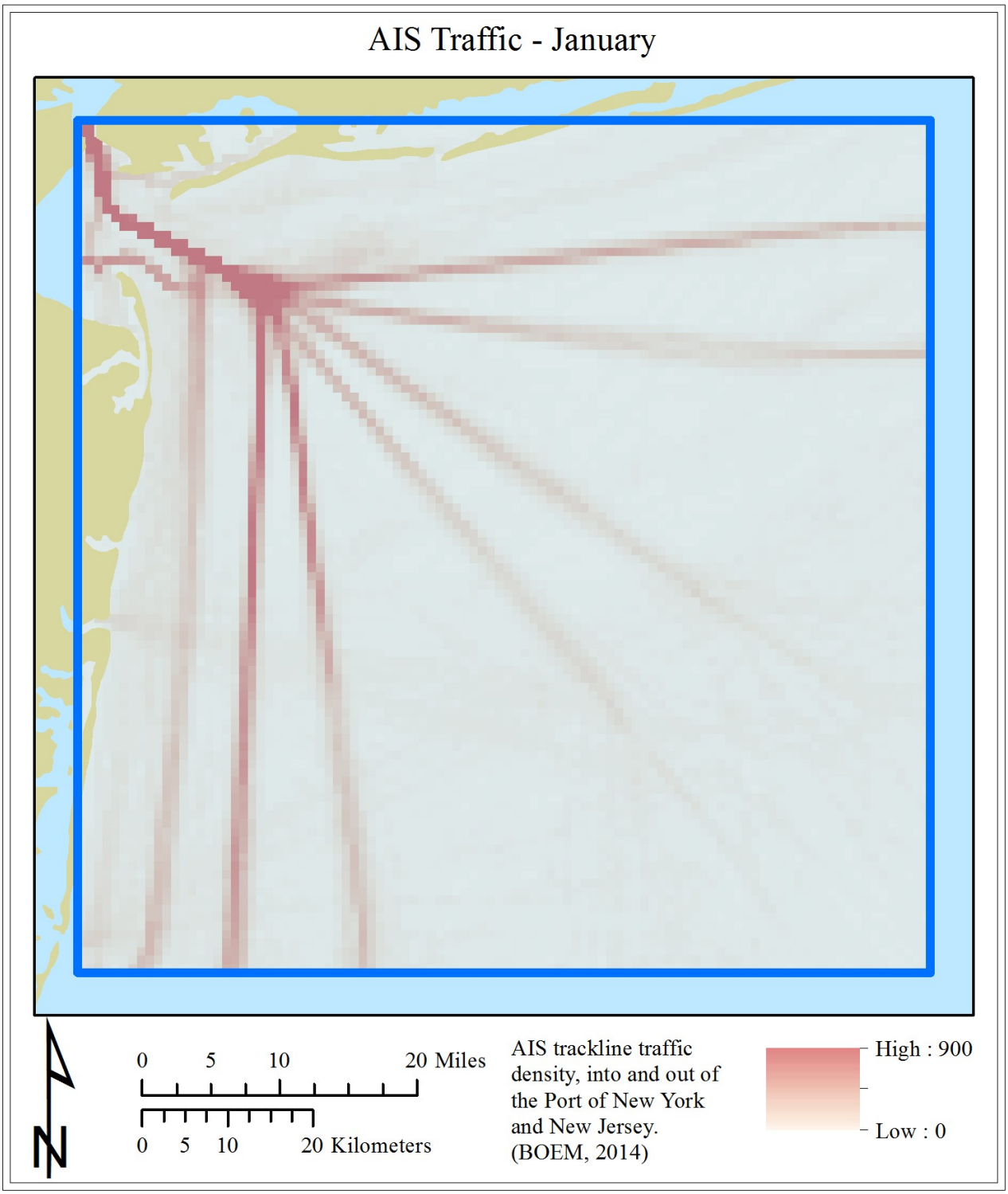

Figure 4.31 *AIS track line density into and out of the Port in January of 2014.*

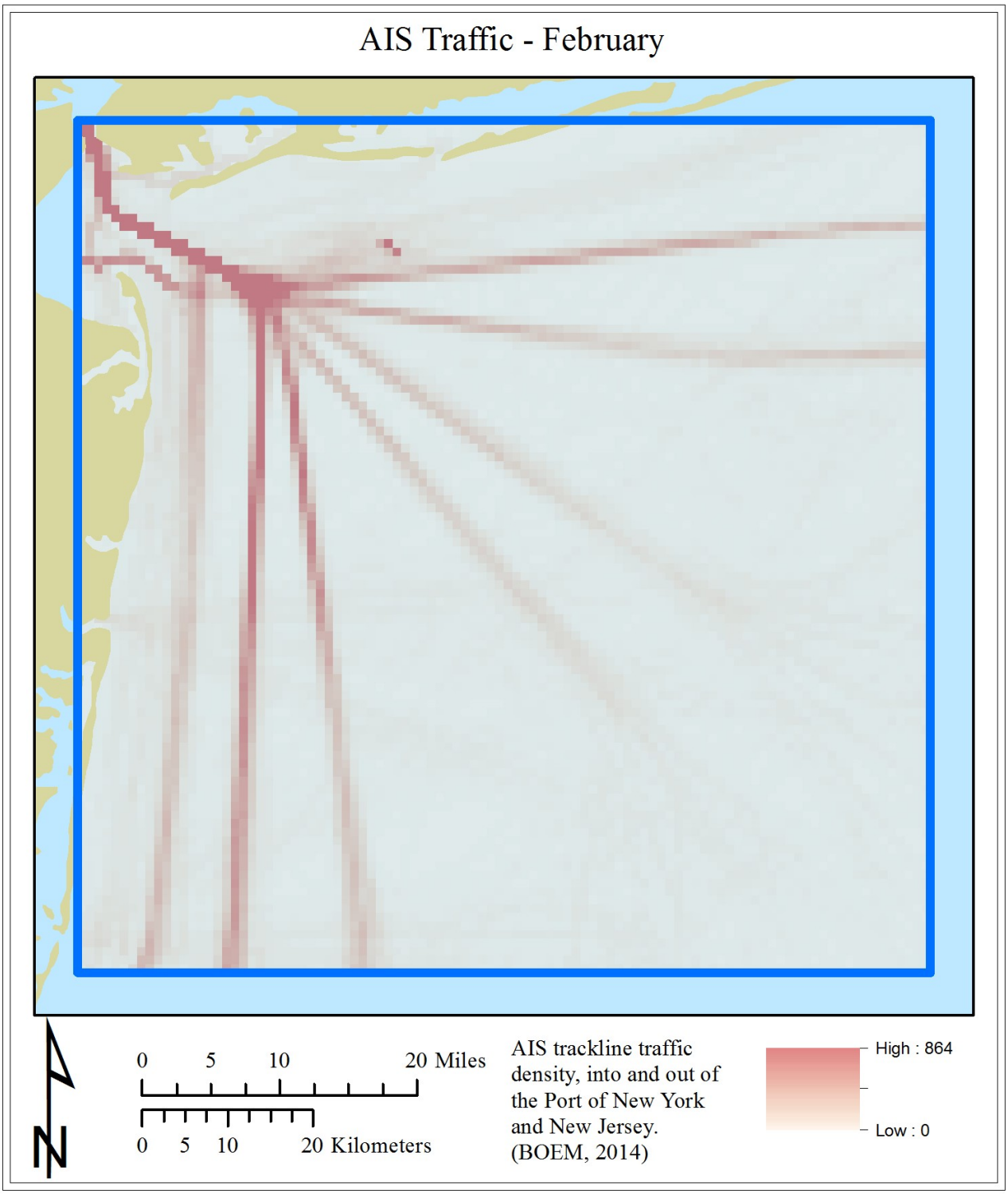

Figure 4.32 *AIS track line density into and out of the Port in February of 2014.*

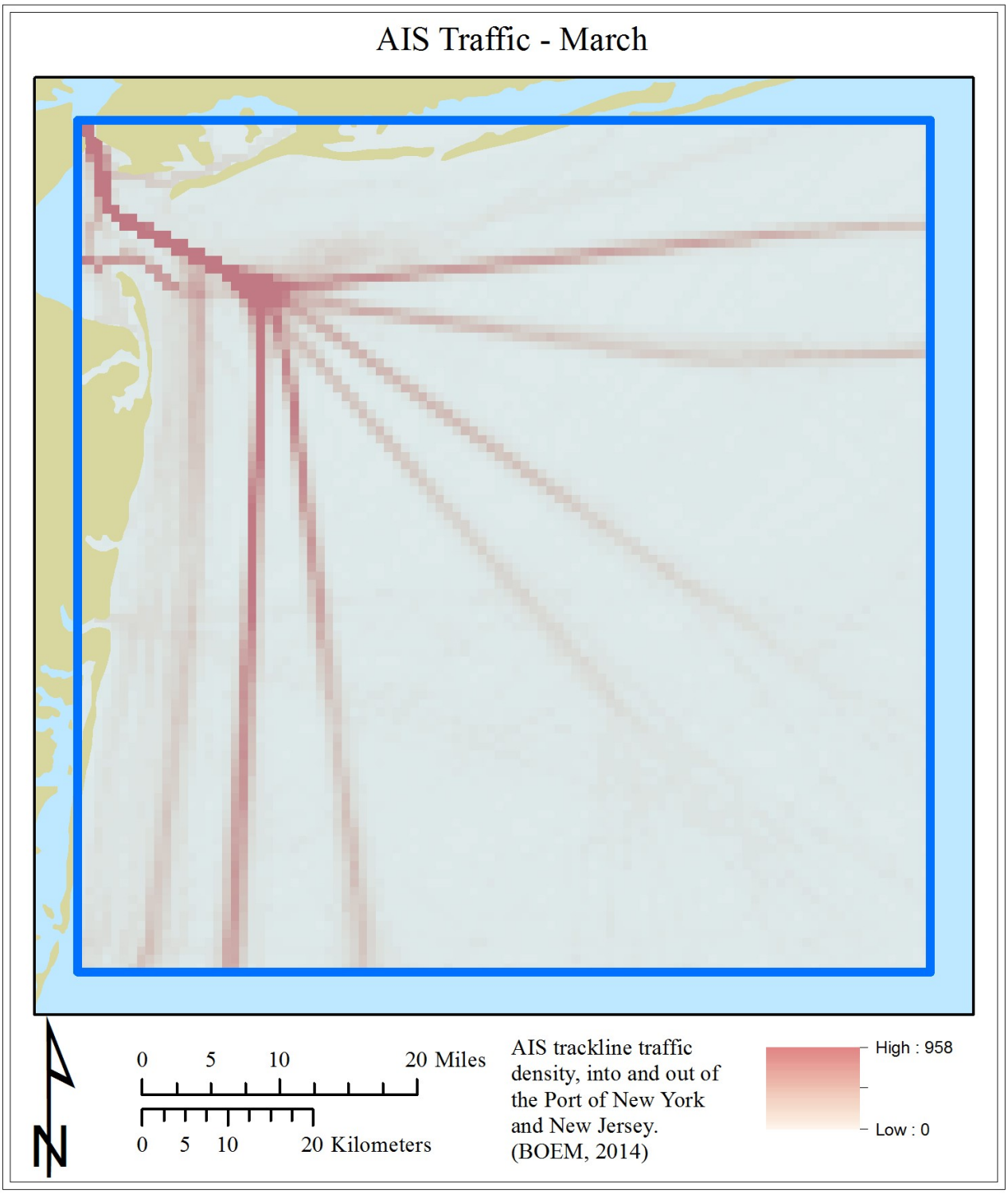

Figure 4.33 *AIS track line density into and out of the Port in March of 2014.*

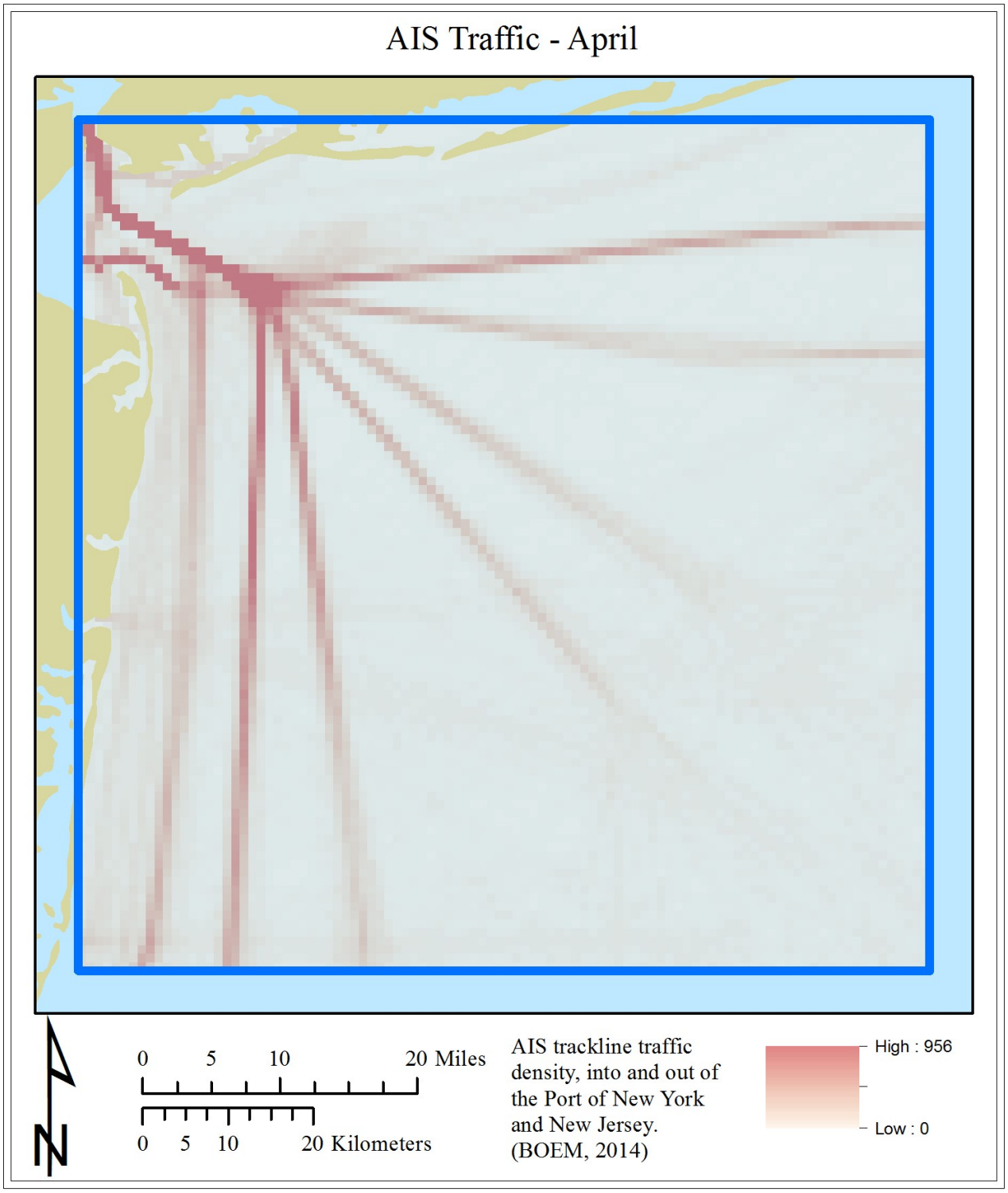

Figure 4.34 *AIS track line density into and out of the Port in April of 2014.*

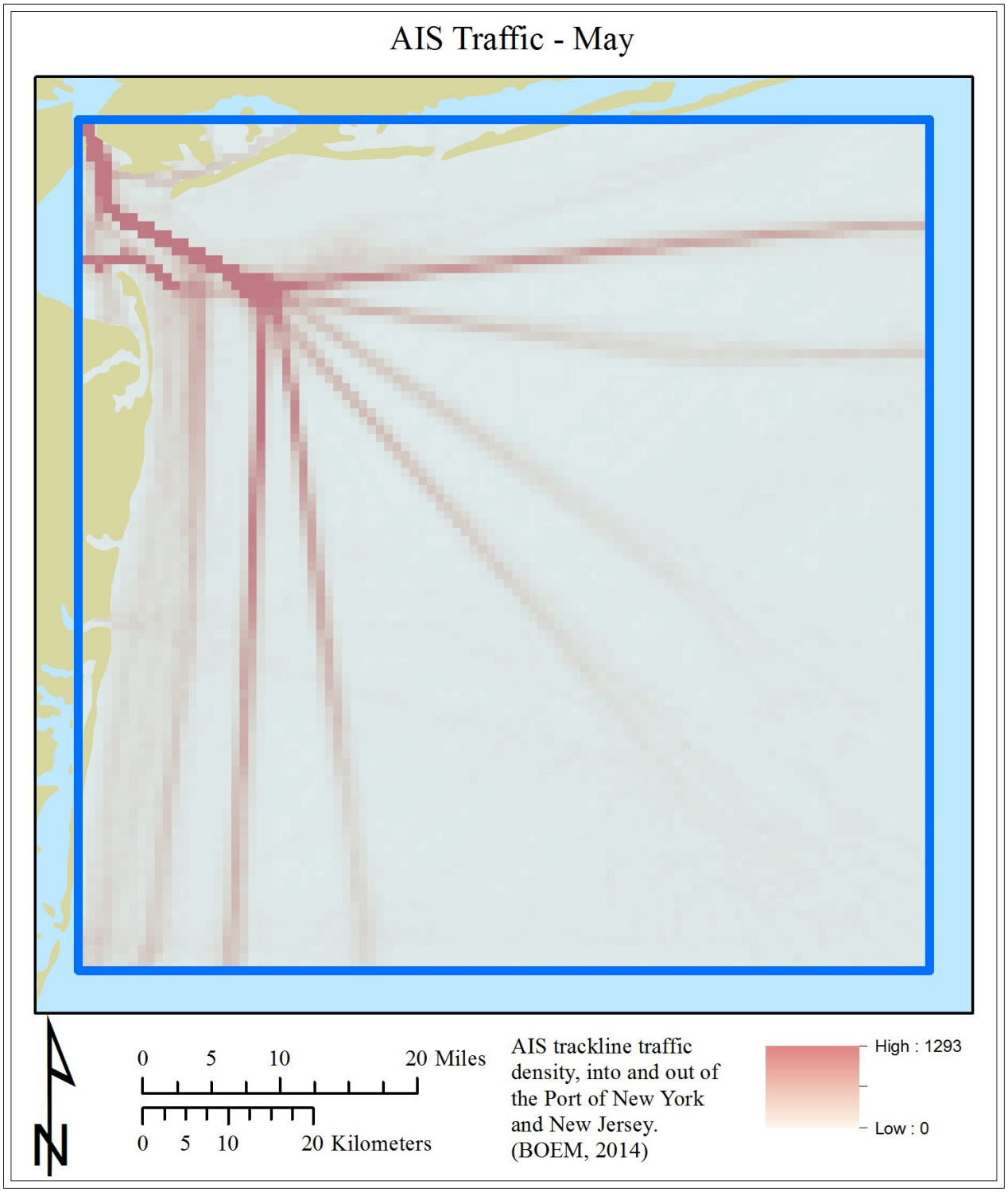

Figure 4.35 *AIS track line density into and out of the Port in May of 2014.*

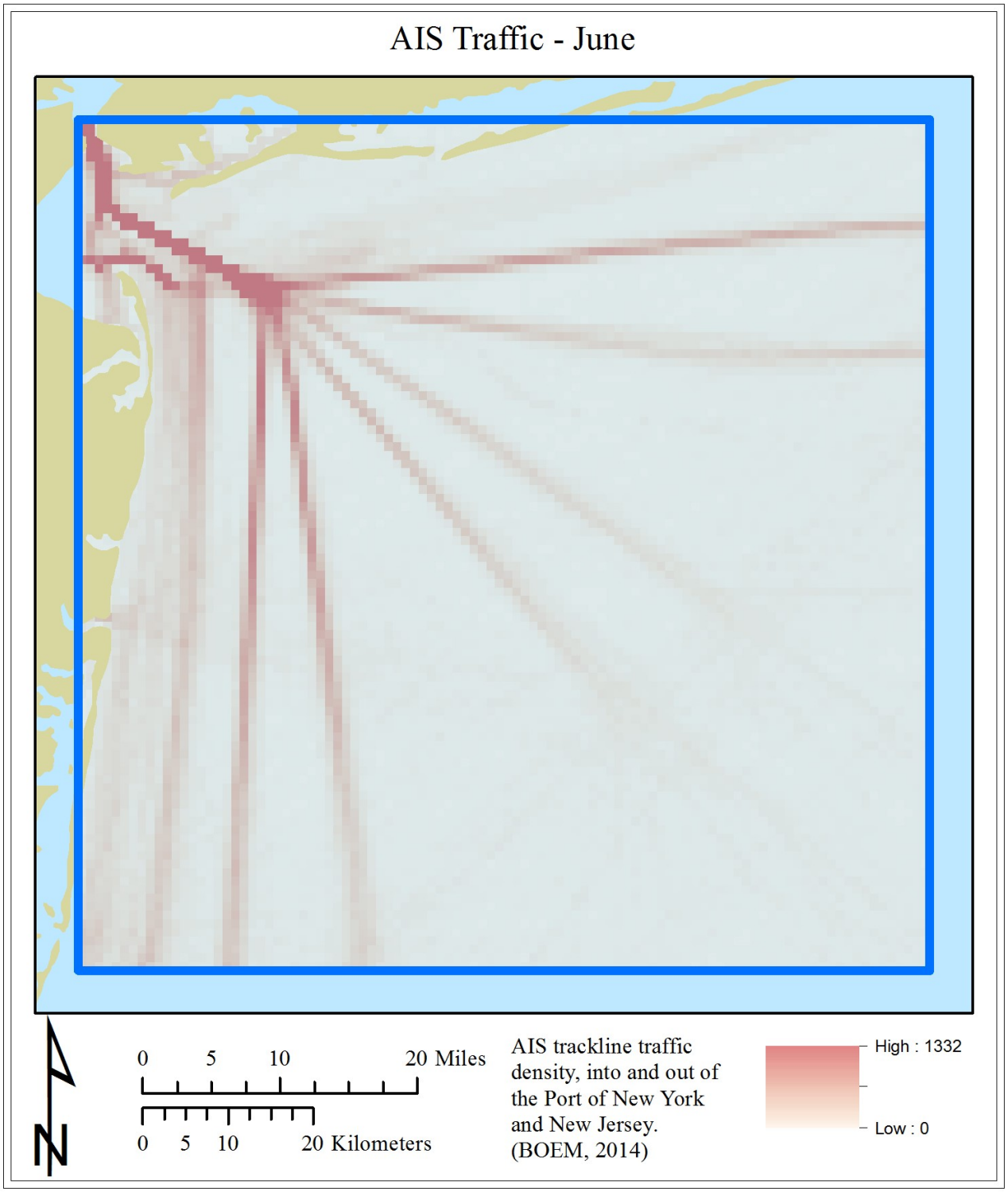

Figure 4.36 *AIS track line density into and out of the Port in June of 2014.*

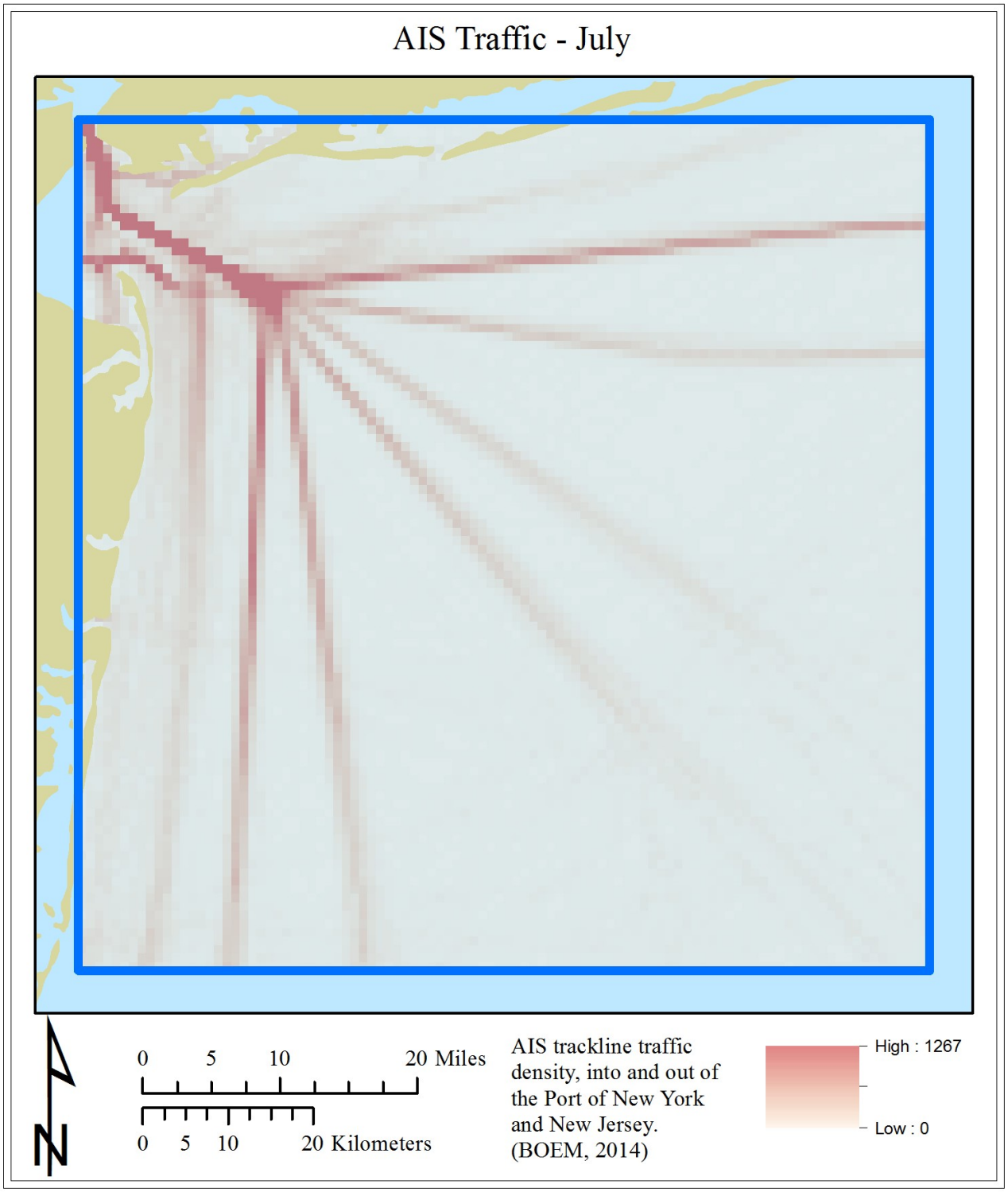

Figure 4.37 *AIS track line density into and out of the Port in July of 2014.*

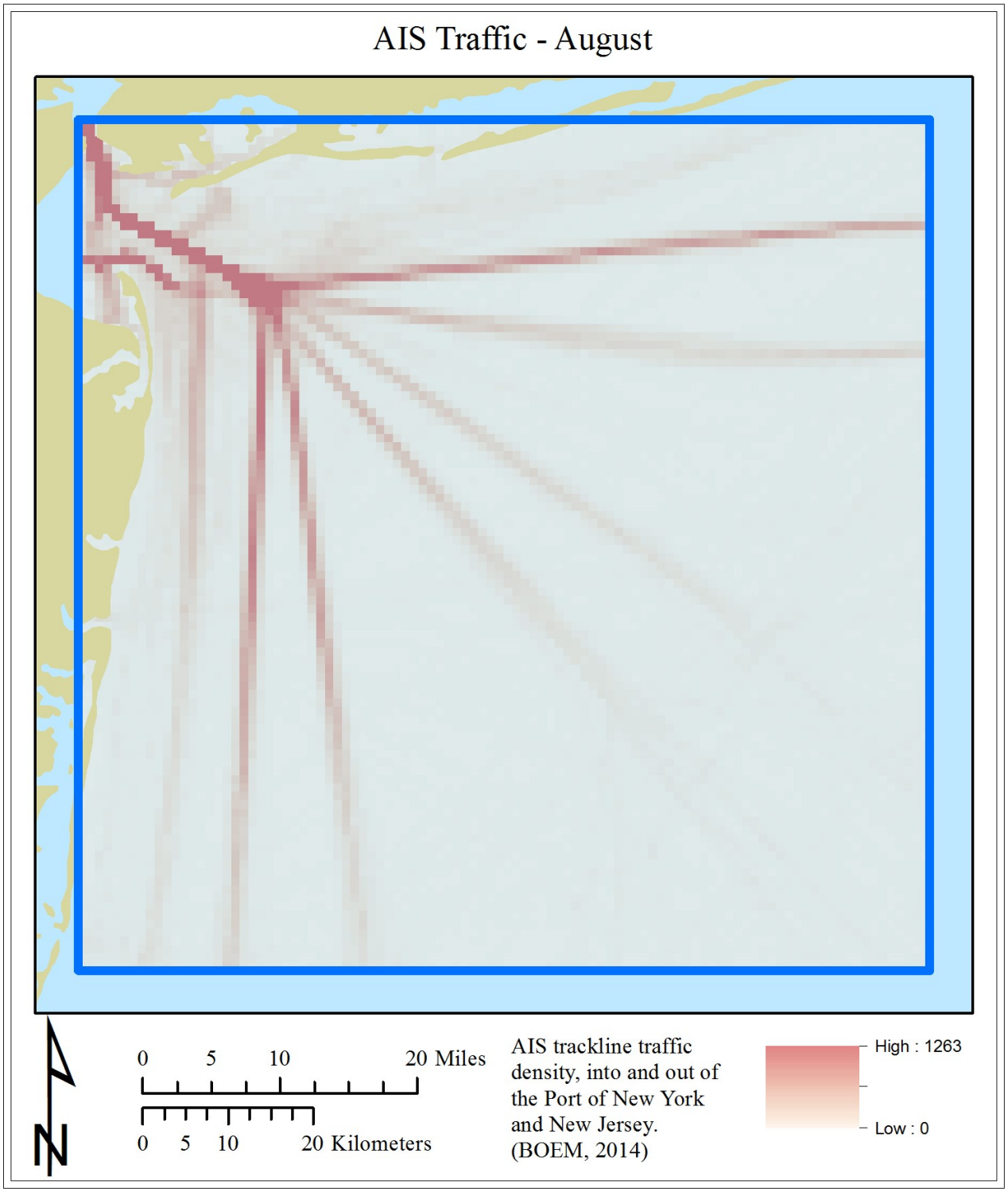

Figure 4.38 *AIS track line density into and out of the Port in August of 2014.*

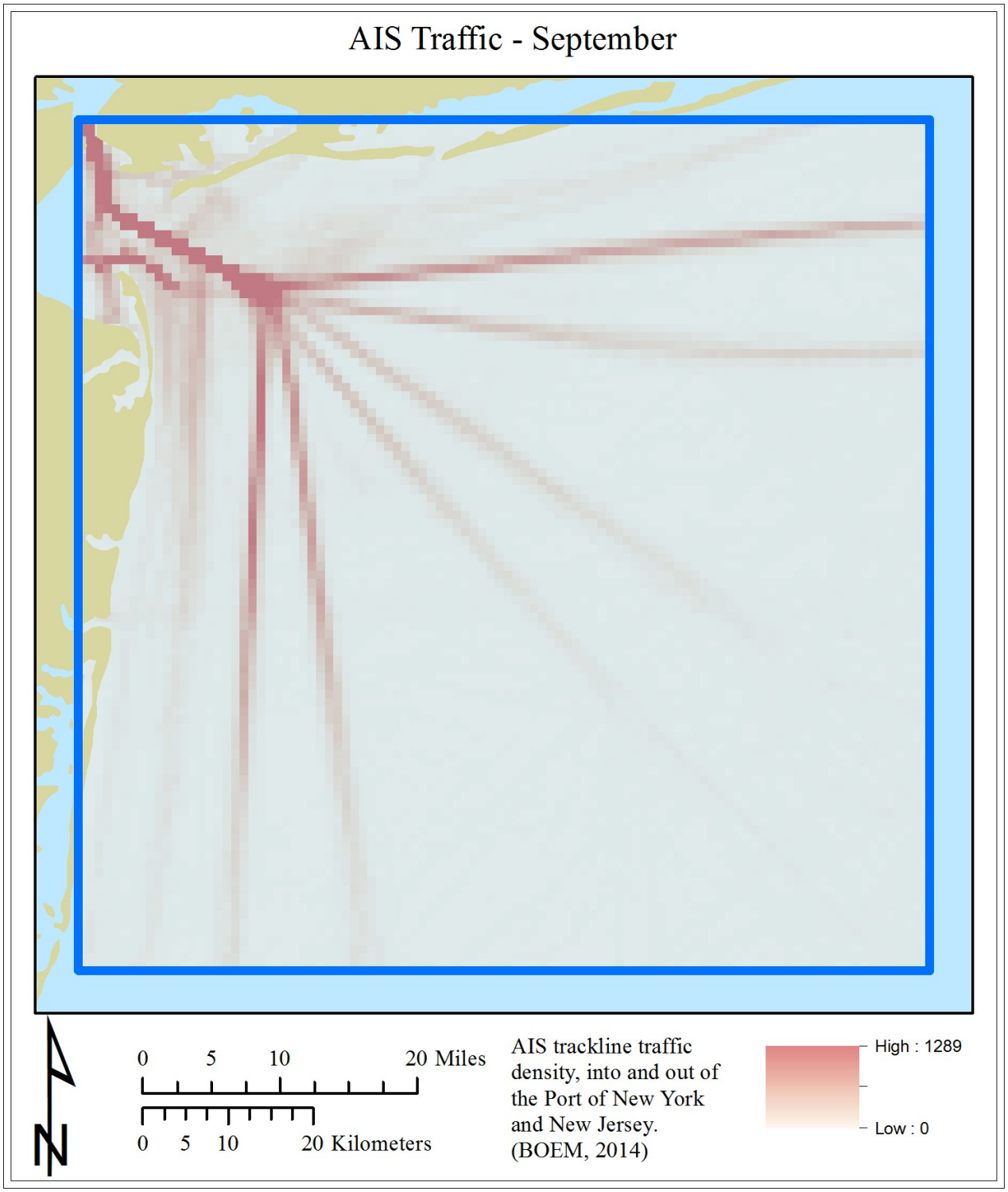

Figure 4.39 *AIS track line density into and out of the Port in September of 2014.*

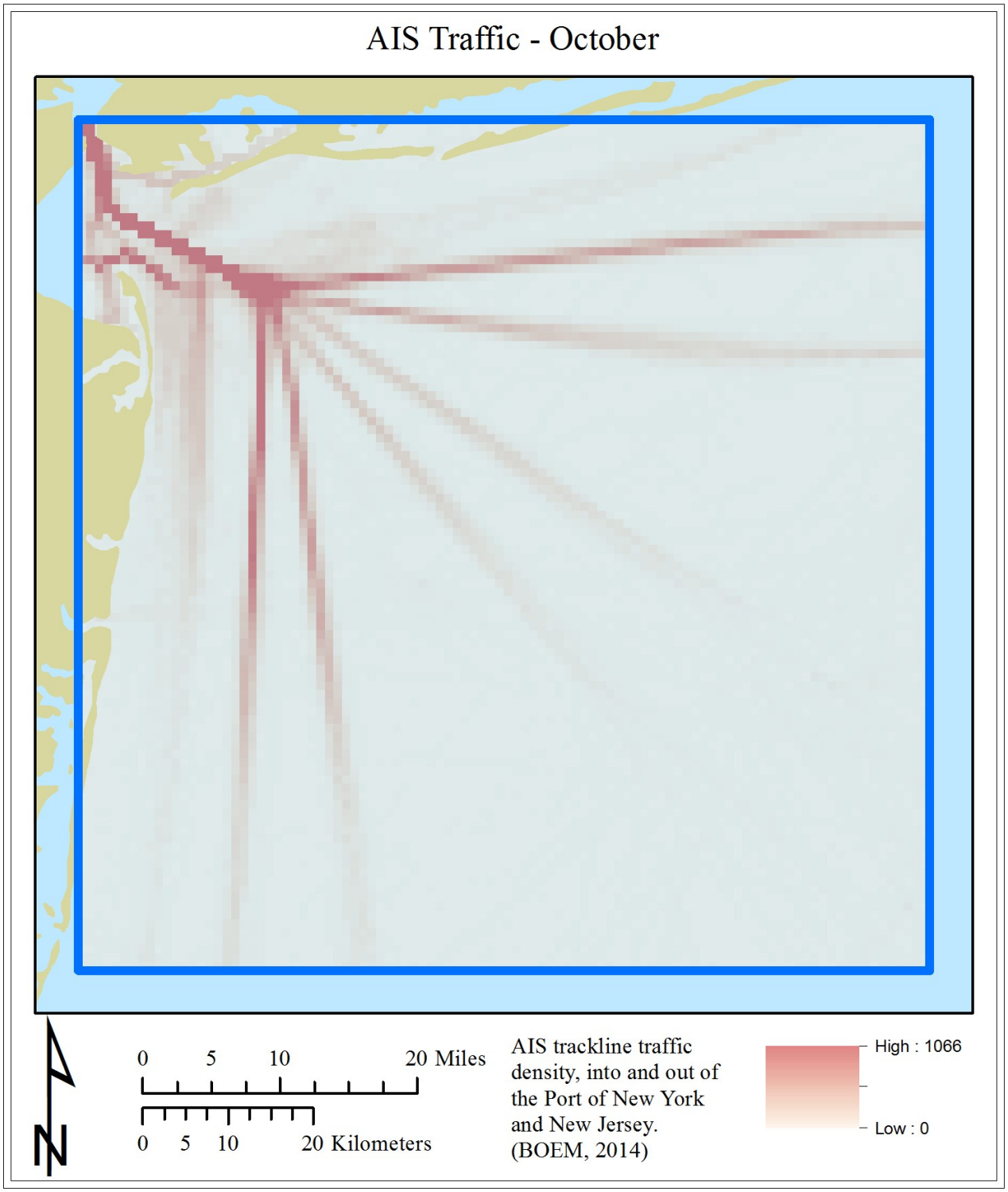

Figure 4.40 *AIS track line density into and out of the Port in October of 2014.*

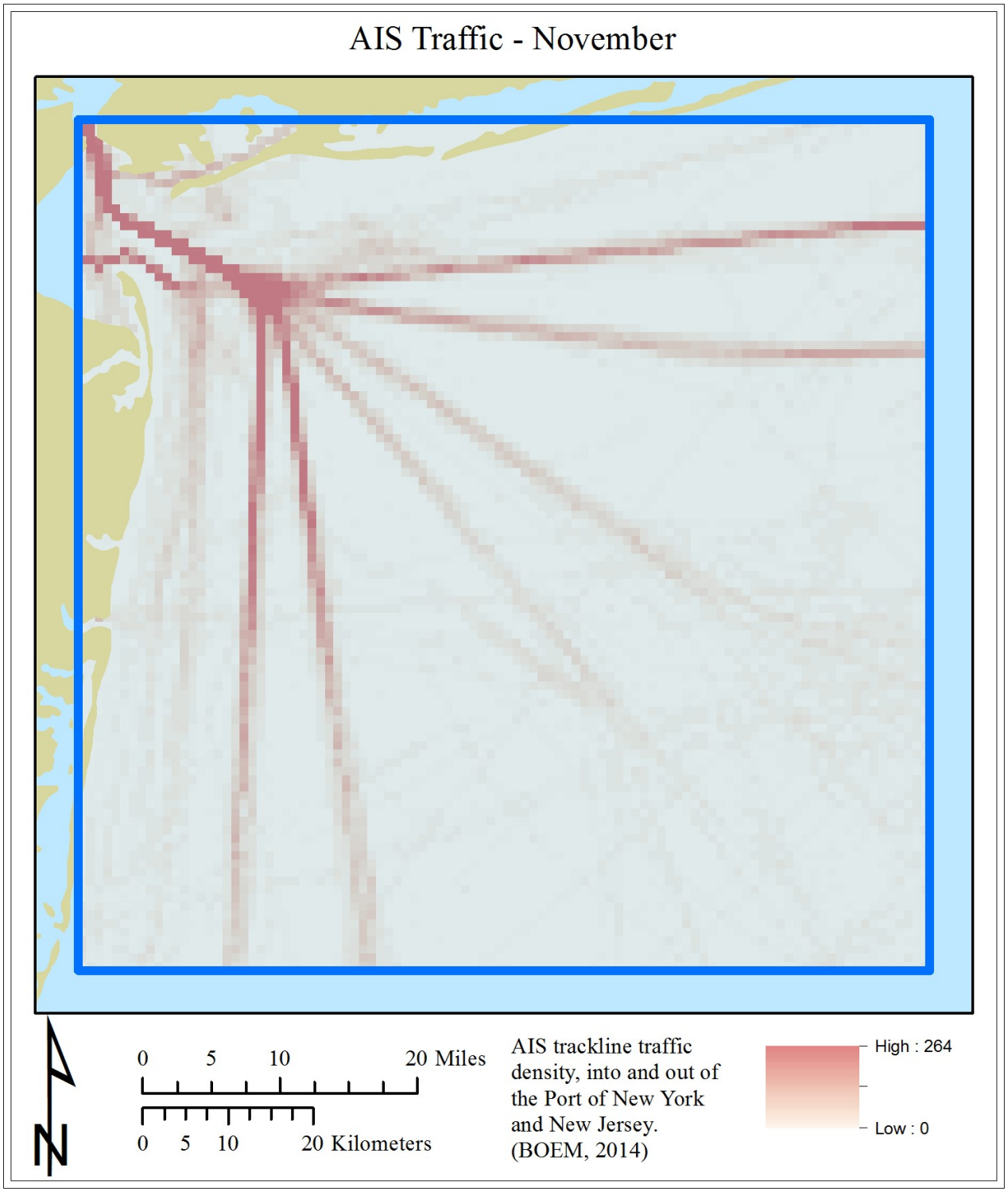

Figure 4.41 *AIS track line density into and out of the Port in November of 2014.*

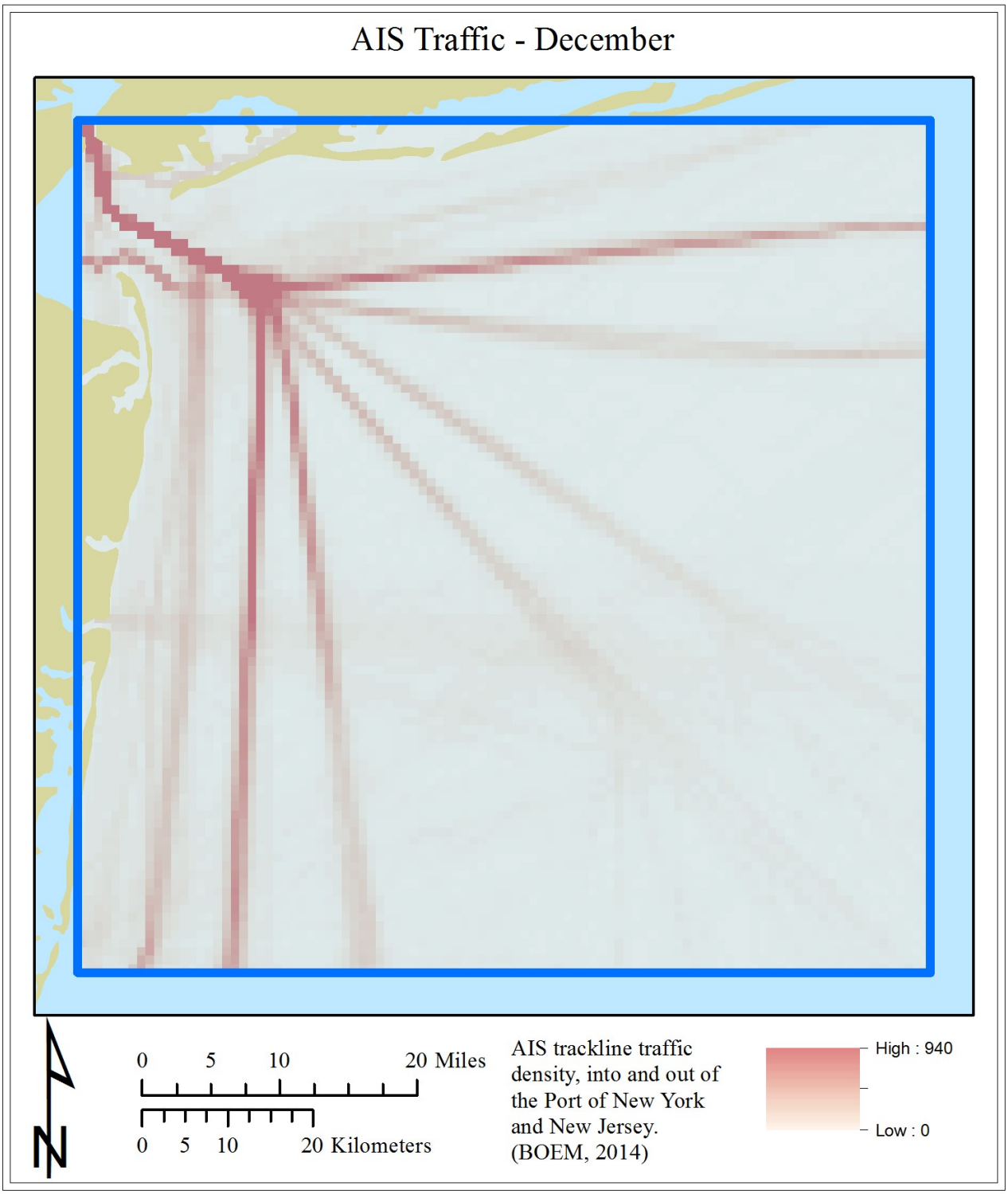

Figure 4.42 *AIS track line density into and out of the Port in December of 2014.*

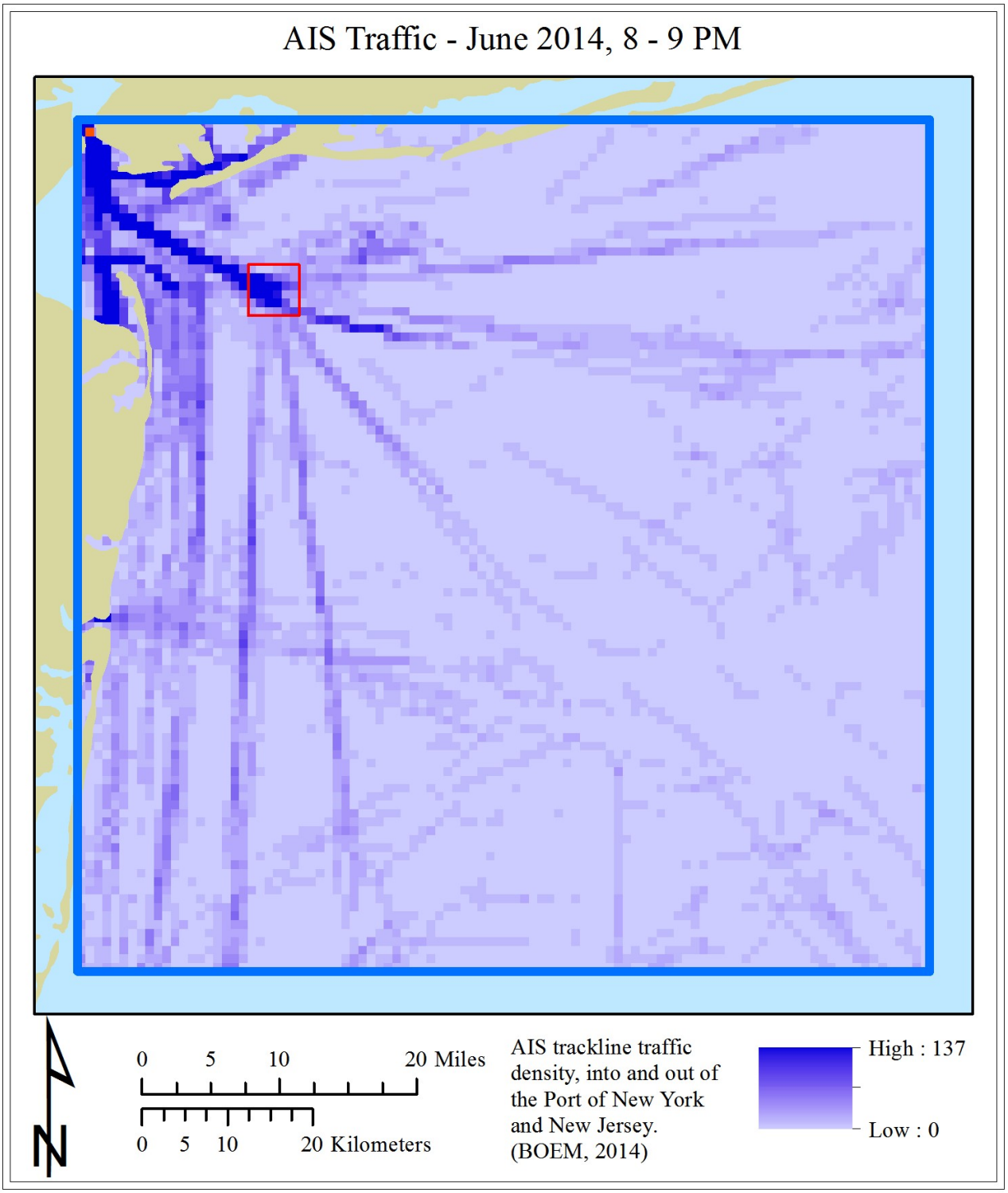

Figure 4.43 *Number of unique voyages per square kilometer during of the hour between 20:00 and 21:00 during the month of June, 2014.*

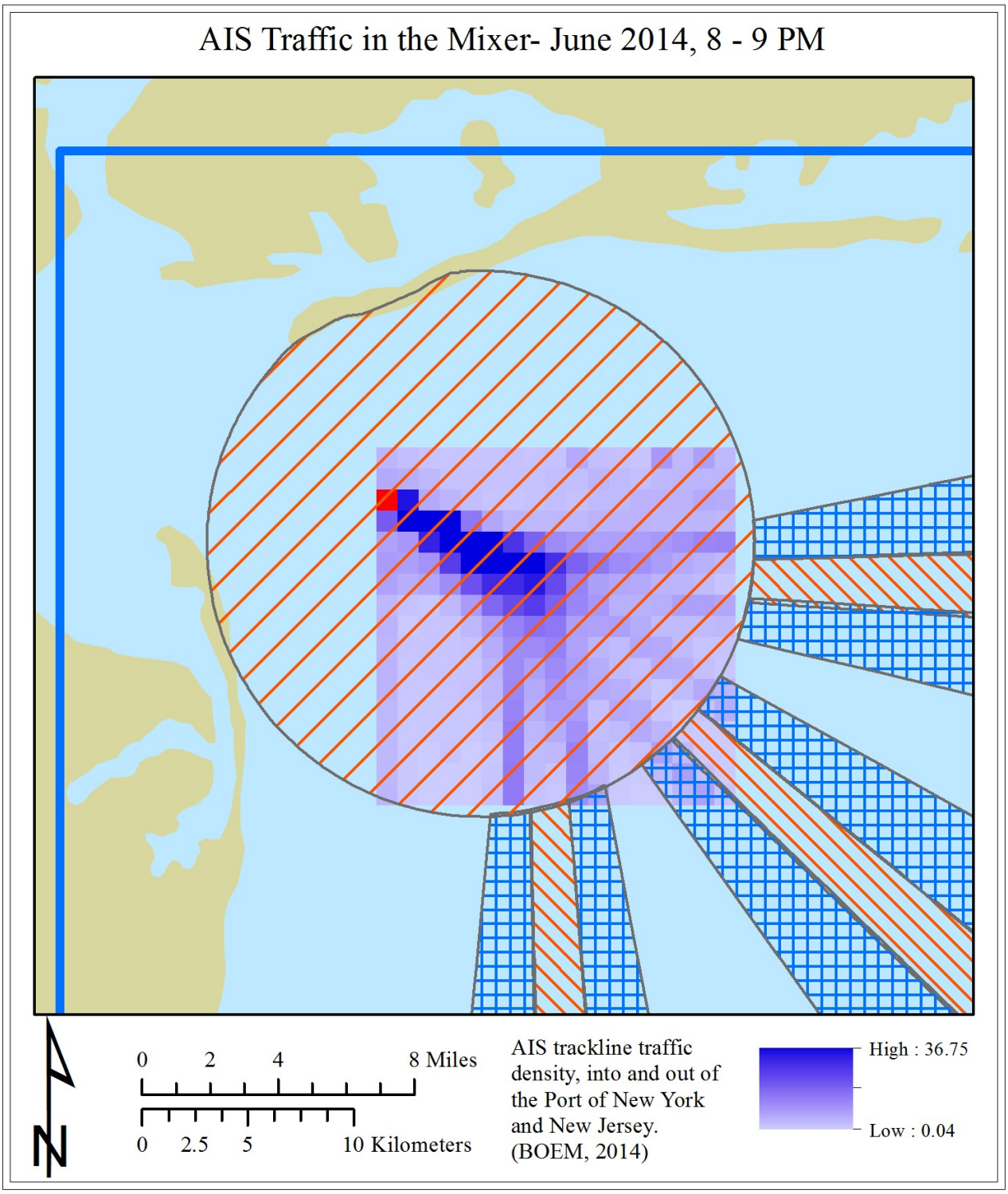

Figure 4.44 average tracking density within the aggregation of traffic lanes into the Ambrose Channel in June 2014 during the 20:00 hour.

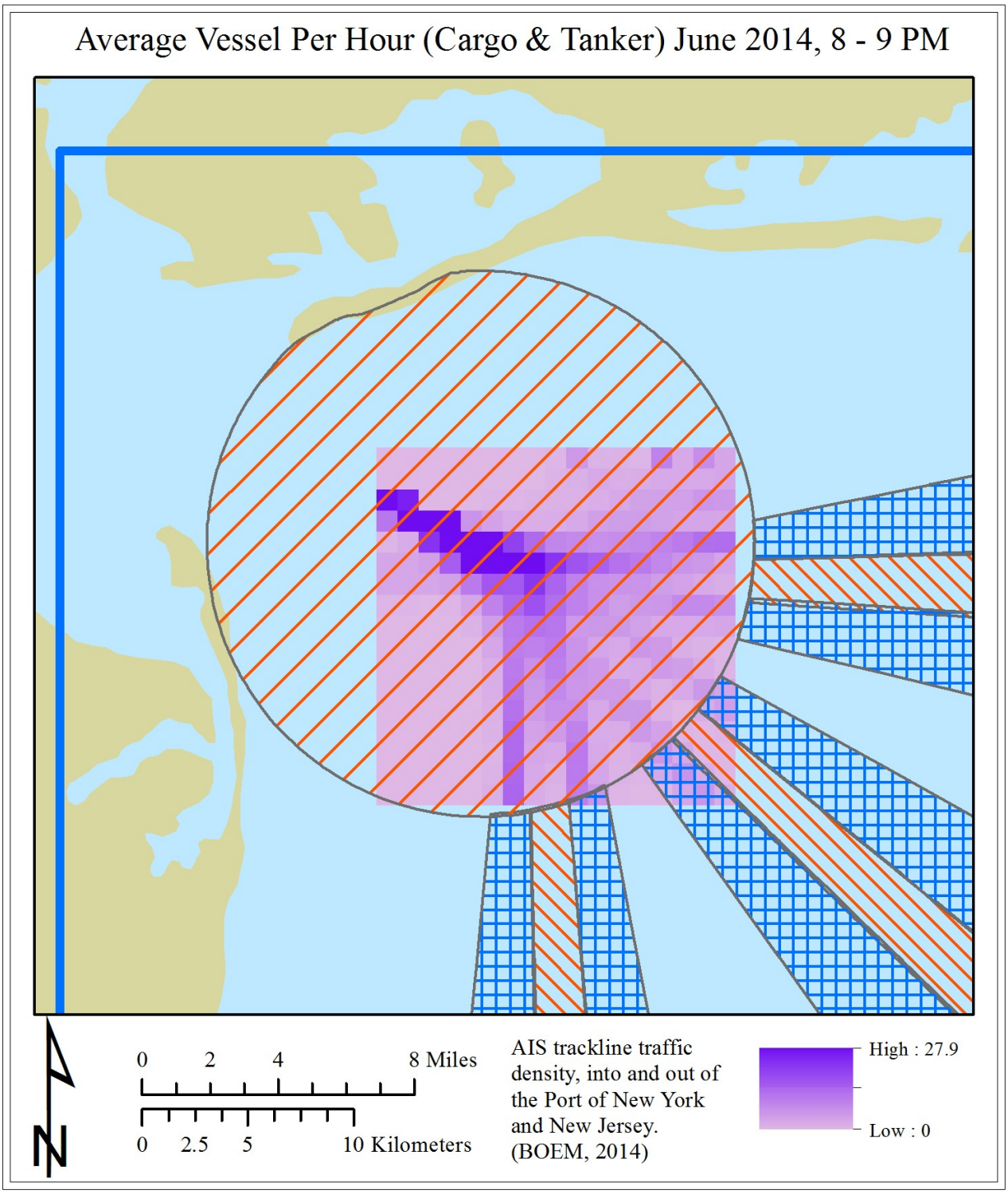

Figure 4.45 *average track line density for Cargo Vessels and Tankers within the Ambrose Channel aggregation area. Note, the largest concentration of vessels occurs within the Ambrose Channel, however the traffic lanes into and out of the Port only average between 4 and 6 vessels per hour.*

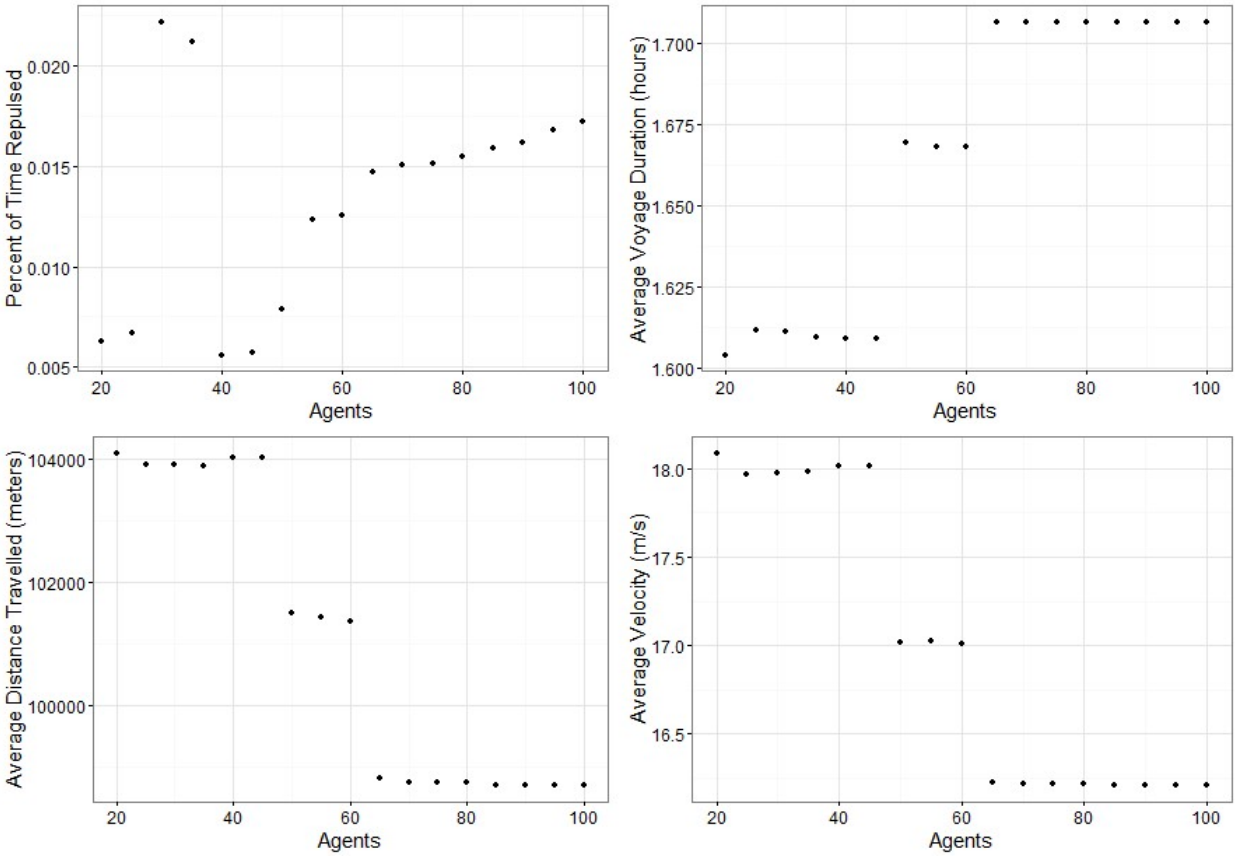

Figure 4.46 panel figure for the no wind farm simulation showing the percent of time repulsed, average voyage duration, average distance travelled and average velocity of the original 20 agents as a function of the number of agents in a simulation. Note the dramatic increase in percent of time repulsed at 30 and 35 agents, however this bump is not noted in the voyage duration or average distance travelled so its effect is minimal

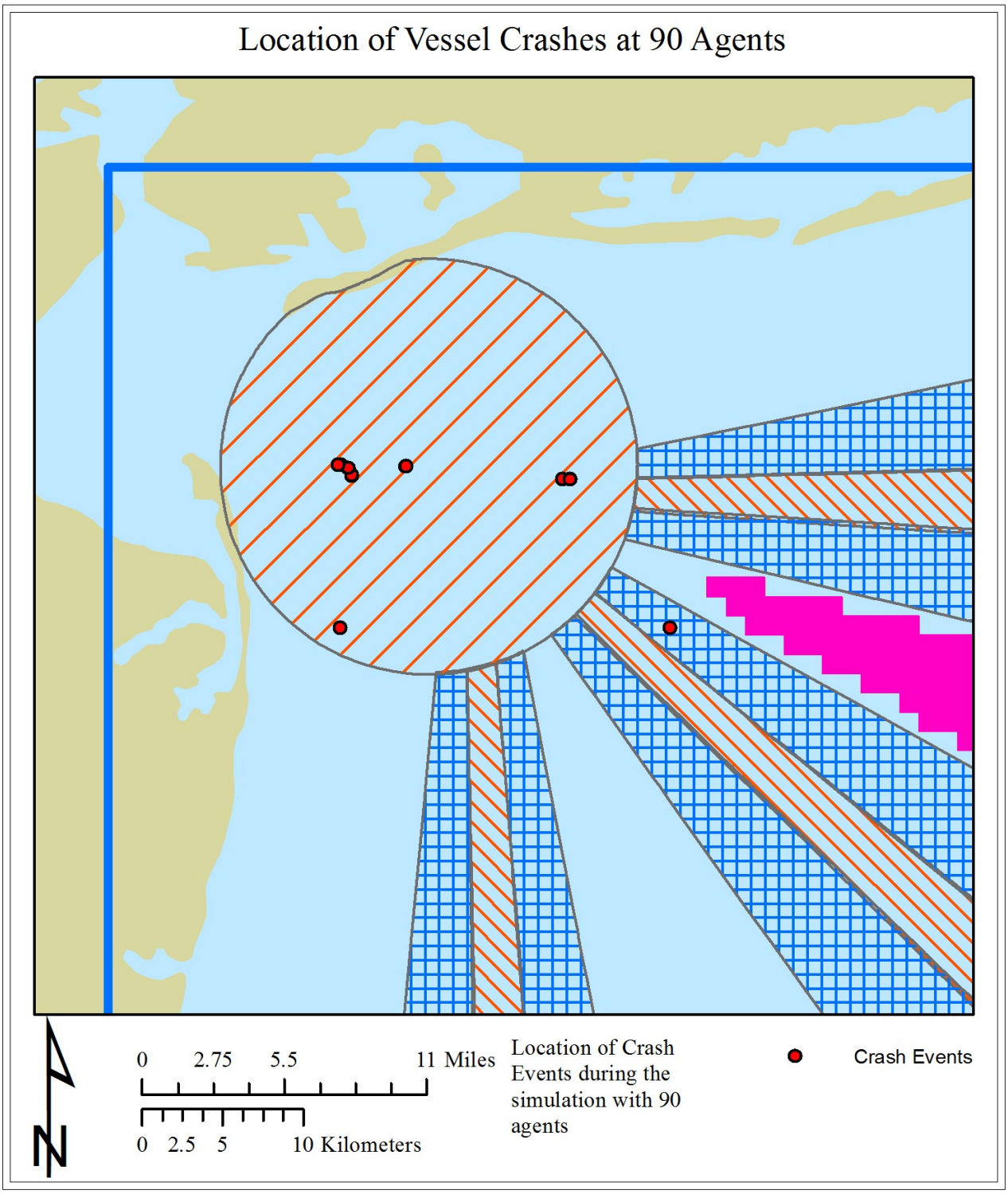

Figure 4.47 Location of all vessel crashes during a simulation with 90 agents. Note no crashes occur with the wind farm, and all are a result of increased traffic within the USCG precautionary area. These incidents are due to heavy traffic situations with such a large number of agents.

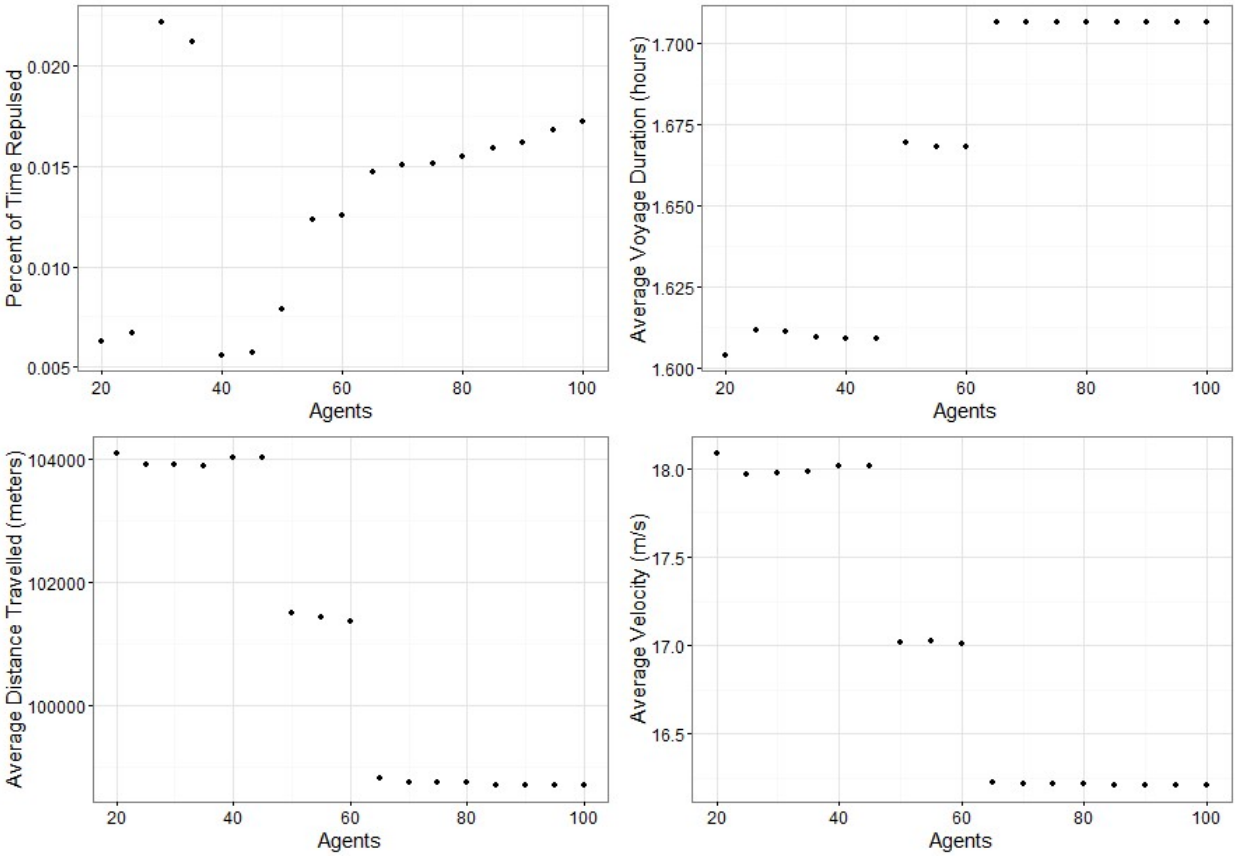

Figure 4.48 panel figure for the wind farm simulation showing the percent of time repulsed, average voyage duration, average distance travelled and average velocity of the original 20 agents as a function of the number of agents in a simulation. Note the dramatic increase in percent of time repulsed at 30 and 35 agents, however this bump is not noted in the voyage duration or average distance travelled so its effect is minimal.

4.7 Summary

A suite of numerical experiments tested an agent's inertial stopping capabilities, acceleration, and maneuvering. For the inertial stop experiments, the mass, wetted area, block coefficient, and drag coefficient were tested in individual experiments while holding all other variables constant. As the mass of a vessel increases, it's stopping capability decreases. As the size of the vessel (wetted area) increases, the hull has more resistance and the agent decelerates faster. In the third experiment as the block coefficient increases, so does resistance, and the vessel decelerates quicker. In the fourth experiment, as drag coefficient increases, so does resistance and the vessel decelerates quicker. To test how an agent accelerates, propeller diameter and cross sectional area were varied in separate experiments. In the first

acceleration experiment, a larger propeller produces more thrust and an agent may accelerate faster. An interesting phenomenon occurs when the propeller diameter is undersized for a vessel. The vessel attains maximum RPS (Figure 4.) meaning it cannot maintain the desired acceleration. The second acceleration experiment varied cross sectional area. As the area increases, so does resistance, and the vessel's propeller must spin faster to achieve the desired acceleration. The final set of numerical experiments tested an agent's maneuvering by adjusting the Nomoto K and T indices. As K increases and T decreases, a vessel can make tighter turns, while a large T and small K will produce a large turning radius. Following the numerical experiments, the Euclidean shortest path route finding algorithm tested agent's route finding capabilities with and without obstacles.

Prior to embarking on a voyage, an agent will identify the shortest route to its destination from its starting point with the Euclidean shortest path algorithm as adopted from Hong and Murray (2013). Provided that the origins and destinations among a populaiton of agents are unique, their shortest path routes will not be coincident (Figure 4.). However, when obstacles are introduced into the problem, routes converge and agents are forced to compete for space and the COLREGs will determine which agent has movement priority. Following the shortest path experiments, a new set of experiments were designed to test for the presence of chaos.

Chaotic systems are deterministic, sensitive to initial conditions, and will produce emergent properties of interest to resource managers through individual interaction. The first set of experiments found that if no variable in the system were changed, than the outcome of any two model runs will be identical. In other words, the agent based model was found to be determinisitc (Figures 4.13 - 4.15). Following the initial experiment, we incrementally altered beam, draft and tonnage by small amounts and we found that the agent based model was sensitive to initial conditions (Figures 4.16 - 4.26). The final chaos experiment looked for the presence of emergence. Of interest to marine spatial planners are the secondary effects stemming from the location of a wind farm. A model was set up that intentially funnelled agents through a bottleneck. The experiment produced kinematic waves, a tell-tale sign of

traffic jams. The potential for traffic jams at sea means longer voyage times and an increased risk of collision. With these results, the model was deemed to reproduce complex adaptive systems. Following the chaos experiments, the agent based model was validated against real ship maneuvering data.

The wheelhouse poster presents information on the maneuverability, which pilots use to guide vessels into port. Information from the wheelhouse poster was used to derive a set of K and T indices for the vessel of interest. Then a turning simulation validated the maneuvering model, producing a turn to port that closely matched the refernece vessel. After validating the turning model, we simulated the entrance to the port of New York and New Jersey.

The agent based model of the entrance to the Port of New York and New Jersey simulated incoming and outgoing vessel traffic with and without a wind farm. While the presence or absence of a wind farm had no effect on the population of vessels, increasing the vessel density past a threshold led to accidents. When vessels from multiple pathways converge at the Ambrose Channel, they interact with each other and must slow down. This decrease in speed produces a cascade of effects throughout the system. In high density simulations, vessels must slow down prior to approaching the speed regulated areas. In these instances, vessels cannot decelerate fast enough to meet intersecting traffic and crashes occurred. Generally, the more vessels in the system, the more crashes occurred. There is a clear upper limit to the amount of traffic within an hour that the current system can sustain.

Chapter 5

Discussion and Conclusion

5.1 Introduction

As the nuclear energy infrastructure in the northeast United States ages and we begin to transition away from fossil fuel energy sources, renewable energy sources must become a prominent feature of our energy landscape. With the siting of WEAs by BOEM in coastal waters along the continental shelf of the eastern United States, marine space will be managed in a manner that regulates activity into appropriate resource use areas. The allocation of space towards a single use will exclude other resource users leading to economic displacement and potential for socio-economic change within the coastal economy. Socio-economic systems that are not resilient enough to withstand change may falter. Displacement has real economic cost to the marine trade and transport sector as it leads to increased time at sea, greater fuel

costs and lower profit margins. These impacts will have direct consequences for the shipping lines and may reduce the profitability of ports as shippers look to other less congested sea lanes and ports. While these displacement costs are real, few researchers have evaluated their potential on the marine landscape. The purpose of this study was to implement methods that can anticipate the displacement of mutually exclusive activities resulting from foregone space by studying the effect of a WEA within close proximity of a shipping lane through the use of an ABM. The ABM simulated individual ships competing for space within a shipping lane while abiding by COLREGs. The study employed ABMs because they offer a way to experiment with the spatial configuration of a plan prior their implementation rather than studying the effects after the fact.

5.2 Evaluating the Impact of Wind Energy Areas Using Agent Based Modeling

Agent based models have been around for a number of years and have solved numerous geographic problems (An, Linderman, Qi, Shortridge, & Liu, 2005 and Crooks, 2010), increased our knowledge of the natural world (Graniero & Robinson, 2006 and Bennett & Tang, 2006) and have studied human interaction in crowds (Arentze, Pelizaro, & Timmermans, 2010 and Batty, Desyllas, & Duxbury, 2003). Recently, the USCG has ruled that there is not enough information to warrant the development of offshore renewable energy infrastructure, particularly wind farms, off of the Atlantic coast because there is a lack of information on their potential effects (USCG, 2016). Agent based models present an opportunity to understand the potential impacts of offshore wind on the navigability of coastal waterways, and have the opportunity to satiate the concerns of regulatory agencies that are hesitant to allow for the construction of the first major development. Assuming the model is validated for conditions without the presence of a wind farm, when one is added to the study area, the resulting population level impacts can provide resource agencies with the information they need to assess the implications of a project. This

agent based model is constructed of numerous modules that control the maneuverability of vessels and agent interaction.

The first group of modules control the maneuverability of each ship agent and aim to approach physical reality. The main advantage of the numerical models employed in this application are their simplicity and elegance. The models are simple enough to be solved in near real time and ranged between 5,609 and 33,692 seconds depending upon the number of agents in the simulation and Python IDE used. This allows an ordinary desktop computer to run the application with simple open source tools (Python 2.7.5) without having to rely upon parallelization over a computerized network, parallelization over a graphics processing unit (GPU) or the use a super computer. While the model enjoys simplicity and efficiency, each numerical model has its drawback.

The first such module employs gravity for collision avoidance and navigation. The inverse of the apparent gravitational force between two agents act to push agents away from danger, while the attractive force of each waypoint acts to pull the agents toward their destination. However, the collision avoidance procedures also require complex logic in order to comply with COLREGs. The COLREGs are a set of regulations that govern ship interactions in open water (USCG, 2015). Thus, guiding a ship requires intelligence, institutional (tacit) knowledge, and foresight, all of which are not contained within the gravity model.

Intelligence is the ability to recognize the severity of each interaction scenario and react accordingly. Currently, the agents have no decision-making ability, they simply react to stimuli in much the same way instinctual decisions are made by animals – they are ingrained with the ability to minimize risk of collision through gravity models. With Institutional knowledge, ships of different types and sizes have inherent differences in their stopping, maneuvering and accelerating capabilities. Hence the requirement for wheelhouse posters for pilots. Thus, a significant amount of tacit knowledge only learned from years of experience are required before a captain can master their ship. This knowledge is completely lost upon

the modeler, and therefore absent from any code contained herein. The gravity model also lacks foresight. The agents cannot "see" a situation developing in front of them and react before it becomes a problem because they do not have the intelligence and institutional knowledge that real ship captains generate after years of experience. In future iterations, it may be necessary to employ some of these capabilities so that the model approaches reality and accurately simulates the real world. The next set of modules govern the maneuverability vessels, with the first describing the ability of a ship agent to stop and accelerate.

The agent based model is limited in its applicability because it only has models for rigid, single hull ships with single propellers. Ships come in many shapes, sizes, and designs, some of which have multiple propellers and hulls. Further, tug boats often tow massive barges that do not have any source of propulsion. Thus, their physics are significantly different than a rigid monohull design. Therefore, the types of vessels that can be modeled with this application are limited. There are other factors in the open ocean that affect how a vessel can decelerate or accelerate including resistance from wind and waves and the effects of tidal currents

5.3 Summary and Future Research

Future iterations of this agent based model can incorporate other forms of resistance, including wind, waves and tide, to improve the accuracy of the model and incorporate scenarios that are impossible given the current configuration. Wind resistance could easily be accounted for by taking the cross-sectional area the vessel's windward profile and the direction and strength of the wind. Incorporating resistance from waves is more difficult because a realistic wave model must couple wind conditions throughout the study area and run in real time alongside the agent based model. Tidal forces are easier to incorporate because they act upon the hull of the ship in much the same way as thrust and resistance. Further, tidal forces are simpler than wind and waves because they are usually unidirectional for a given study area. While it is possible to incorporate wind, wave and tidal forces into the model, doing so would increase the

number of computations and model complexity, which may affect one of the main advantages of the model, its simplicity and real time computation on personal desktop computers. There must be a tradeoff between model simplicity and realism, and more study is required to determine where this tradeoff lies, and if it is even required for the type of open water simulations we are employing here. The final module governing ship movement concerns maneuverability.

The Nomoto model is the most common used model for heading in autopilot systems (Fossen, 2005) and is a generally accepted method for simulating ship maneuvering. However, the maneuvering model does not take into account added resistance to the hull when the rudder is activated. This source of resistance will slow a vessel considerably during a turn, and must be accounted for in future iterations. After calibrating the Nomoto K and T indices, the model was able to accurately simulate the test vessel's advance and transfer. Validation of the Nomoto model proved successful, however the amount of calibration data received from the shipping community was paltry. The researcher initiated communication with ship builders, ship owners, regulatory agencies, rating firms, pilot associations and consulting firms that perform sea trials and was met with near universal rejection. There was only a single pilot, on a single vessel that provided appropriate data for calibration. Due to these setbacks, the model is currently limited in its applicability and is simulating vessel maneuverability with unverifiable but published ranges of K-T indices (Kawaguchi, Xiong, Inaishi, & Kondo, 2004). If this application is to become accepted practice for assessing the potential effects of offshore energy installations on the commercial shipping industry, then the industry must be more cooperative. Perhaps there will be regulatory pressure for the industry to comply after the Coast Guard's latest report (USCG, 2016) that found considerable potential for impact from these competing industries.

With the limitations of the physical models and lack of calibration data for the entire shipping industry, it is important to discuss the limitations of this model. The ABM lacks physical models describing the effects of wind, wave, and tides on the maneuverability of ships. Therefore, it is

inappropriate to model the interaction of the shipping industry with offshore renewable energy installations in storm conditions and locations with considerable tidal currents, which may be of interest to regulatory agencies. Future iterations of the ABM should incorporate these modules. The lack of K-T index calibration data means that the model relies upon the unverifiable published limits (Kawaguchi, Xiong, Inaishi, & Kondo, 2004) for cargo vessels and tankers. Further only having limits for cargo vessels and tankers means that the model can only simulate these types of vessels, but according to Table 4.5, many other types of vessels exist within the Port. Further research and industry compliance is required before the model is appropriate for assessing the impact to the entire shipping industry. Until then, the model is only appropriate for assessing impacts to cargo vessels and tankers, which happen to be the two largest components of vessel traffic in the study area (Table 4.5). The maneuvering models and physics described in this application are appropriate for single screw, single rigid hull vessels. It cannot simulate vessels with multiple propellers or hulls, nor can it simulate towed barges. Lastly, the Nomoto model is not appropriate for simulating movement at velocities close to steerage speed. At these low speeds the rudders are no longer effective and vessels cannot turn without the aid of bow thrusters or assistance from tug boats.

While the application has considerable limitations, it was still able to simulate commercial traffic in and around the traffic separation schemes that are well outside the entrance to the port. These locations are dominated by traffic from cargo vessels and tankers, which we have calibration data for and can simulate well. While the agent based model simulated crashes when the number of vessels were high, the modeled vessel density when crashes occurred was far greater than what occurs presently. The vessel crashes were not a result of the proposed wind farm considering the two sets of simulations (one with and one without the wind farm) were identical. The proposed wind farm does not affect the initial route selection of cargo vessels and tankers, nor does it increase the vessel density within the channels leading to an increase in collision avoidance procedures. Therefore, at this time, the proposed wind farm appears to have no effect on the socio-economic well-being of the marine trade and transport industry.

In all experiments, the model produced results indicative of chaotic systems. The agent based model was deterministic, sensitive to small changes in initial states, and is capable of producing emergent phenomena of interest to spatial planners. Theoretically, the model is similar to Ruelle's billiard ball experiment (Ruelle, 1991), so the fact that it is chaotic comes as no surprise. The results of the ESP algorithm as iterated over a population of agents (Figure 4.12 and Figure 4.13) may also be chaotic. Not only will the shortest distance pathways change with small changes in the initial locations of the agents, but they will also change with small changes in the locations of obstacles.

While interesting from a theoretical standpoint, making sense out of the simulated interactions of complex adaptive systems may prove difficult for spatial planners. Through individual interaction guided by simple behavioral rules, agent based models reproduce the complex tapestry of behaviors on display across a landscape. After comparing the emergent pattern of a model with that of a real system, a plausible causal explanation arises that is not readily apparent from a traditional reductionist approach. Further, agent based models, or any model of a complex adaptive system, provides a mechanism for the study of thresholds, where small changes in an individual parameter leads to a profound change in system state. In the case of traffic problems, laminar flow can seize into gridlock, which eventually give way to smooth laminar flow. Described as kinematic waves (Lighthill and Whitham, 1955), pulses of interrupted traffic (gridlock) travel longitudinally through a column of traffic. With two-dimensional traffic in continuous space, disruptions lead to a deflection in course as well as a reduction in speed (Figure 4.29). While not the intention of the model, crashes are inevitable in every transportation system.

It is possible for the model to exhibit all three states of physical matter, gas, liquid and solid within a single simulation. At low traffic densities, the population of agents behaves like a gas. As density increases, the traffic begins to behave as a fluid. At a critical density threshold, the agents may collide in a process similar to crystallization, the shape of which is in the form of the kinematic wave that was progressing through the population before the initial contact occurred. Once the first two vessels within a

wave collide, a chain reaction occurs with each trailing vessel colliding with the vessel in front of it. Accidents like this are common on our highways, and the model exhibited this behavior during some extreme scenarios. Considering each vessel is massive with incredible amounts of momentum, it is nearly impossible to stop quickly and an accident in close quarters easily sparks a chain reaction of accidents.

In conclusion, this agent based model of the commercial shipping industry in and around the Port of New York and New Jersey offers great promise to understand the potential effects from developing wind energy in coastal waters. The model was able to reproduce current behavior of cargo vessels and tankers, and with better calibration data and physical models incorporating the effects of wind, waves and tides, this application could become an important tool for regulators and spatial planners alike.

Chapter 6

Bibliography

Abbott, J. K., & Hayne, A. C. (2012). What are we protecting? Fisher behavior and the unintended consequences of spatial closures as a fishery management tool. Ecological Applications, 22(3), 762-777.

Abbott, R. (2007). Putting complex systems to work. Complexity, 13(2), 30-49.

Agardy, T., Notarbartolo di Sciara, G., & Christie, P. (2011). Mind the gap: Addressing the shortcomings of marine protected areas through large scale marine spatial planning. Marine Policy, 35, 226-232.

Alexander, K. A., Janssen, R., Arciniegas, G., O'Higgins, T. G., Eikelboom, T., & Wilding, T. A. (2012). Interactive Marine Spatial Planning: Siting Tidal Energy Arrays around the Mull of Kintyre. PLoS ONE, 7(1), 1-9.

Alexander, K. A., Wilding, T. A., & Heymans, J. J. (2013). Attitudes of Scottish fishers towards marine renewable energy. Marine Policy, 37, 239-244.

An, L., Linderman, M., Qi, J., Shortridge, A., & Liu, J. (2005). Exploring Complexity in a Human-Environment System: An Agent-Based Spatial Model for Multidisciplinary and Multiscale Integration. Annals of the Association of American Geographers, 95(1), 54-79.

Arentze, T., Pelizaro, C., & Timmermans, H. (2010). An agent-based micro-simulation framework for modelling of dynamic activity and travel rescheduling decisions. International Journal of Geographical Information Science, 24(8), 1149-1170.

Baird, A. J. (2007). The economics of Motorways of the Sea. Maritime Policy & Management, 34(4), 287-310.

Barthelmie, R. J., Pryor, S. C., Frandsen, S. T., Hansen, K. S., Schepers, J. G., Rados, K., . . . Neckelmann, S. (2010). Quantifying the Impact of Wind Turbine Wakes on Power Output at Offshore Wind Farms. J. Atmos. Oceanic Technol., 27(8), 1302-1317.

Batty, M., Desyllas, J., & Duxbury, E. (2003). The discrete dynamics of small-scale spatial events: agent-based models of mobility in carnivals and street parades. International Journal of Geographical Information Science, 17(7), 673-697.

Bennett, D. A., & Tang, W. (2006). Modelling adaptive, spatially aware, and mobile agents: Elk migration in Yellowstone. International Journal of Geographical Information Science, 20(9), 1039-1066.

BOEM. (2014, October). Vessel Traffic Data. Vessel Traffic Data. Retrieved from http://marinecadastre.gov/ais/

Bone, C., Dragicevic, S., & White, R. (2011). Modeling-in-the-middle: bridging the gap between agent-based modeling and multi-objective decision-making for land use change. International Journal of Geographical Information Science, 25(5), 717-737.

Bonissone, P. P. (1980). A fuzzy sets based linguistic approach: theory and applications. Proceedings of the 12th conference on Winter simulation, (pp. 99-111).

Borenstein, J., & Koren, Y. (1991). The vector field histogram-fast obstacle avoidance for mobile robots. Robotics and Automation, IEEE Transactions on, 7(3), 278-288.

Brooks, D. A. (2011). The hydrokinetic power resource in a tidal estuary: The Kennebec River of the central Maine coast. Renewable Energy, 36(5), 1492-1501.

Cada, G. F., & Bevelhimer, M. S. (2011). Attraction to and Avoidance of Instream Hydrokinetic Turbines by Freshwater Aquatic Organisms. Tech. rep., Oak Ridge National Laboratory.

Campbell, M. S., Stehfest, K. M., Votier, S. C., & Hall-Spencer, J. M. (2014). Mapping fisheries for marine spatial planning: Gear-specific vessel monitoring system (VMS), marine conservation and offshore renewable energy. Marine Policy, 45(0), 293-300.

Campling, L., Havice, E., & Howard, P. M. (2012). The Political Economy and Ecology of Capture Fisheries: Market Dynamics, Resource Access and Relations of Exploitation and Resistance. Journal of Agrarian Change, 12(2-3), 177-203.

Carter, D. W. (2003). Protected areas in marine resource management: another look at the economics and research issues. Ocean & Coastal Management, 46(5), 439-456.

Castro, J. L. (1995). Fuzzy logic controllers are universal approximators. Systems, Man and Cybernetics, IEEE Transactions on, 25(4), 629-635.

Chang, Y.-T., Lee, S.-Y., & Tongzon, J. L. (2008). Port selection factors by shipping lines: Different perspectives between trunk liners and feeder service providers. Marine Policy, 32(6), 877-885.

Chen, Y., Li, X., Liu, X., & Liu, Y. (2010). An agent-based model for optimal land allocation (AgentLA) with a contiguity constraint. International Journal of Geographical Information Science, 24(8), 1269-1288.

Chen, Y., Li, X., Wang, S., & Liu, X. (2012). Defining agents' behavior based on urban economic theory to simulate complex urban residential dynamics. International Journal of Geographical Information Science, 26(7), 1155-1172.

Clark, X., Dollar, D., & Micco, A. (2004). Port efficiency, maritime transport costs, and bilateral trade. Journal of Development Economics, 75(2), 417-450.

Conlisk, J. (1996). Why Bounded Rationality? Journal of Economic Literature, 34(2), pp. 669-700.

Crooks, A. T. (2010). Constructing and implementing an agent-based model of residential segregation through vector GIS. International Journal of Geographical Information Science, 24(5), 661-675.

Crowder, L., & Norse, E. (2008). Essential ecological insights for marine ecosystem-based management and marine spatial planning. Marine Policy, 32, 772-778.

Cullinane, K., & Khanna, M. (2000). Economies of scale in large containerships: optimal size and geographical implications. Journal of Transport Geography, 8(3), 181-195.

Curtin, R., & Prezello, R. (2010). Understanding marine ecosystem based management: A literature review. Marine Policy, 34, 821-830.

Dijkstra, E. W. (1959). A note on two problems in connexion with graphs. Numerische mathematik, 1(1), 269-271.

Douvere, F., & Ehler, C. (2009). Marine Spatial Planning: A Step-By-Step Approach toward EBM. International Marine Conservation Congress (IMCC). Washington, DC.

Ehler, C. (2008). Conclusions: Benefits, lessons learned, and future challenges of marine spatial planning. Marine Policy, 32, 840-843.

Epstein, J. M. (1999). Agent-based computational models and generative social science. Complexity, 4(5), 41-60.

Fagerholt, K. (2004). Designing optimal routes in a liner shipping problem. Maritime Policy & Management, 31(4), 259-268.

Fayram, A. H., & de Risi, A. (2007). The potential compatibility of offshore wind power and fisheries: An example using bluefin tuna in the Adriatic Sea. Ocean \& Coastal Management, 50(8), 597-605.

Fishburn, P. C. (1970). Utility theory for decision making. Tech. rep., DTIC Document.

Foley, M. M., Halpern, B. S., Micheli, F., Armsby, M. H., Caldwell, M. R., Crain, C. M., . . . Steneck, R. S. (2010). Guiding ecological principles for marine spatial planning. Marine Policy, 34, 955-966.

Fossen, T. I. (1994). Guidance and Control of Ocean Vehicles. New York, NY: John Wiley & Sons, Inc.

Ge, S. S., & Cui, Y. J. (2002). Dynamic Motion Planning for Mobile Robots Using Potential Field Method. Autonomous Robots, 13(3), 207-222.

Gillies, S. (2013). The Shapely User Manual. The Shapely User Manual. Retrieved from http://toblerity.org/shapely/manual.html

Graniero, P. A., & Robinson, V. B. (2006). A probe mechanism to couple spatially explicit agents and landscape models in an integrated modelling framework. International Journal of Geographical Information Science, 20(9), 965-990.

Greenstreet, S. P., Fraser, H. M., & Piet, G. J. (2009). Using MPAs to address regional scale ecological objectives in the North Sea: modelling the effects of fishing effort displacement. ICES Journal of Marine Science.

Gross, D., & Strand, R. (2000). Can agent-based models assist decisions on large-scale practical problems? A philosophical analysis. Complexity, 5(6), 26-33.

Gunderson, L. H., & Holling, C. S. (Eds.). (2002). Panarchy: Understanding Transformations in Human and Natural Systems. Washington: Island Press.

Hagberg, A. A., Schult, D. A., & Swart, P. J. (2008). Exploring network structure, dynamics, and function using NetworkX. Proceedings of the 7th Python in Science Conference (SciPy2008), (pp. 11-15). Pasadena, CA USA.

Halley, J. D., & Winkler, D. A. (2008). Classification of emergence and its relation to self-organization. Complexity, 13(5), 10-15.

Harrill, R. (1999). Political Ecology and Planning Theory. Journal of Planning Education and Research, 19, 67-75.

Heppenstall, A. J., Crooks, A. T., See, L. M., & Batty, M. (Eds.). (2012). Agent-Based Models of Geographic Systems. New York, NY: Springer.

Hewlett, J. C. (1994). Ship Navigation Simulation Study, Houston-Galveston Navigation Channels, Texas. Report 1. Houston Ship Channel, Bay Segment. Tech. rep., DTIC Document.

Hilborn, R. (2007). Managing fisheries is managing people: what has been learned? Fish and Fisheries, 8, 285-296.

Holling, C. S. (1973). Resilience and Stability of Ecological Systems. Annual Review of Ecology and Systematics, 4, 1-23.

Hong, I., & Murray, A. T. (2013). Efficient measurement of continuous space shortest distance around barriers. International Journal of Geographical Information Science, 27(12), 2302-2318.

Jogiste, K., Moser, W. K., & Mandre, M. (2005). Disturbance dynamics and ecosystem-based forest management. Scandinavian Journal of Forest Research, 20(56), 2-4.

Johnson, K., Kerr, S., & Side, J. (2013, March). Marine renewables and coastal communities: Experiences from the offshore oil industry in the1970s and their relevance to marine renewables in the 2010s. Marine Policy, 38, 491-499.

Johnson, N. F. (2009). Simply Complexity: A Clear Guide to Complexity Theory. Oneworld.

Jones, E., Oliphant, T., Peterson, P., & others. (2001). SciPy: Open source scientific tools for Python. {SciPy}: Open source scientific tools for {Python}. Retrieved from http://www.scipy.org/

Jorgensen, S. E., & Fath, B. D. (2011). 9 - Individual-Based Models. In S. E. Jørgensen, & B. D. Fath (Eds.), Fundamentals of Ecological Modelling (Vol. 23, pp. 291-308). Elsevier.

Journee, J. M., & Pinkster, J. A. (2001, January). Ship Hydromechanics, Part 1: Introduction. Draft Edition, Ship Hydromechanics Laboratory, Delft University of Technology, Mekelweg, Delft, The Netherlands.

Kao, S.-L., Lee, K.-T., Chang, K.-Y., & Ko, M.-D. (2007). A fuzzy logic method for collision avoidance in vessel traffic service. Journal of Navigation, 60(01), 17-31.

Kawaguchi, A., Xiong, X., Inaishi, M., & Kondo, H. (2004). A computerized navigation support for maneuvering clustered ship groups in close proximity. Best session paper in the 10th International Conference on Information Systems Analysis and Synthesis (ISAS'04), Orlando, Florida, (pp. 313-318).

Kellner, J. B., Tetreault, I., Gaines, S. D., & Nisbet, R. M. (2007). Fishing the Line Near Marine Reserves in Single and Multispecies Fisheries. Ecological Applications, 17(4), 1039-1054.

Kerr, D. (2007, April). Marine Energy. Philosophical Transactions: Mathematical, Physical and Engineering Sciences, 365(1853), 971-992.

Kildow, J. T., Colgan, C. S., & Scorse, J. (2009). State of the U.S. Ocean and Coastal Economies. Tech. rep., National Ocean Economics Program. Retrieved from http://www.oceaneconomics.org/Market/

Klein, C. J., Steinback, C., Watts, M., Scholz, A. J., & Possingham, H. P. (2010). Spatial marine zoning for fisheries and conservation. Frontiers in Ecology and the Environment, 8(7), 349-353.

Koren, Y., & Borenstein, J. (1991, Apr). Potential field methods and their inherent limitations for mobile robot navigation. Robotics and Automation, 1991. Proceedings., 1991 IEEE International Conference on, 2, pp. 1398-1404.

Lee, H., Kong, G., Kim, S., Kim, C., & Lee, J. (2002). Optimum Ship Routing and Its Implementation on the Web. In W. Chang (Ed.), Advanced Internet Services and Applications (Vol. 2402, pp. 125-136). Springer Berlin Heidelberg.

Lee, S.-M., Kwon, K.-Y., & Joh, J. (2004). A fuzzy logic for autonomous navigation of marine vehicles satisfying COLREG guidelines. International Journal of Control Automation and Systems, 2, 171-181.

Levin, S. A., & Lubichenco, J. (2008). Resilience, Robustness, and Marine Ecosystem-based Management. BioScience, 58(1), 27-32.

Lighthill, M. J., & Whitham, G. B. (1955). On kinematic waves. II. A theory of traffic flow on long crowded roads. Proceedings of the Royal Society of London. Series A. Mathematical and Physical Sciences, 229(1178), 317-345.

Lorenz, E. N. (1963). Deterministic nonperiodic flow. Journal of the atmospheric sciences, 20(2), 130-141.

Macal, C. M., & North, M. J. (2005). Tutorial on agent-based modeling and simulation. WSC '05: Proceedings of the 37th conference on Winter simulation (pp. 2-15). Winter Simulation Conference.

Malchow, M. B., & Kanafani, A. (2004). A disaggregate analysis of port selection. Transportation Research Part E: Logistics and Transportation Review, 40(4), 317-337.

Manson, S. M. (2006). Bounded rationality in agent-based models: experiments with evolutionary programs. International Journal of Geographical Information Science, 20(9), 991-1012.

Martin, R., & Sunley, P. (2007). Complexity thinking and evolutionary economic geography. Journal of Economic Geography, 7(5), 573-601.

Martins, M. R., & Maturana, M. C. (2013). Application of Bayesian Belief networks to the human reliability analysis of an oil tanker operation focusing on collision accidents. Reliability Engineering & System Safety, 110, 89-109.

Mascia, M. B., Claus, C. A., & Naidoo, R. (2010). Impacts of Marine Protected Areas on Fishing Communities. Conservation Biology, 24(5), 1424-1429.

MCA. (2008). Offshore Renewable Energy Installations (OREIs) - Guidance on UK Navigational Practice, Safety and Emergency Response Issues. Marine Guidance Note, Maritime and Coastguard Agency.

McKay, B. J., & Jones, P. J. (2011). Marine Protected Areas and the Governance of Marine Ecosystems and Fisheries. Conservation Biology, 25(6), 1130-1133.

Merrick, J. R., van Dorp, J. R., Blackford, J. P., Shaw, G. L., Harrald, J., & Mazzuchi, T. A. (2003). A traffic density analysis of proposed ferry service expansion in San Francisco Bay using a maritime simulation model. Reliability Engineering & System Safety, 81(2), 119-132.

Montes, A. A. (2005). Network shortest path application for optimum track ship routing. Ph.D. dissertation, Monterey, California. Naval Postgraduate School.

Moon, J. N., & Tudhope, D. S. (2006). An agent-directed marine navigation simulator. Journal of Navigation, 59(03), 461-475.

Mori, A. S. (2011). Ecosystem management based on natural disturbances: hierarchical context and non-equilibrium paradigm. Journal of Applied Ecology, 48, 280-292.

Morrissey, K., O'Donoghue, C., & Hynes, S. (2011). Quantifying the value of multi-sectoral marine commercial activity in Ireland. Marine Policy, 35(5), 721-727.

Nikitakos, N., & Fikaris, G. (2009). Marine Navigation and Safety of Sea Transportation. CRC Press.

Nir, A.-S., Lin, K., & Liang, G.-S. (2003). Port choice behavior--from the perspective of the shipper. Maritime Policy & Management, 30(2), 165-173.

Northam, J. (2016). Amid Industry Downturn, Global Shipping Sees Record-Low Growth. Amid Industry Downturn, Global Shipping Sees Record-Low Growth. Retrieved from http://www.npr.org/sections/parallels/2016/08/20/490621376/amid-industry-downturn-global-shipping-sees-record-low-growth

Northam, J. (2016). Container Ships Stranded at Sea After South Korean Company Goes Bankrupt. Container Ships Stranded at Sea After South Korean Company Goes Bankrupt. Retrieved from http://www.npr.org/sections/parallels/2016/09/08/493157924/container-ships-stranded-at-sea-after-south-korean-company-goes-bankrupt

Notteboom, T. E. (2006). The time factor in liner shipping services. Maritime Economics & Logistics, 8(1), 19-39.

NTNU. (2009). Chapter 8 - Course Autopilots`. Chapter 8 - Course Autopilots`. Retrieved from http://www.itk.ntnu.no/fag/gnc/lecture_notes/2009/L7.pdf

PANYNJ. (2016, April). 2014 Trade Statistics. 2014 Trade Statistics. Retrieved from http://www.panynj.gov/port/pdf/historical_stats_2004-2014_trade-stats.pdf

Peel, D., & Lloyd, M. G. (2004). The Social Reconstruction of the Marine Environment: Towards Marine Spatial Planning? The Town Planning Review, 75(3), 359-378.

Pelc, R., & Fujita, R. M. (2002). Renewable energy from the ocean. Marine Policy, 26, 471-479.

Perera, L. P., Carvalho, J. P., & Soares, C. G. (2009). Autonomous guidance and navigation based on the COLREGs rules and regulations of collision avoidance. In Proceedings of the International Workshop: Advanced Ship Design for Pollution Prevention, (pp. 205-216).

Peterson, A., & Stead, S. (2011, 8). Rule breaking and livelihood options in marine protected areas. Environmental Conservation, 38, 342-352.

Python. (2016). python. python. Retrieved from https://www.python.org/

Reynolds, C. S. (2002). Ecological Pattern and ecosystem theory. Ecological Modelling, 158, 181-200.

Ruelle, D. (1991). Chance and Chaos. Princeton, NJ: Princeton University Press.

Salamon, T. (2011). Design of Agent-Based Models: Developing Computer Simulations for a Better Understanding of Social Processes. Czech, Republic: Repin - Zinonin Academic Series.

Samhouri, J. F., Levin, P. S., & Ainsworth, C. H. (2010). Identifying Thresholds for Ecosystem-Based Management. PlosOne, 5(1), 1-10.

Sengupta, R. R., & Bennett, D. A. (2003). Agent-based modelling environment for spatial decision support. International Journal of Geographical Information Science, 17(2), 157-180.

Shi, C., Zhang, M., & Peng, J. (2007). Harmonic potential field method for autonomous ship navigation. Telecommunications, 2007. ITST'07. 7th International Conference on ITS, (pp. 1-6).

Shields, M. A., Woolf, D. K., Grist, E. P., Kerr, S. A., Jackson, A. C., Harris, R. E., . . . Side, J. (2011). Marine renewable energy: The ecological implications of altering the hydrodynamics of the marine environment. Ocean & Coastal Management, 54(1), 2-9.

Smierzchalski, R. (1999). An intelligent method of ship's trajectory planning at sea. Intelligent Transportation Systems, 1999. Proceedings. 1999 IEEE/IEEJ/JSAI International Conference on, (pp. 907-912).

Statheros, T., Howells, G., & Maier, K. M. (2008, 1). Autonomous Ship Collision Avoidance Navigation Concepts, Technologies and Techniques. The Journal of Navigation, 61, 129-142.

Sutulo, S., Moreira, L., & Soares, C. G. (2002). Mathematical models for ship path prediction in maneuvering simulation systems. Ocean Engineering, 29(1), 1-19.

Tang, W., & Bennett, D. A. (2010). The Explicit Representation of Context in Agent-Based Models of Complex Adaptive Spatial Systems. Annals of the Association of American Geographers, 100(5), 1128-1155.

Teh, L. C., Teh, L. S., & Pitcher, T. J. (2012). A tool for site prioritization of marine protected areas under data poor conditions. Marine Policy, 36(6), 1290-1300.

Thrift, N. (1999). The Place of Complexity. Theory, Culture \& Society, 16(3), 31-69.

Tongzon, J. L., & Sawant, L. (2007). Port choice in a competitive environment: from the shipping lines' perspective. Applied Economics, 39(4), 477-492.

Torrens, P. M. (2012). Moving Agent Pedestrians Through Space and Time. Annals of the Association of American Geographers, 102(1), 35-66.

Torrens, P. M., & McDaniel, A. W. (2013). Modeling Geographic Behavior in Riotous Crowds. Annals of the Association of American Geographers, 103(1), 20-46.

Ueng, S.-K., Lin, D., & Liu, C.-H. (2008). A ship motion simulation system. Virtual reality, 12(1), 65-76.

USCG. (2015). Navigation Rules: International-Inland. Navigation Rules: International-Inland (COMDTINST M16672.2D).

USCG. (2016). Atlantic Coast Port Access Route Study. Tech. rep., United States Coast Guard.

Van Der Walt, S., Colbert, S. C., & Varoquaux, G. (2011). The NumPy array: a structure for efficient numerical computation. Computing in Science & Engineering, 13(2), 22-30.

Villa, F., Tunesi, L., & Agardy, T. (2002). Zoning Marine Protected Areas through Spatial Multiple-Criteria Analysis: the Case of the Asinara Island National Marine Reserve of Italy. Conservation Biology, 16(2), 515-526.

Xiao, F., Ligteringen, H., van Gulijk, C., & Ale, B. (2012). Artificial Force Fields for Multi-agent Simulations of Maritime Traffic: A Case Study of Chinese Waterway. Procedia Engineering, 45, 807-814.

Xue, Y., Clelland, D., Lee, B. S., & Han, D. (2011). Automatic simulation of ship navigation. Ocean Engineering, 38(17-18), 2290-2305.

Zubaly, R. B. (1996). Applied Naval Architecture. Cornell Maritime Press.